Republic of Iraq
Ministry of Higher Education and Scientific Research
University of Babylon
College of Materials Engineering
Department of Ceramic Engineering and Building Materials

Effect of Doping By Fe^{+3} and Sc^{+3} on The Characteristics of $MgAl_2O_4$

A Thesis
Submitted to the Department of Ceramics Engineering and Building Materials at college of Materials Engineering / University of Babylon in Partial fulfillment of the Requirements for Obtaining a Master's Degree in Materials Engineering /Ceramic

By

Al-khuder Mohammed Fadil Alwan
(B.Sc. In Ceramic and Building Materials, 2018)

Supervised by

Prof. Dr. Shaker J. Edress **Assist. Prof. Dr. Shaima Jaber Karim**

2021-2022 A.D
1442-1443 A.H

بسم الله الرحمن الرحيم

(وَقُل رَّبِّ زِدْنِي عِلْمًا)

صدق الله العلي العظيم

سورة طه_الآية (114)

Supervisor Certificates

We Certify that this thesis, entitled " **Effect of Doping by Fe^{+3} and Sc^{+3} on The Characteristics of $MgAl_2O_4$**" was prepared by (**Al-khuder Mohammed Fadil)** under our supervision at the Department of Ceramic Engineering and Building materials / College of Materials Engineering / University of Babylon in Partial Fulfilment of the requirements for the degree of Master in Ceramic Engineering.

Signature :

Name : ***Prof. Dr. Shaker J. Edress***

(supervisor)
Date : / / 2022

Signature :

Name : ***Assist. Prof. Dr. Shaima Jaber Karim***

(Co-supervisor)
Date : / / 2022

Signature:

Prof. Mohsin Abbas Aswad (Ph. D)
Head of Ceramics Engineering and Building Materials

Date: / /2022

(Examining Committee Approval Sheet)

We certify that we have read this thesis entitled **"Effect of Doping by Fe^{+3} and Sc^{+3} on The Characteristics of $MgAl_2O_4$"** and as an examining committee, we have examined the student ***(Al-khuder Mohammed Fadil)*** in contents and that is related to it. And that in our opinion it meets the standard of a thesis for the degree of Master in Ceramic Engineering .

Signature
Prof. Ghazi K. Saeed (PhD)
Committee Chair
Date: / / 2022

Signature
Prof. Imad A. Disher (PhD)
Committee Member
Date: / / 2022

Signature
Lect .Mohammed N. Hassan (PhD)
Committee Member
Date: / / 2022

Signature
Prof. Shaker J. Edress (PhD)

Supervisor Member
Date: / / 2022

Signature
Asst. Prof. Shaima Jaber Karim (PhD)

Supervisor Member
Date: / / 2022

Approval of the Department of
Ceramic Engineering and building materials
Head of Department.

Signature
Prof. Mohsin Abbas Aswad (PhD)
Date: / / 2022

Approval of the College
of Materials Engineering
Dean of college.

Signature
Prof. Imad Ali Disher (PhD)
Date: / / 2022

Dedication

To our Prophet Muhammad and his good and pure family With All love

Al-Khuder Mohammed Fadil

Acknowledgement

In the name of Allah, the most gracious, the most merciful. First of all, great thanks be to (ALLAH His MAJESTY) and very grateful to **Imam Ali Ibn Musa Al-Ridha** for enabling me to finish this study,

My sincere appreciation and deepest gratitude are due to the Department of Ceramic Engineering and building materials , I would like to thanks **Prof. Dr Shaker J.Edress** and **Assist. Prof. Dr. Shaima Jaber Karim** whom I had the honour of being under their guidance and supervision, their constructive suggestion, patience and continuous encouragement are highly acknowledged through this study.

Special thanks be to my family **(mam and dad)** for supporting me, my **brothers, sisters** and **friends** for encouraging me through the time of the study,

To Mr. Dean of the College of Materials Engineering **Imad A. Disher** who was always available to give support in difficult times during this study.

Al-Khuder Mohammed Fadil

2022

ABSTRACT

Magnesium aluminate spinel ($MgAl_2O_4$) is one of the most famous ceramic material type of metal-oxide with special properties. Nanocrystallines of doped and undoped ($MgAl_2O_4$) spinel were synthesis by modified sol–gel method using aluminum nitrate, magnesium nitrate, iron nitrate, scandium nitrate and citric acid were used as precursor materials with a molar ratio Al/Mg = 2. After obtained a dry powder, the precursor was heat-treated at desired temperatures (800 °C) for 4h at rate of 5 °C/min.

In the present work, two main groups of undoped and doped $MgAl_2O_4$ samples were prepared by using sol–gel method. The first is $MgAl_{2-x}Fe_xO_4$ doped samples, where (x=0.0, 0.01, 0.02, 0.03, 0.04, 0.05) and the second is $MgAl_{1.95}Fe_{0.05-y}Sc_yO_4$ doped samples group, where (y= 0. 0.01, 0.02, 0.03, 0.04, 0.05).

The XRD results for undoped and doped samples demonstrated that all the samples have a single set of peaks matching with the $MgAl_2O_4$ cubic phase. From the XRD analysis, the major diffraction peak of all the doped samples have found to be shifted to lower 2θ. The lattice parameter, the inter-planner d space, and the size of crystallites were varied according to the concentration of doping Fe^{+3} and Sc^{+3} ions. The FTIR spectrum obtained from the synthesized material indicate the formation of $MgAl_2O_4$ spinel The peaks appearing in the range of 531-690 cm^{-1} . The molecular structures for the doped and undoped samples of $MgAl_{2-x}Fe_xO_4$ and $MgAl_{1.95}Fe_{0.05-y}Sc_yO_4$ samples have the same framework, but the doped samples have a variation in the broad of peaks. Furthermore, there were variation in the intensities due to incorporate of Fe^{+3} and Sc^{+3} ions the fingerprint area between 1000-400cm^{-1}.

From the images of the SEM test, the shape of the nanoparticles showed several different nanoparticles appear, they are angular, plate-like, or semi-spherical and contain porous channels due to the accumulation of particles. The purity of all samples was confirmed by EDX analysis.

As it was observed from the TEM selection images, the shape of the nanoparticles showed that they are spherical or spherical shapes with needle shapesand a little agglomerated overlaps resulting from the ratios of Sc^{+3} ion additions.

STM was used to study the dimensions of calcined doped and undoped magnesium aluminate particles to an improved understanding of the basic physical phenomena relating magnetism. In the case of $(MgAl_{2-x}Fe_xO_4)$, there were larger particles and particle clusters. Higher $MgAl_2O_4$ average particle and cluster sizes are due to the Fe^{+3} ion, resulting in an intensified individual particle growth. From the specific surface area of as-burnt powders, we can see that as-burnt powders have a mesoporous character. Because of calcination, the products showed a clear decrease of the surface areas because sub-micrometer sized primary particles have been agglomerated into larger secondary particles. $MgAl_{1.95}Fe_{0.05-y}Sc_yO_4$ samples have the same framework, but the doped samples have a variation in the dark and bright spots at a scale that is characterized by the nanometer dimensions.

The results of the magnetism were measured by the VSM test, where the results showed that the values of magnetic saturation, Ms, depend on the doping ratios. And the maximum magnetic value for the $(MgAl_{2-x}Fe_xO_4)$ group is at x=0.05 for the sample $(MgAl_{1.95}Fe_{0.05}O_4)$, while the maximum magnetic value was recorded for the $MgAl_{1.95}Fe_{0.05-y}Sc_yO_4$ nanogroup when y=0.04 for a sample of $MgAl_{1.95}Fe_{0.01}Sc_{0.04}O$, the results of the magnetism assumed that both doping ions Fe^{+3} and Sc^{+3} in different proportions and oxygen gaps play an important role, in addition to this the appearance of three types of hysteresis loops.

Table of Contents

List of Figures

List of Tables

List Of Abbreviations

Abbreviate	Meaning
AFM	Atomic Force Microscopy
CA	Citric Acid
EDX	Energy Dispersive X-Ray
FCE	F-Center excchange
FTIR	Fourier Transform Infrared
H_c	Coercivity
IR	Infrared
MB	Magnetic Moment
MNPs	Metallic Nanoparticles
M_R	Remanent Magnetization
M_S	Saturation Magnetization
NMR	Nuclear Magnetic Resonance
NMS	Non-magnetic Semiconductors
NPs	Nanoparticles
PEG	Poly Ethylene Glycol
R	Reflection
RE	Rare Earth
REE	Rare Earth Element
SEM	Scanning Electron Microscopy
Sq	Roughness Mean Square
STM	Surface Tunneling Microscope
TEM	Transmission Electron Microscope
TM	Transition Metal
UV	Ultraviolet
VSM	Vibrating Sample Magnometer
XRD	X-Ray Diffraction
μ_{eff}	Effective magnetic moment

List Of Units Used

Units Used	Meaning
μm	micro meter
nm	nanometer
m	meter
Å	angstrom
g/cm^3	gram/centimeter cube
^oC	degree Celsius
h	hour
min	minute
V	volt
Cm^{-1}	reciprocal centimeter

Chapter 1

Introduction

1-1 Introduction

Spinel compounds are the group of minerals that are oxides of Magnesium, Iron, Manganese or Aluminum. The term spinel is derived from spina (Latin, thorn) in reference to its pointed octahedral, crystal habit. Spinel minerals are widely distributed in the earth, in meteorites' and in rock from moon [1-3]. While the ideal spinel formula is AB_2O_4, some 30 elements, with valence from 1 to 6, are known to substitute in the A and B cation sites, having the spinel crystal structure [4]. The name spinel minerals that have so far been recorded in nature are oxides that occur as a matrix of A^{+2} versus B^{+3} cations [5-7] .

Due to the unique magnetic, structural and other properties, spinels are very attractive subjects for material research and engineering applications. Aluminous spinels are highly refractory, varying from translucent to transparent and from colorless to green, blue, brown and black [8].

The compounds $MgAl_2O_4$ refers to the spinel structure type (space group Fd_3m and Z=8). The magnesium aluminate spinel belongs to normal spinels, its formula is $(Mg^{+2})[Al^{+3}]O_4$.The round and square bracket denote the tetrahedral and octahedral sites respectively, while the oxygen ions are arranged in cubic closed packed structure [9-10].

Furthermore, spinel-structured aluminates exhibit properties such as, stability at high temperature and resistance against alkalis. In this context, they are widely used in applications such as buffer-layers, optical ceramics, refractories, electromagnetic windows and magnetic memory devices etc. [11].

Spinel $MgAl_2O_4$ doped with transition ions has been studied in bulk form for many years, to both understand their magnetic behavior and correlate it to their structural properties, where the Ferromagnetic lead to strong developments during the last two decades due to improvement in the field of nanotechnology [12].

Previously, the effect of transition metal (TM) doping on spinel structures has been examined and reported by several research groups exploring their various physical properties [13-15]. The TM (3*d*) levels interact with defect-levels of the host $MgAl_2O_4$ by affecting the valance electrons of the doped elements. Because of this interaction, the *A* or *B*-site cations can be purposely substituted by TM-ions, in order to tune the band structure desired for particular applications. For example, in the case of Fe-doped $MgAl_2O_4$, the magnetic properties of aluminates are determined primarily by Fe^{+2} A-site impurities [16].

Depending on the nature (magnetic or non-magnetic) and distribution of cations among A and B sublattices, spinel aluminate doped with (TM) can exhibit properties of different type magnets, like: ferromagnet, antiferromagnet and paramagnet. The inter-sublattice interactions (J_{AB}: A-O-B) is much stronger than the intra-sublattice interactions (J_{AA}: A-O-A and J_{BB}: B-O-B) in spinel doped with transition ions with collinear ferrimagnetic structure. Extensive works on certain spinel $MgAl_2O_4$ have been carried out for the last few decades, because of their theoretical understanding and potential applications in science and technology [17-18].

Recently, the evolution of power electronics toward higher frequency, the downsizing of ceramics from microstructure to nanometer scale, the increasing price of rare-earth elements and the development of magnetic

materials put light again on the study of spinel [19]. The presence of magnetically active centres determines a variety of interesting magnetic properties and applications of $MgAl_2O_4$ spinels doped (TM). This can be accomplished by creating nanoparticulate materials. In other words, the particle size of a spinel has a direct influence on, and thus magnetism. [20].

Thus, the preparation of magnesium aluminate powders with high purity, chemical homogeneity, control of stoichiometry, fine particle size, narrow particle size distribution, and minimum particle agglomeration with high sinter activity has received considerable attention in order to improve the material properties [21].

So as to prepare undoped and doped $MgAl_2O_4$ multiple formulation routes were included, such as combustion, modified sol-gel method, green synthesis, co-precipitation, liquid-phase technique, aerogel routes, hard templating pathways, microwave sol-gel technique, and spinning disk reactor [22-25]. The modified sol-gel process was chosen as one of the total chemical synthesis techniques number achieved in the formulation of pureness and doped $MgAl_2O_4$ at relatively low temperatures to improve the sinter ability and fabrication fine particles because it's key function was to synthesise magnetic materials, catalysts, ceramics, and high temperature superconductors [26]. The procedure prefers good stoichiometric management, homogeneity, and particle morphological control. The modified sol-gel method involves combining a metal precursor with water and citric acid. The chemical basis of this method is dehydration (esterification) of a carboxylic acid [27].

1.2 Aim of research:

1. This work was a comprehensive Investigation the effect of different doping concentration of Fe^{+3} ion ($MgAl_{2-x}Fe_xO_4$) of samples group and Fe^{+3} and Sc^{+3} ions of ($MgAl_{1.95}Fe_{0.05-y}Sc_yO_4$) samples group on structural and morphology of preparation samples by modified sol gel method, were (x= 0.0, 0.01, 0.02, 0.03, 0.04, 0.05) and (y= 0.0, 0.01, 0.02, 0.03, 0.04, 0.05).
2. This study focuses on the preparation of doped and undoped $MgAl_2O_4$ in nanoscale. Many applications of the aluminate at microscale have many problems like high coercive field, inhomogeneous magnetic spin structure. In addition to the problems in synthesis steps, it needs a long time of preparation and high calcination temperature. The goal of using modified sol-gel technique is to synthesis nanoparticles of doped and undoped $MgAl_2O_4$ with using acid to improve the magnetic properties, reduce the impurity phases, homogeneous spin structure, short time preparation, and low temperature.

Chapter 2

Theoretical Part

&

Literature Review

2-1 Introduction:

The electronics technology has the miniaturization of the device to nanometer sizes but with greatly improved final performance, as this raises many issues related to new materials to achieve specific and selective functions. The unique properties and improved performance of nanomaterial's are determined by their sizes by enhancing the surface area with a large number of particles present on the surface as well as by unique surface compositions, and interactions between particles [28].

The magnetic properties for nano-sized particulate materials vary from the broad surface to thickness, as the surface atoms are connecting with the neighbouring atoms in a different local area. Unlike ferromagnetic bulk materials, generally forming several magnetic domains, multiple small ferromagnetic particles can only comprise a single magnetic domain. The magnetic characteristics of magnetic spinel's are also affected by the degree for cation dis-order [29].

2.2 Crystalline Spinel Oxide Nanomaterials:

The study of metal oxides has attracted the attention of materials scientists due to their unique optical, electrical, magnetic, mechanical, thermal and catalytic properties, which make them technologically useful in materials science and catalysis, chemical sensing, microelectronics, nanotechnology, environmental decontamination, analytical chemistry, solid-state chemistry and fuel cells. The products of choice for data storage and transmission are ferromagnetic iron oxides, such as γ-Fe_2O_3, spinels applied by formula (AB_2O_4Where A, B = metal cations), and hexaferrites such as $BaFe_{12}O_{19}$ and $SrFe_{12}O_{19}$. Electronic instruments make heavy use of ferroelectric and dielectric oxides of perovskite structures, such as BaTiO_3 & Pb(Zr,Ti)O_3. Electrical, chemical, mechanical, and optical properties differ depending on the composition of perovskite oxides. LaMnO_3 is an antiferromagnetic insulating oxide, while LaNiO_3 is a metallic oxide. The

correlation between both the structure of oxide materials and their chemical and physical properties, as well as their applications, is important [30].

The spinels have the general formula AB_2X_4. In the crystal structure of the cubical (Isometric) spinals are arranged oxide anions in the clamping cube, Where the tetrahedral (A^{II}= a divalent cation like $Mg, Mn, Co, Fe, Cu, Ni, Zn, Sn, Cd$), the octahedral ($B^{III}$= a trivalent cation like $Al, Ga, Ti, V, Cr, Mn, Fe, Fe, Co, Ni$), and the ($X = O, S, Se\ etc.$). In the same manner, ($A^{II}$) and ($B^{III}$) as in Fe_3O_4 as ($Fe^{+2}Fe_2^{+3}O_4^{-2}$), may also be metal for various loads. The spinel structure can also be found in sulphide, selenides, tellurides, and a some halides, but the spinel minerals are mainly oxides[31] .

The structure of a spinel compound is identical to the strongly symmetric structure of diamond, which accounts for its high hardness and density. The location of the tetrahedral ions is about the same as that in the carbon atoms of diamond structures and The structure of the other ions favours the crystal structure octahedral conforming to diamond structure symmetry [32]. Additionally, the equilibrium of the spinel lattice cations is based on ionic radii, electrostatic energy and the effect on polarization. The structure of the spinel is only stable if the cations are very medium size and, therefore, the radii in the same compound of the various ionic species are not very different, so that in the oxide spinels, the sizes of two types of cations are not usually quite different. The same applies to the sulfides spinels , for example: $Ni^{+2}CO_2^{+3}S_4$. In the halide spinels, however, for example $Li_2^{+1}Fe^{+2}Br$, cations limit the total cation to charges 1^+ and 2^+, for balance of the cation: anion ratio of 3: 4 [33].

2.3 Type of spinel

The position of cations at the two main sites, tetrahedral site and octahedral site, divides spinels into three types [34], according to the following description:

2.3.1 Normal Spinel (AB_2O_4)

The divalent A^{II} ions occupy the tetrahedral voids, whereas the trivalent B^{III} ions occupy the octahedral voids in the close packed arrangement of oxide ions. The following is a representation of a normal spinel: $(A^{II})^{tet}(B^{III})^{oct}O_4$. For examples are $MgAl_2O_4$ (known as spinel)$Mn3O4, ZnFe2O4, FeCr2O4$ $(chromite)$ etc [35]

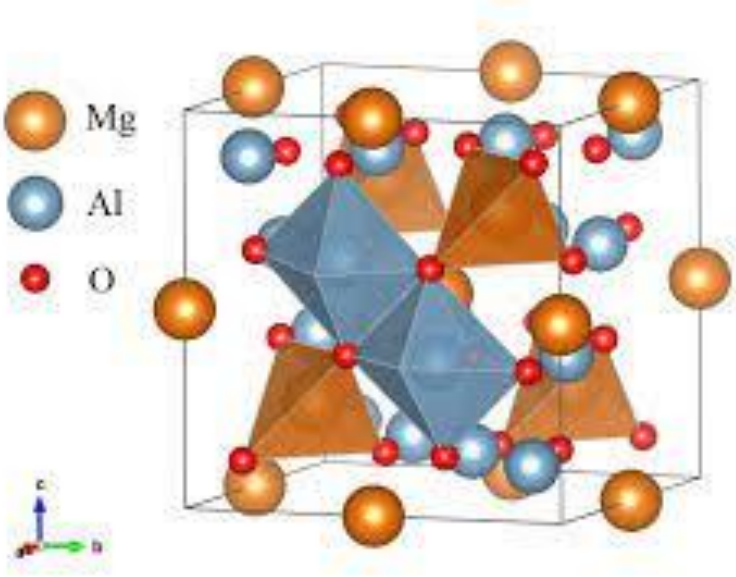

Figure (2-1) Normal Spinel's (AB_2O_4) [36].

2.3.2 Inverse spinel ($B(AB)O_4$) The A^{II} ions occupy the octahedral voids, whereas half of BIII ions occupy the tetrahedral voids. It can be represented as: $(B^{III})^{tet}(A^{II}B^{III})^{oct}O_4$. For examples are $CoFe_2O_4$, $NiFe_2O_4$ etc. [37]. The above inverse spinels can also be written as:

$$Fe_3O_4 = Fe^{III}(Fe^{II}Fe^{III})O_4,\ CoFe_2O_4 = Fe^{III}(Co^{II}Fe^{III})O_4$$

$$NiFe_2O_4 = Fe^{III}(Ni^{II}Fe^{III})O_4$$

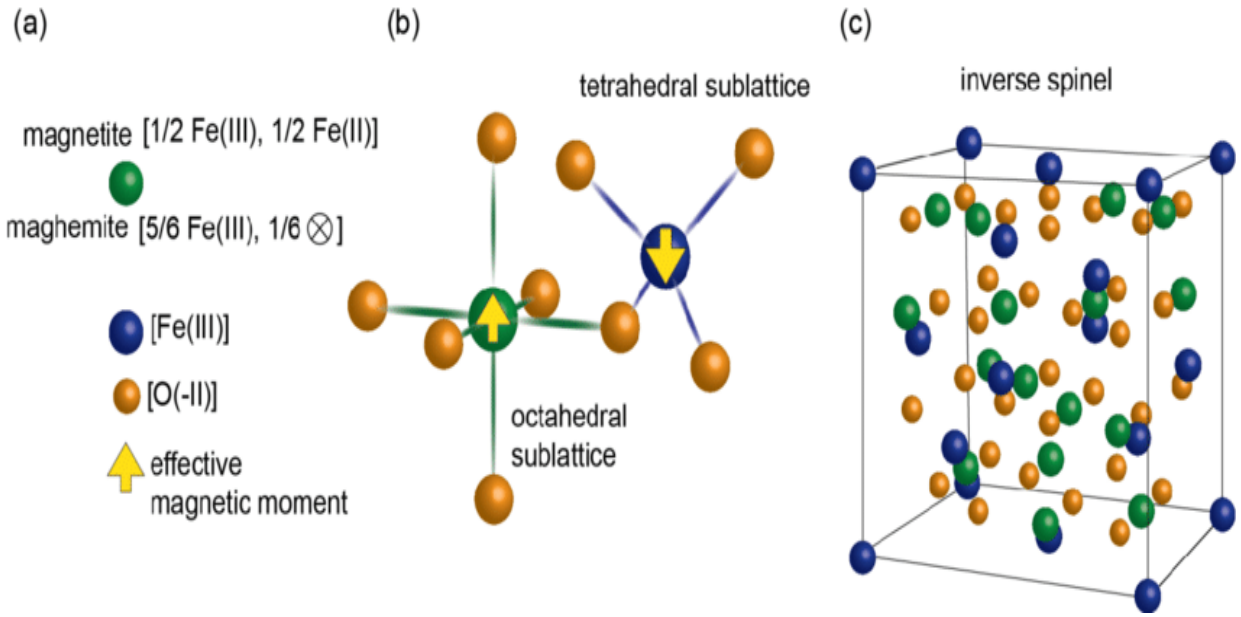

Figure (2-2) Invers Spinel's[38].

2.3.3 Random Spinel: The number of octahedral sites occupied may be ordered or random. The random occupation leads to defected spinels. has a cation distribution that is intermediate, with cations scattered at both the octahedral and tetrahedral locations. For examples are $NiAl_2O_4$ for which the formula can be written as $(Al_{0.75}Ni_{0.25})^{tet}\ [Ni_{0.75}Al_{1.25}]^{octa}O_4$. Another defected spinel is γ-Al_2O_3. A reversal parameter "i" may be used to measure the cation distribution, which equals the part (A) of the sites of octahedral [39].

$$Normal \quad (A^{II})^{tet}(B^{III})^{oct}O_4 \quad i = 0$$

$$Inverse \quad (B^{III})^{tet}(A^{II}B^{III})^{oct}O_4 \quad i = 1$$

$$Random \quad (Al_{0.75}Ni_{0.25})^{tet}\ [Ni_{0.75}Al_{1.25}]^{octa}O_4 \quad i = 0.67$$

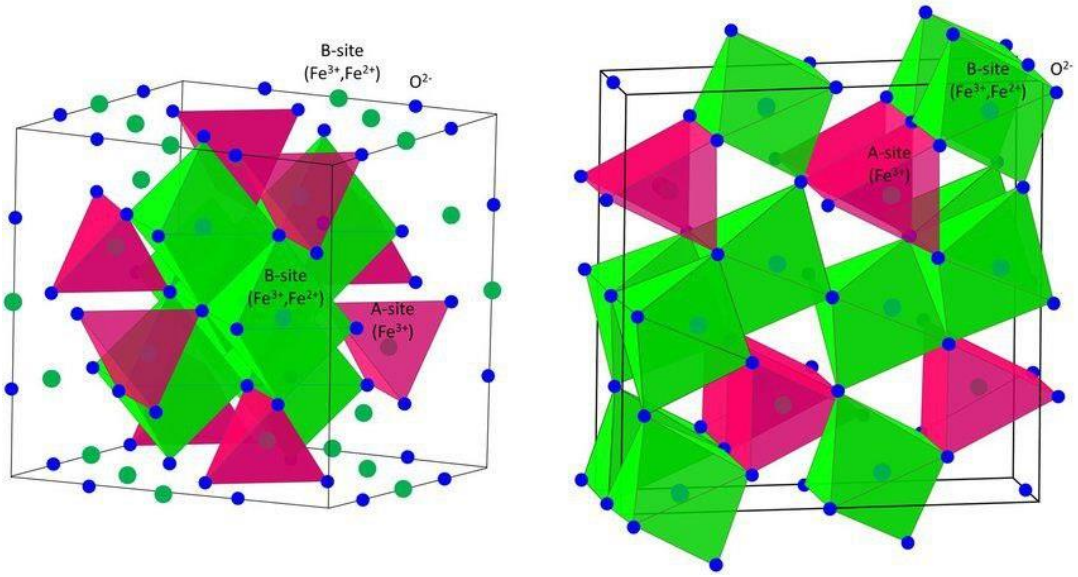

Figure (2-3) Random Spinel [40].

2.4 Magnesium aluminate

2.4.1 Structure of Spinel $MgAl_2O_4$:

The crystal structure of the Magnesium Aluminate is of the spinel type and has a lattic parameter of 8.08 Å and cell volume 528 $Å^3$ and shows the similarities and differences between both MgO and Al_2O_3; in contrast with Al_2O_3, both the MgO and the spinel show a cubic closest packed sample of oxide ions, and the Al^{+3}ions occupy the octahedral sites of both Al2O3 and spinel, whereas the Mg^{+2} ions are octahedral in MgO but tetrahedral in $MgAl_2O_4$. Gorter was the first to publish a study of the cation array in spinels (1954). Each cubic unit cell contains eight $MgAl_2O_4$, resulting in $32O^{-2}$ [41].

This close packing contains 64 tetrahedral sites $(8a, 8b\ and\ 48f)$ and 32 octahedral sites $(16c\ and\ 16d\ sites)$, 1/8 of the tetrahedral sites are occupied by the Mg^{+2} ion surrounded by $4O^{-2}$; MgO4, and half of the octahedral sites are occupied by Al^{+3} ion surrounded by $6O^{-2}$-; AlO_6. The Mg^{+2} ion in the tetrahedral

site, $8a$ $(A-site\ tetrahedra)$ in $MgAl_2O_4$ spinel are isolated from each other and share corners with the neighboring Al^{+3} ions in octahedral site, $16c$ $(B-site\ octahedra)$ $(Fig.\ 2.4)$. [42].

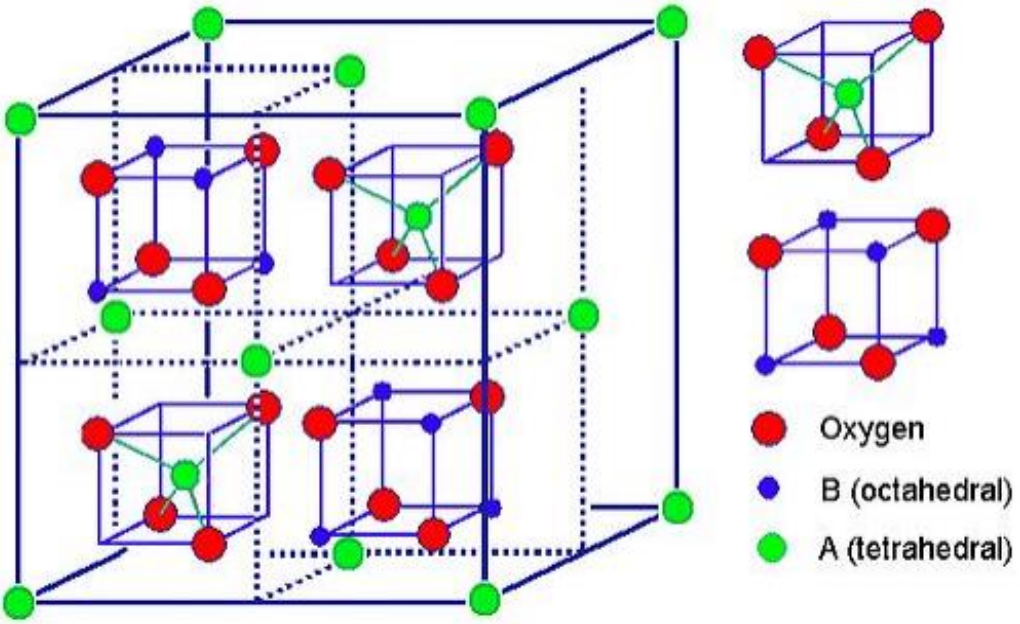

Figure 2.4: The arrangement of ions in the spinel [43]

$No\ edge\ sharing\ occurs$ between A-site tetrahedra and the other A- or B-site polyhedral and B-site octahedral. The Al^{+3}ions in the octahedral site share six out of twelve $O-O$ edges with the nearest–neighbor B-site octahedral. The other six edges are shared with the octahedral that surround 16c vacant sites. The $O-O$ edges that are shared by the Al^{+3}ions form chains in the lattice along the (110) directions (Fig. 2.5). The $B-B$ distance in $MgAl_2O_4$ is 2.86 Å [44, 45].

A polyhedral view of a spinel unit cell is shown in $Fig.\ 2.5$. The two different equipoints with point symmetries $43m\ and\ 3m$ are possible choices for the unit-cell origin. Moreover, the origin can be assigned to either a vacant site or an occupied lattice site. The coordinates of the anions at equipoint 32e are not special: they vary according to a single parameter, u, for a perfect ccp anion arrangement, u^{43m} ideal = 3⁄8 (0.375) and u^{3m} ideal =1⁄4 (0.250), for origins at $43m\ and\ 3m$, respectively [46].

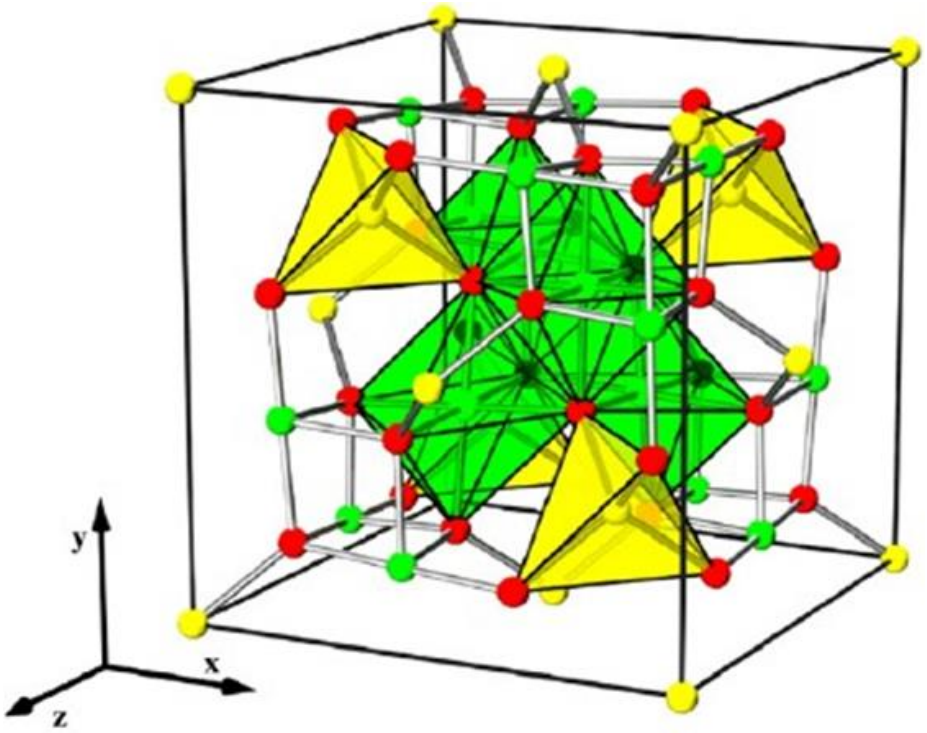

Figure 2.5: The spinel structure with the tetrahedrally coordinated Mg^{+2} ions (yellow) and octahedrally coordinated Al^{+3} ions (green) while O2- ions are represented in red [47]

Because of the high electro negativity of oxygen, ionic type bonds exist in spinel, resulting in high electrical resistivity, and these compounds are categorised as insulators, although the term low-mobility semiconductors is sometimes used. This is not the case for the other bivalent anions (S, Se, Te), which have far smaller electro negativities [48].

The presence of cationic disorder, or the dispersion of Mg^{+2} and Al^{+3} cations between the tetrahedral and octahedral positions, is a structural feature of $MgAl_2O_4$ crystals. As a result of the inversion, charged defects $(Mg^{+2}\ oct)^{-}$ and $(Al^{+3}tet)^{+}$are formed, which are known as anti-site defects and may play an essential role in ion-surface interaction processes. The binding energy of surface ions, in particularly, will change when the cation distribution amongst polyhedra

changes, and bulk-surface diffusion during sputtering will be affected by the concentration of charged anti-site defects [49].

The spinel structure of organically formed $MgAl_2O_4$ spinel is similar to that of regular spinel. It means that the smaller Al^{+3} cation prefers the octahedral positions thermodynamically. However, computations of the point–defect formation energies show that the energy consumed in the cation antisite reaction (i. e. , $Mg_A + Al_B \rightarrow Al^{\cdot}{}_A + Mg'_B$) is less than that for any other point–defect formation energy [50], implying that these defects develop rapidly. As a result, the synthesized $MgAl_2O_4$ spinel is invariably partly inverse, with inversion values ranging from 0.1 to 0.6. [51]

The tetrahedral and octahedral sites are always the same and are unaffected by the type of the component cations. The overall location of anions, however, is determined by the relative size of A and B cations [52]. For example, in natural spinel $MgAl_2O_4$, $a = 0.80898\, nm$. Anions in spinel are often dilated away from their optimal ccp locations, and this dilation has numerous key crystallographic repercussions, including changes in bond lengths, bond angles, interstices volumes, and coordination polyhedron symmetries. [53]

2.4.2 Properties of Spinel $MgAl_2O_4$:

Magnesium aluminate has a high melting point (2135 ℃), low-density ($3.58\ g/Cm^3$), excellent strength at extremely high temperatures (flexural strength of 140 MPa , Knoop hardness of 1150 $kg/mm^2$and Young' modulus of 190 GPa) and good resistance against chemical attacks. It has $(80-87\%)$ optical transmittance in the region between $(0.3-5\ \mu m)$, low thermal conductivity $(15\ W/mK)$, high electrical resistivity $(105\ \Omega\ cm)$, low dielectric constant (8.2) and low dielectric losses (0.01) [54-55].

Such properties are used in a variety of applications, including catalysts or catalyst support materials, refractories, humidity sensors, dielectric capacitors in electronic devices, insulators and radiation resistant materials, electromagnetic radiation absorbers and transparent armour materials. [56].

Spinel $MgAl_2O_4$ pure and doping is a very revealing crystal organization for sympathetic and designing the magnetic properties of nanomaterials through chemical manipulations. The interest in nanoscale materials stems from the new properties acquired at this length scale and, also the properties change with their size or shape. Oxide spinels can show unique chemical properties, due to their limited size and a high density of corner or edge surface sites. [57].

Properties of $MgAl_2O_4$ depend upon several factors such as composition, a method of preparation, substitution and doping of different cations, sintering temperature and time, sintered density, grain size and their distribution [58].

2.4.3 Application of Spinel $MgAl_2O_4$:

$MgAl_2O_4$ Plays a significant role in geophysics [59] as one of the early-condensed minerals and a common constituent of the shallow upper mantle. The elastic behavior of its polymorphs can be used to predict seismic velocities, and some of its high-pressure forms have been proposed as a constituent of shock-metamorphosed meteorites [60]. Refractories are the materials which have high melting points and hence with strong interatomic bonds. These characteristics make it an excellent component in refractory materials and used in steel ladles, cement rotary kilns, vacuum induction furnaces, continuous casting tundishes and glass industries, transition and burning zones of cement rotary kilns, side walls and bottom of steel teeming ladles and checker work of glass tank of furnace regenerators etc. [61]. Table 2.1 shows properties applications of $MgAl_2O_4$ [62].

Magnesium aluminate spinel has demonstrated a strong resistance, under irradiation, to the formation of large defect aggregates such as dislocation loops and voids [63]. Consequently, it has the ability to withstand neutron irradiation over wide range without degradation of its mechanical properties. This ability is thought to be the result of two factors. (i) high intrestial-vacancy recombination rate. (ii) the ability of the lattice to tolerate significant intrinsic antisite disorder on the cation sub-lattice. Spinel ($MgAl_2O_4$) is therefore being considered for application as an insulating and structural material in fusion reactors [64] and as an inert matrix target material in the nuclear transmutation of radioactive actinides [65].

Table 2.1 shows properties applications of magnesium aluminate spinel [62].

Fields of interest	Respective properties	Applications
Nuclear	radiation resistance, strength at high temperatures, refractoriness	nuclear fuel, nuclear fuel cladding, control materials, moderating materials
Optical	optical condensing, fluorescence, translucence, optical conductivity	laser diode, light emitting diode, communication cable, heat resistant translucent porcelain
Electrical and magnetic	electrical insulation, electrical conductivity,semi-conductivity, dielectric, piezoelectric	integrated circuits substrates, varistor sensors, resistance heating elements, piezoelectric filters
Mechanical	High strength, wear resistance, low thermal expansion, lubrication	tools & jigs, abrasion, turbine blades, solid lubricants
Chemical	catalysis, adsorption, corrosion resistance	artificial bone & teeth, catalyst carrier, heat exchanger, chemical equipment
Thermal	insulation, refractoriness, heat collection, thermal conductivity	high temperature industrial furnace lining, electrode material, heat sinks for electronic parts

2.5 Effect of transitions ions of magnetic properties:

The design and synthesis of transition metal oxide materials provide a variety of applications of electronic [66] and magnetic devices [67], heterogeneous catalysis [68] and a number of other applications. Although design and synthesis of materials is one of the challenges in materials chemistry, it is far from achieving this goal universally. Synthesis of materials can be achieved but the success has been limited. To accomplish the target properties, the right structure and composition have to be achieved. [69].

Transition metal oxides play a vital role in several areas of chemistry, physics, materials science etc. The unusual properties of transition metal oxides are clearly due to the unique nature of the valence d-electrons. The affluent diversity of compositions, structure-properties relations of metal oxides has led to extensive applications in electronics, engineering, and catalysis. By using a variety of synthetic techniques [70], one can justifiably induce a large diversity of properties in the oxide materials. The desire for novel functions or properties generate a vast demand for new materials, which has to be fabricated with well defined, controllable properties and structures on the nanometer scale afforded by new nanocomposite oxide materials. This has generated mostly the special interest in oxide materials in tailoring the properties on the molecular and nanoscale level, generating novel materials that either shows characteristics in between the original phases or even new properties. Tailoring specific properties of solids such as magnetic, optical, electronic etc. is important to utilize the solid as a material. However, it is necessary to ensure if the material is monophasic and to what extent for such applications [71]. The phenomenal range of electronic and magnetic properties exhibited by transition metal oxides is also noteworthy [72].

Rare earth - transition metal composite oxide materials Apart from the oxide materials containing only the transition metals as mentioned above, currently the increasing interest in designing and preparing rare earth - transition metal composite oxides have also received extensive attention due to their unique 3d-4f orbital interactions. This 3d-4f orbital interactions results in fascinating chemical and physical properties such as electronic energy band structures and magnetic ordering that results from two different types of orbitals with distinct energy levels (3d of transition metal and 4f of rare-earth ions). In these materials, the 4f electrons of the rare earth ions polarize their 5d bands, which give the 5d-3d short range interaction with the transition metal. The 5d band polarizations are oriented parallel to 4f moments because the local 4f-5d exchange interactions are positive [73].

It is known that in ferromagnetic materials the magnitude of the magnetic moments oriented in either way differ, so that there always exists sultanate compensated magnetic moment. The various factors that determine the magnetic properties of this spinel are the nature of cations, heat treatment, preparative methods, site preference energy of cations and the Madelung energy. According to Neel, spinel exhibit a magnetic structure distinctly different from any previously recognized structure. Neel explained the spontaneous magnetization of these spinel based on Heisenberg's exchange forces [74].

One of the reasons of being $MgAl_2O_4$ are interesting is their high resistivity. The resistivity of spinel varies from $10^2$to 10^{10} ohm-cm which is about 15 orders of magnitude higher than that of iron. This outstanding property of spinel makes them highly demandable for high frequency applications. Other reasons, which make Magnesium aluminate to be the most important, are their applicability at a higher frequency, lower price, greater heat resistance and higher corrosion resistance [75].

2.6 Magnetic Materials:

Materials are classified by their response to an externally applied magnetic field. Descriptions of orientations of the magnetic moments in a material help to identify different forms of magnetism observed in nature as shown in table (2.2).

Five basic types of magnetism can be described: diamagnetism, paramagnetism, ferromagnetism, antiferromagnetism and ferrimagnetism. In the presence of an externally applied magnetic field, the atomic current loops created by the orbital motion of electrons respond to oppose the applied field. All materials display this type of weak repulsion to a magnetic field known as diamagnetism. However, diamagnetism is very weak and therefore any other form of magnetic behavior that a material may possess usually overpowers the effects of the current loops. In terms of electronic configuration of materials, diamagnetism is observed in materials with filled electronic subshells where the magnetic moments are paired and overall cancel each other. Diamagnetic materials have a negative susceptibility ($\chi < 0$) and weakly repel an applied magnetic field (e.g., quartz SiO_2 and calcite $CaCO_3$).

All other types of magnetic behavior observed in materials are at least partially attributed to unpaired electrons in atomic shells, often in the 3d or 4f shells of each atom. Material atomic magnetic moments are uncoupled display paramagnetism. Thus, paramagnetic materials moments have small positive magnetic susceptibility ($\chi \approx 0$); e.g., montmorillonite and pyrite [76].

Table 2.2 A summary of the different types of magnetic behavior [77].

Type	Example	Atomic / Magnetic behavior		
Diamagnetism	Inert gases; many metals Au, Cu, Hg; non-metalic elements B, Si, P, S; ions Na^+, Cl^-; molecules H2, N2; H2O	Atoms have no magnetic moment. Susceptibility is small and negative, -10^{-6} to -10^{-5}	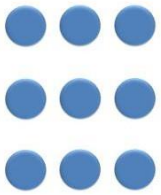	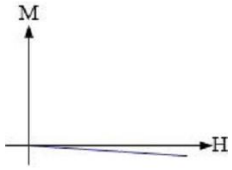
Paramagnetism	Some metals Al, some diatomic gases O2, NO; ions of transition metals and rare earth metals; rare earth oxides	Atoms have randomly oriented magnetic moments. Susceptibility is small and positive, 10^{-5} to 10^{-3}	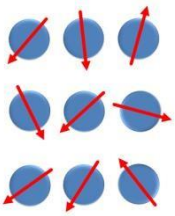	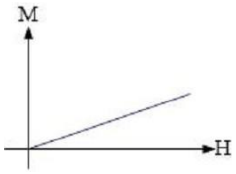
Ferromagnetism	Transitions metals Fe, H, Co, Ni, alloys of ferromagnetic elements; some alloys of Mn, MnBi, Cu2MnAl	Atoms have parallel aligned magnetic moments. Susceptibility is large (below T_C)	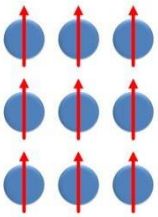	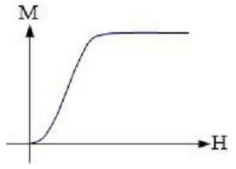
Anti-ferromagnetism	Transition metals Mn, Cr and many of their compounds, MnO, CoO, NiO, Cr2O3, MnS, MnSe	Atoms have antiparallel aligned magnetic moments. Susceptibility is small and positive 10^{-5} to 10^{-3}	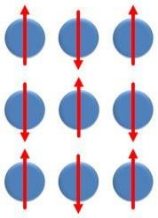	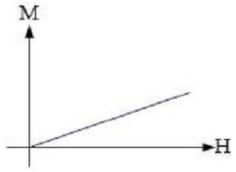
Ferrimagnetism	Fe_3O_4 (magnetite); mixed oxides of iron and other elements such as Sr ferrite	Atoms have mixed parallel and antiparallel aligned magnetic moments. Susceptibility is large (below T_C)	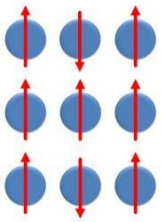	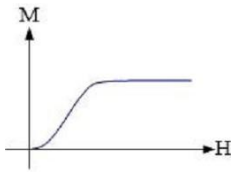

Ferromagnetism in materials are shown equal magnitude of aligned atomic magnetic moments and their crystalline structure allows for direct coupling interactions between the moments, which may strongly enhance the flux density (e.g., Fe, Ni and Co). Furthermore, the aligned moments in ferromagnetic materials can confer a spontaneous magnetization in the absence of an applied magnetic field. Materials having atomic magnetic moments of equal magnitude that arranged in an antiparallel fashion display antiferromagnetism (e.g., troilite FeS and ilmenite $FeTiO_2$). The exchange interaction couples the moments such that they are antiparallel therefore leaving a zero net magnetization [78]. Above the Neel temperature(T_N), (or magnetic ordering temperature is the temperature above which an antiferromagnetic material becomes paramagnetic that is, the thermal energy becomes large enough to destroy the macroscopic magnetic ordering within the material),thermal energy is sufficient to cause the equal and oppositely aligned atomic moments randomly fluctuate leading to a disappearance of their long-range order. In this state, the material exhibits paramagnetic behavior. Ferrimagnetism is a property exhibited by materials whose atoms or ions tend to assume an ordered but non-parallel arrangement in zero applied field below a Neel temperature (e.g., Fe_3O_4 and Fe_3S_4). In the usual case, within a magnetic domain, a substantial net magnetization results from the antiparallel alignment of neighboring non-equivalent sublattices [79].

2.7 Hysteresis loop:

The most commonly measured magnetic parameters are schematically illustrated in figure (2.6) shown as a hysteresis loop (magnetization versus field). The application of a sufficiently large magnetic field causes the spins within a material to align with the field. The maximum value of the magnetization achieved in this state is called the saturation magnetization, Ms. As the magnitude of the magnetic

field decreases, spins cease to be aligned with the field and the total magnetization decreases. In ferromagnets, a residual magnetic moment remains at zero field. The value of the magnetization at zero field is called the remanent magnetization, Mr. The ratio of remanent magnetization to the saturation magnetization, Mr/Ms, is called the remanence ratio and varies from (0 to 1). [80].

The coercive field Hc is the magnitude of the field that must be applied in the negative direction to bring the magnetization of the sample back to zero. The shape of the hysteresis loop is especially of interest for magnetic recording applications [81].

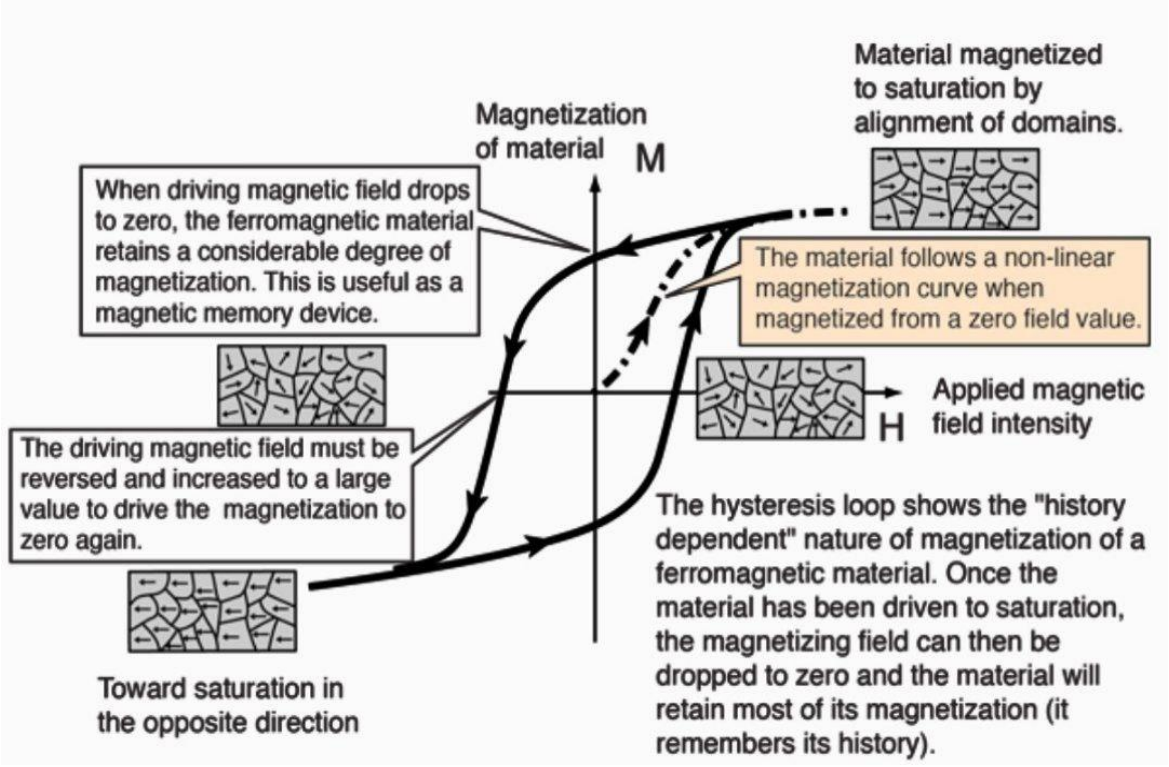

Figure (2.6) Hysteresis Loop [82].

2.8 Chemical techniques:

The syntheses of nanoscale materials are generally grouped into two broad categories: “bottom-up” and “top-down.” Those preparations based on building up from atomic or molecular precursors, which come together to form clusters, and subsequently nanoparticles are referred to as “bottom up.” Conversely, when the nanoscale is reached by physically tearing down larger building blocks, the process is referred to as “top-down.” The “bottom-up” route is particularly interesting because of the possibilities to manipulate the properties (such as size, shape, stoichiometry, surface area, pore size, and surface decoration) of the product [83].

Various methods which were used so far for the synthesis of ($MgAl_2O_4$) spinel are flame fusion growth, solid state method, co-precipitation, thermal decomposition, spray pyrolysis technique, sol-gel method, aerosol method, freeze drying method, mechanical activation, combined gelation-precipitation, chemical vapor deposition, micro emulsion, oxide one pot synthesis (OOPS), etc.,[84]. Based on the physical condition of the starting material, all of the procedures employed to date for the synthesis of magnesium aluminate spinels may be classified into the following kinds. There are four types of methods: (i) gaseous phase, (ii) liquid phase, (iii) solid phase, and (iv) mixed phase. Chemical vapour deposition (gaseous phase), co-precipitation, and the sol-gel techniques (liquid phase), solid state method (solid phase), and microwave combustion are some of the most prevalent processes (liquid-solid phase). [85].

The sol-gel process has been used to produce porous nanomaterials with well-defined structures and complicated forms. It is well known that the sol-gel technique is reasonably simple and provides for control of the distribution of the components in molecules via network pre-orientation. As a result, the prospective uses of

materials synthesised using this process can be competitive (also in terms of production costs) [85]. are briefly discussed below.

2.8.1 Sol-gel method:

In the sol-gel process, the starting material normally inorganic salts or a solution of metal alkoxides, M(OR)x, or a suspension of very fine particles in an appropriate alcohol (the sol), is converted by a poly condensation reaction into a semi rigid mass (the gel). The polymerization of the species formed by the hydrolysis and condensation reactions together with interlinking and cross-linking of the polymer chains eventually leads to a marked increase in the viscosity of the reaction mixture forming either aerogel or xerogel. Aging and the drying of the gel result in the removal of water and volatile components from the gel ensuing in the contraction of the gel. Aging before drying helps to strengthen the gel network and thereby reduce the risk of fracture. The sintering of a gel at a particular temperature results in the breakdown of pore structure and the formation of the product occurs[86].

The chemical and physical properties of the final product are primarily determined by the hydrolysis and drying steps. Slower and more controlled hydrolysis typically leads to smaller particle sizes and more unique properties. Hydrolysis and condensation rates depend on the electro negativity of the metal atom, the alkoxy group, solvent system, and the molecular structure of the metal alkoxide. Those metals with higher electronegativities undergo hydrolysis more slowly than those with lower electronegativities. For alkoxides that have low rates of hydrolysis, acid or base catalysts can be used to enhance the process. The relatively negative alkoxides are protonated by acids creating a better leaving group and eliminating the need for proton transfer in the transition state. Alternatively, bases provide better nucleophiles (OH^-) for hydrolysis, however; deprotonation of metal hydroxide groups enhances their condensation rates. [86].

Ingredients of high purity may be created because to the ease with which liquids (as the starting materials for the process) can be purified. Because the ingredients are mixed at the molecular level, materials with extraordinary chemical homogeneity may be created, and the lower densification temperature further promotes modified sol-gel method. However, the starting materials (e.g., the metal alkoxides) can be fairly expensive. Due to the difficulties of conventional drying, cracking, warping, and considerable shrinkage also occur [87].

The significant advantage of sol-gel processing of ceramic powders is that homogeneous compositions can be prepared at temperatures lower than required for conventional powder processes. Furthermore, the reactants used in sol-gel processing are available in very high purities, which allow the formation of high-purity powders [88].

Sol-gel processing is versatile because it can be used to produce ceramics in a number of different forms:

1. Powders—because we can make very small particles and control the composition, example application: bioactive glass powders, with a composition of SiO2–CaO–P2O5
2. Coatings—because the sol is a viscous liquid and can be applied to a substrate by spinning, example application: TiO2-based antiglare coatings on Glass.
3. Fibers—because we can pull a thread out that is liquid and dry it, example application: SiO2 fibers used for space shuttle tiles [88].

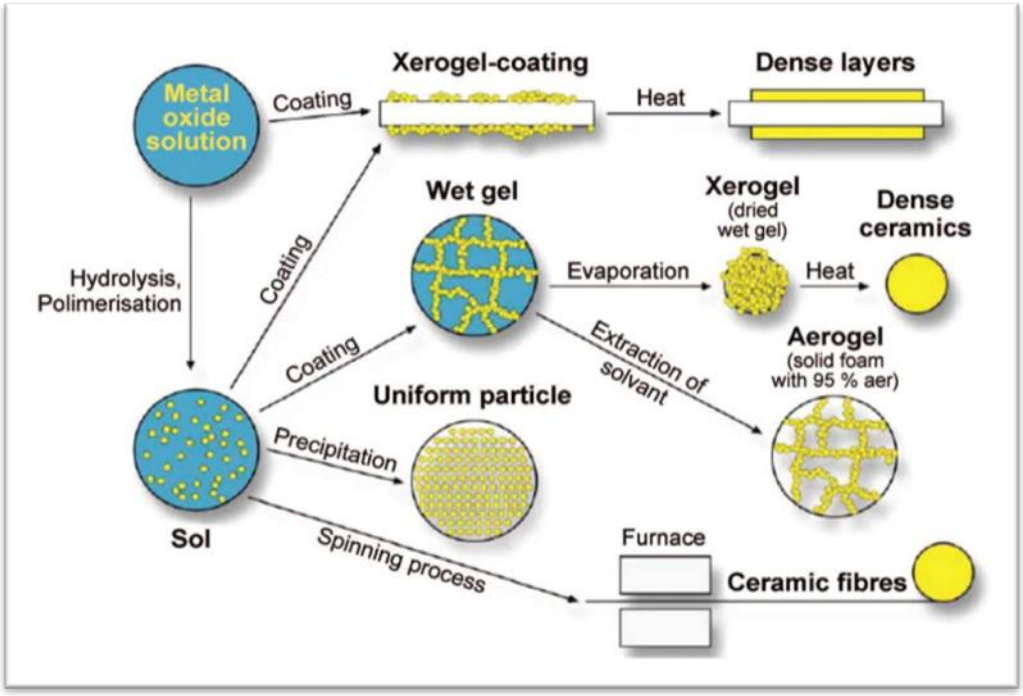

Figure (2.7) the Routes that Could be Followed in modified Sol–Gel method [89]

2.9 Synthesis and characterization of magnesium aluminate: Literature Survey

The history of the spinel dates back to 1887 when the spinel crystals were prepared artificially by heating a mixture of magnesia, aluminum chloride, cryolite, alumina and traces of potassium bichromate in graphite crucibles for five to six hours. In 1930, artificially synthesized $MgAl_2O_4$ crystals were developed for use as a diamond replacement. Its application as a refractory material was investigated in 1955. When Yoneda researched the catalytic exchange process between H2 and D2, employing magnesium aluminate spinel as a catalyst, in 1959, the catalytic characteristics of spinel were investigated. The following is a review of the literature over the previous ten years, with a brief explanation of research activity on magnesium aluminate spinel.

Chandradass et al. (2010) [90] reported the synthesis of magnesium aluminate spinel nanoparticles using micro-reactors made of poly(oxyethylene) nonylphenyl ether/water/cyclohexane microemulsions. The influence of water to surfactant ratio on the resulting particle size of $MgAl_2O_4$ was investigated. The average particle size was found to increase with the increase in water to surfactant molar ratio and the average particle size increased from 13 to 17 nm on increasing the molar ratio from 2 to 8. Water to surfactant ratio is a major factor in controlling the final particle size of $MgAl_2O_4$ powder.

Wiglusz et al. (2010) [91]. Nanoplates of the $MgAl_2O_4$ spinel doped with Eu^{+3} ions were prepared by a microwave assisted hydrothermal method, Structural properties of the precursor calcined at 700 and 1000 ℃. The results show XRD patterns the formation of single-phase spinels after calcinations was confirmed. The average spinel particles was determined to be 11 nm after the calcinations at 700 ℃ and it increased up to 14 nm after calcinations at 1000 ℃. The photoluminescent properties of prepared powders with different Eu^{+3} ion concentrations (0-5 % mol) were investigated using excitation and emission spectroscopy at room and low temperatures (77K).

Torkian et al.(2010) [92] synthesized nanocrystalline $MgAl_2O_4$ single-phase powders by two different chemical routes, the co-precipitation and the combustion methods. In the first procedure, a combination of precipitation and gelation process was used to prepare the spinel from aluminum and magnesium sulfates. The other involved a rapid evaporation of polyvinyl alcohol (PVA) that was added to a mixed metal nitrate solution, followed by pyrolysis of the dried mass. Data indicated that the average size of nanoparticles is around 30 nm. The BET surface areas of the prepared powders were measured to be 8.1 and 28.2 m2/g for the material synthesized by coprecipitation and the PVA combustion routes, respectively.

Ianos et al.(2011) [93] prepared $Mg_{1-x}NixAl_2O_4$ (x = 0, 0.25, 0.5, 0.75 and 1) solid solutions were prepared by combustion synthesis. After annealing the combustion-synthesized powders at 1273 K for 3 h, single-phase $Mg_{1-x}NixAl_2O_4$ was obtained over the entire range of compositions. The lattice parameter of $Mg_{1-x}NixAl_2O_4$ gradually increased from 8.049 Å ($NiAl_2O_4$) to 8.085 Å ($MgAl_2O_4$), which certified the formation of the spinel solid solutions. All samples prepared by combustion synthesis had blue color shades, denoting the inclusion of Ni^{+2} in the spinel structure in octahedral and tetrahedral configuration.

Jian & Da (2012) [94] Preparation of nanocrystalline $MgAl_2O_4$ powders using polymer gel reaction is technically simpler, more cost effective, and more time and energy efficient than other technology. Synthesis of powders by calcining at 900°C formed single phase spinel. Calcining at different firing temperatures up to 900°C led to progressive crystallization of the amorphous materials to form nanocrystalline spinel with a maximum crystallite size of about 20nm.

Nassar et al. (2014) [95] have prepared Pure phase of $MgAl_2O_4$ nanoparticles by a facile sol-gel auto combustion method using different organic fuels urea, oxalic and citric acid at 250 °C then the burnt product was calcined at 350 °C, separately, for 3h.The Effect of fuels on the crystallite size of $MgAl_2O_4$ products was studied. The pure spin*el* $MgAl_2O_4$ with average crystallite size 27.7, 14.6 and 15.65 nm was obtain at 800 °C .

Sanjabi, S., & Obeydavi, A. (2015). [96] Nanocrystallines of magnesium aluminate spinel ($MgAl_2O_4$) were synthesis by modified sol–gel method using aluminum nitrate, magnesium nitrate, citric acid and diethylene glycol monoethyl ether were used as precursor materials with a molar ratio Al/Mg = 2. After obtained a dry powder, the precursor was heat-treated in air at desired temperatures (700–900 °C) for 2 h. According to obtained XRD patterns the formation of single phase $MgAl_2O_4$

completed up 700 °C. The average crystallite's sizes spinel and specific surface area at 800 °C were estimated about 11.07 nm and 154 $m^2 g^{-1}$, respectively. The results of FESEM analysis show that the nanoparticles shape are as spherical shape, uniform and a little agglomerated. The dimension of nanoparticles used by HRTEM was measured to be about 12 nm by averaging 20 particles at 800 °C.

Mahmood et al. (2016) [97] Magnesium aluminate ($MgAl_2O_4$) nanoparticles doped with different concentrations of Na have been synthesized by solution combustion method. The XRD data showed that the samples have nanocrystalline single phase spinel and the average grain size of the undoped and 6% Na doped samples were about 21.84 nm and 16.58 nm. The SEM image shows several pores in the particles due to escaping gases during combustion reaction. FTIR studies confirmed the presence of AlO_6 group which indicate the formation of $MgAl_2O_4$. It has low calcination temperature which was detected by TGA.The optical properties including absorbance, transmittance, and band gap have optimum value for optimum amount of 6% Na doped samples.

Habibi, N. et al. (2017). [98] A simple, template-free and scalable modified sol-gel route was developed for the synthesis of mesoporous flake-like magnesium aluminate spinel ($MgAl_2O_4$) at low temperature (700 °C). The result materials reveal that the textural properties of the $MgAl_2O_4$ product are strongly associated with the nature and amount of addictive solvent and calcination temperatures.

Ahmad et al.(2018) [99] have been investigated the dielectric response of Potassium (K)-doped magnesium aluminates nanoparticles ($Mg_{1-x}KxAl_2O_4$, x = 0:0, 0.25, 0.5, 0.75, 1.0) as a function of frequency (20 Hz to 2 MHz) at room-temperature. Interestingly, the behavior of dielectric constant indicated the ionic or space charge polarization in the low-frequency range and it remains almost constant at high frequency. However, the value of conductivity increases at higher frequencies which is consistent with the previously reported results for the parent compound $MgAl_2O_4$.

Motloung, S.V., et al. (2019).[100] A series of nanocrystalline ($0 \leq x \leq 1.25\%$) x% In^{3+}:$MgAl_2O_4$ (IMAO) phosphor powders have been successfully prepared via citrate sol-gel technique. The x-ray diffraction (XRD) results indicated that the IMAO consists of the cubic phase and average crystallite sizes was found to be 9 nm. Scanning electron microscopy (SEM) revealed that the In^{3+} concentration influences the phosphor morphology. Ultraviolet-visible (UV–vis) results showed that the reflectance and absorption of the IMAO depends on the In^{3+} concentration. The prepared samples exhibited the emission at 395 nm, which is attributed to the defects within the host material. The optimum emission intensity was observed at x = 0.3% In^{3+}. The critical distance (R_c) calculation suggested that the concentration quenching occurs due to the multipole-multipole interaction.

Table 2.3 The summaries of ccurrent studies in doping and undoping $MgAl_2O_4$.

study	authors	year
Effect of water to surfactant ratio (R) on the particle size of $MgAl_2O_4$ nanoparticle prepared via reverse micelle process.	Chandradass, J., Balasubramanian, M., Bae, D.S., Kim, J., & Kim,K. H.	**2010**
Hydrothermal preparation and photoluminescent properties of $MgAl_2O_4$: Eu3+ spinel nanocrystals.	Wiglusz, R. J., Grzyb, T., Lis, S., & Strek, W.	**2010**
Synthesis and Characterization of a Nanorefractory Dimetaloxide Spinel.	Torkian, L., Amini, M. M., & Bahrami, Z.	**2010**
Synthesis of $Mg_{1-x}Co_xAl_2O_4$ blue pigments via combustion route.	Ianoş, R., Lazău, R., & Barvinschi, P.	**2011**
A novel way to synthesis magnesium aluminate spinel powders by polymer Gel reaction.	Tong, J. F., & Chen, D. M.	**2012**
A novel synthetic route for magnesium aluminate ($MgAl_2O_4$) nanoparticles using sol–gel auto combustion method and their photocatalytic properties.	Nassar, M. Y., Ahmed, I. S., & Samir, I.	**2014**
Synthesis and characterization of nanocrystalline MgAl2O4 spinel via modified sol–gel method.	Sanjabi, S., & Obeydavi, A.	**2015**
Synthesis and Characterization of Sodium (Na) Doped Magnesium Aluminate ($MgAl_2O_4$) Nanoparticle by Solution Combustion Method	Al Mahmood, A., Ali, M. M., Rahman, M., Islam, M. M., & Abdul, M.	**2016**
Low-temperature synthesis of mesoporous nanocrystalline magnesium aluminate ($MgAl_2O_4$) spinel with high surface area using a novel modified sol-gel method.	Habibi, N., Wang, Y., Arandiyan, H., & Rezaei, M.	**2017**
Infrared reflectance spectroscopy of $MgAl_2O_4$ nanoparticles substituted by K+ ions	Ahmad, J., Qadeer Awan, M., Yasmin, R., Sabir, M., Anwar, S., Ehsan Mazhar, M., & Hamad Bukhari, S.	**2018**
Effects of In3+ doping concentration on the structural, morphological and photoluminescence properties of x% In3+: $MgAl_2O_4$ nanophosphor prepared via citrate sol-gel method.	Motloung, S. V.	**2019**

Chapter 3

Experimental Part

3-1 Introduction:

In this chapter, deals with the procedures of synthesis undoped and doped spinel nanoparticle with general formula $MgAl_2O_4$. Moreover, it gives the details of the precursors and chemicals used, processing conditions, and techniques used in the present study for structural and magnetic characterizations of spinel $MgAl_2O_4$ will be briefly described.

This chapter was classified into three stages:

- Preparation of the powder specimens stage and
- Completion of the examination stage. Figure (3-1) shows the schematic diagram, which illustrates all experimental stages.

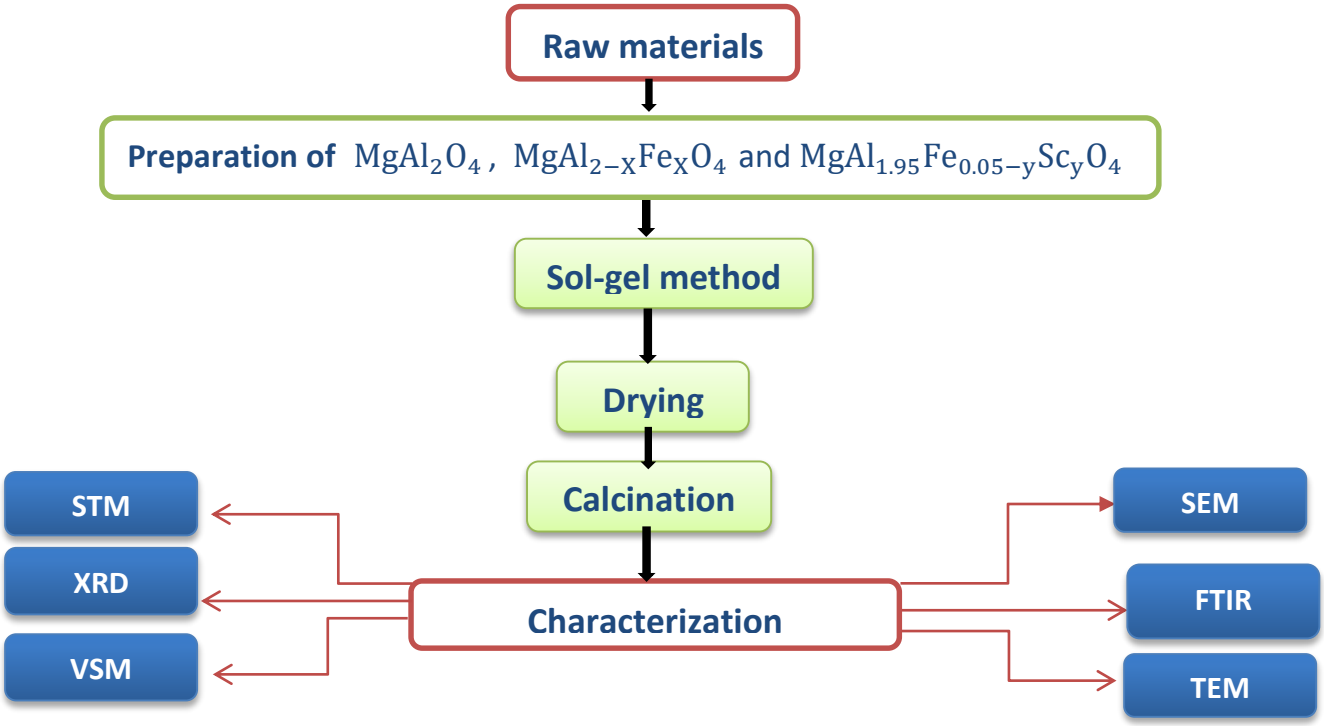

Figure (3-1) Diagram Shows the Preparation Steps.

3-2 Starting Materials for modified Sol-Gel Method:

In this method the Starting materials was chosen with very high purity, to avoid any influence on the compound properties. Table (3-1) shows the Starting materials that have been used in this work to prepare the sample using modified sol-gel method and its purity as shown in the labels of the cans of materials.

Table 3.1: The Starting materials in modified Sol-gel method.

Raw materials	Manufacturer	Country manufactured	The purity
$Mg(NO_3)_2.6H_2O$	THOMAS BAKER	Indian	98 %
$Al(NO_3)_3.9H_2O$	THOMAS BAKER	Indian	98 %
$Fe(NO_3)_3.9H_2O$	THOMAS BAKER	Indian	99 %
$Sc(NO_3)_3$	THOMAS BAKER	Indian	99 %
$C_6H_8O_7$	THOMAS BAKER	Indian	99 %
distilled water H_2O	-	-	99 %

The reaction's general chemical equation can be written as follows, with all undesirable by-products such as (CO_2, H_2O, NO_X), and so on written as " Z "

- Chemical equation for pure magnesium aluminate :

$$Mg(NO_3)_2.6H_2O + 2Al(NO_3)_3.9H_2O + 5C_6H_8O_7 \rightarrow MgAl_2O_4 + Z \quad \ldots (3\text{-}1)$$

- Chemical equation for iron (III) and -doped magnesium aluminate

$$Mg(NO_3)_2.6H_2O + (2-x)Al(NO_3)_3.9H_2O + (x)Fe(NO_3)_3.9H_2O + 5\ C_6H_8O_7$$

$$\rightarrow MgAl_{2-x}Fe_xO_4 + Z \quad \ldots\ldots (3\text{-}2)$$

- Chemical equation for Sc(III) and doped magnesium aluminate :

$$Mg(NO_3)_2.6H_2O + 1.95\ Al(NO_3)_3.9H_2O + (0.05\text{-}y)Fe(NO_3)_3.9H_2O + ySc(NO_3)_3 + 5C_6H_8O_7 \rightarrow MgAl_{1.95}Fe_{0.05-y}\ Sc_yO_4 + Z \quad \ldots(3\text{-}3)$$

3-2-1 Synthesis of magnesium aluminate spinel:

1. In the Preparation of spinel $MgAl_2O_4$, the modified sol-gel method was used.
2. Dissolve (1.80 g) $Mg(NO_3)_2.6H_2O$ in (30 ml) of distilled water and slowly dissolve (6.75 g) of anhydrous citric acid ($C_6H_8O_7$) add the solution.
3. Stirring the solution with a magnetic stirrer model (LMS-1003), heat it at 60℃ for one hour, until the solution is completely homogeneous.
4. After that, (5.27g) $Al(NO_3)_3.9H_2O$ dissolve in (45 ml) of distilled water and add to the solution, at this point the solution is heated to 80 ℃ for one hour.
5. The color of the solution after the addition of hydrated aluminum nitrate turns milky, with further heating of the solution to 140 ° C for one hour, the residue solvent evaporates.
6. The solution becomes viscous and finally turns into a xerogel.
7. To complete drying and removal the organic solvent is placed in a relatively dry xerogel in an oven at 150 °C for 1 hours. Using oven at the Department of Ceramics and Building Material of the College of Engineering Materials/ University of Babylon.
8. In this case, a dark yellow powder is obtained as the precursor.
9. Then calcinated to 800 ℃ in a furnace at 5 ℃/min. using furnace (JYMF-1800, High Temperature Muffle Furnace) at the Department of Ceramics

and Building Material of the College of Engineering Materials/ University of Babylon.

10. This step is called calcination of powder, which is a common heat treatment in the final preparation of nano crystalline powders.
11. The powder obtained from this step is white.
12. The steps in the preparation of magnesium aluminate ($MgAl_2O_4$) spinel nanoparticles are summarized in Figure (3.2).

3-2-2 Synthesis of Fe^{+3} and Sc^{+3} doped magnesium aluminate spinel:

In preparing the powder ($MgAl_{2-x}Fe_xO_4$) and ($MgAl_{1.95}Fe_{0.05-y}\,Sc_yO_4$) in addition to the consumables mentioned in the first stage. Water was used as a solvent for preparing sol. Multiple quantities of iron nitrate (III) and scandium, represented by the symbol "X", were added, where x= (0.01, 0.02, 0.03, 0.04, 0.05) to the solution and it is a solution of colored bricks. According to stoichiometric relationships the chemical formula in this case is $Mg(Al_{2-x}Fe_x)O_4$ and $MgAl_{1.95}(Fe_{0.05-y}\,Sc_y)O_4$. The gel was prepared and placed in a dryer at $150\ C^0$ using oven at the University of Babylon /college of Materials.to obtain a crude powder.

Finally, calcination process for the dried powder calcinate of 800 ° C at a rate of 5 °C / min. using furnace (JYMF-1800, High Temperature Muffle Furnace) at the Department of Ceramics and Building Material of the College of Engineering Materials/ University of Babylon.

The rest of the steps are the same as preparing the $MgAl_2O_4$ powder spinel, with the exception that the synthesized powder is not white. However, different colors appear according to the relative proportions. All the chemical were (THOMAS BAKER) type as shown in Table (3-1).

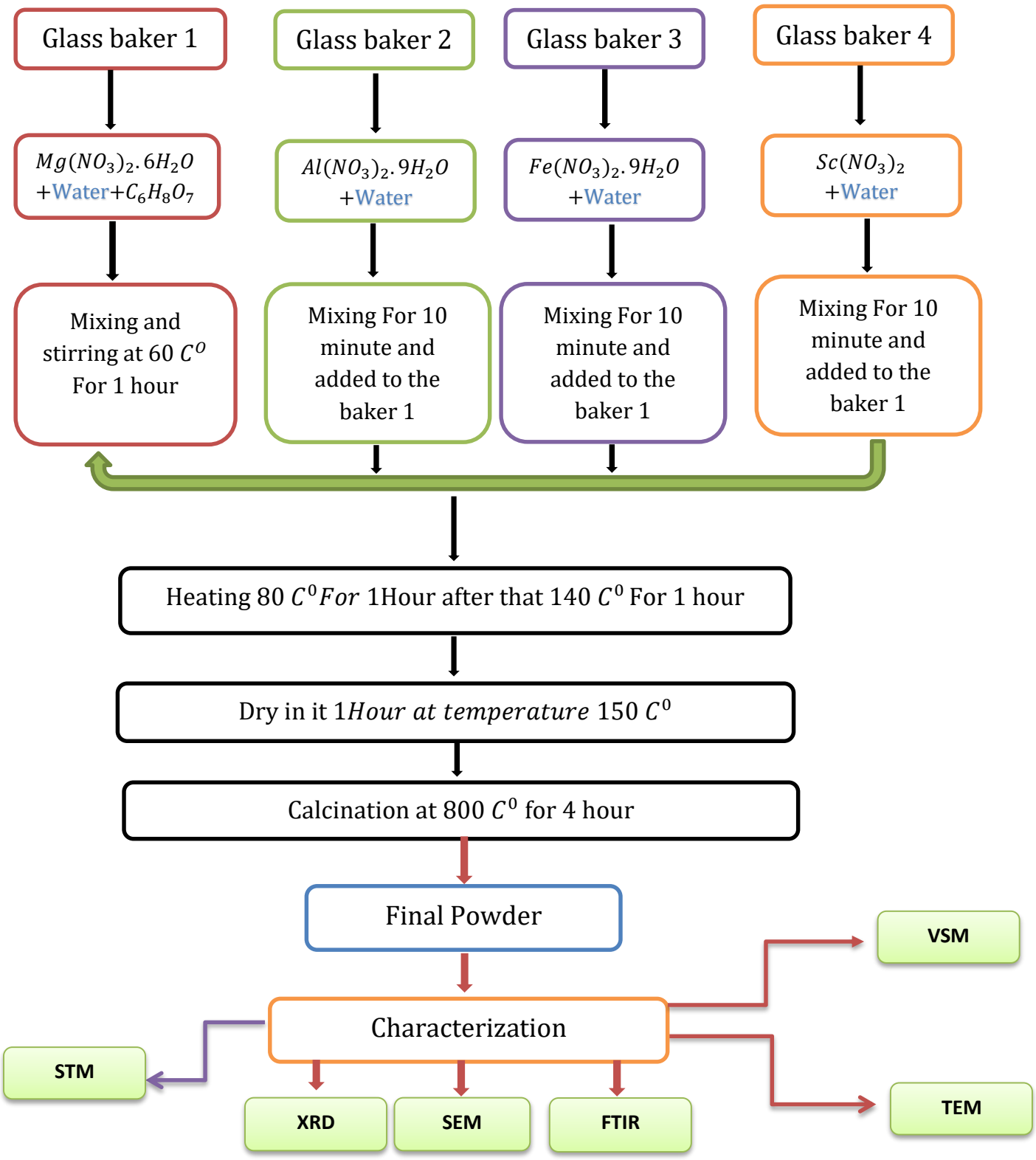

Figure 3-2. Preparation steps of undoped and doped spinel $MgAl_2O_4$ Nanoparticls.

Fig.3-3 Stages of preparation of doped and undoped $MgAl_2O_4$ sample

3-3 Characterization Of The Powder Samples :

X-ray diffraction (XRD), scanning electron microscopy coupled with energy dispersive spectroscope (SEM-EDS), transmission electron microscopy (TEM), Fourier transform infrared spectroscopy (FTIR) are used for the characterization of the synthesized materials. To obtain the Hysteresis loops used to the Vibrating Sample Magnetometer (VSM), while to study structure properties using the scanning tunneling microscopy (STM).

A brief description of the working principle and the practical aspects of each characterization technique employed for the current study is given below.

3-3-1 X-ray Diffraction:

X-ray diffraction (XRD) technique is one of the important structural tools that used to identify material elemental compositions, the nature and the crystal growth of the powder, lattice parameters, and crystal quality and etc.

Crystallite sizes were determined based on (311) plane from XRD data of the samples. In this experiment, the full width at half maximum (FWHM) was used with the Debye–Scherrer according to the formula [101].

$$D=K\lambda / (\beta \cos\theta) \qquad \text{…… Eq (3-4)}$$

Where D stands for the crystallite size in nm, λ refers to the wavelength value of the Cu Kα line (λ= 1:5406 Å), Θ is the Bragg diffraction angle, β is the FWHM of the diffraction peak measured in rad and K is fixed number about 0.9.

This test was performed using x-ray diffractometer (XRD 6000, Shimadzu, Japan) that is exist in (ceramics and building materials laboratories /College of Materials Engineering/ University of Babylon).

3-3-2 Scanning Electron Microscopy and Energy Dispersive X-Ray Spectroscopy (SEM&EDS):

A scanning electron microscope (SEM) is a type of electron microscope that produces images of a sample by scanning it with a focused beam of electrons. The electrons interact with atoms in the sample producing various signals that can be detected and that contain information about the sample's surface topography and composition.

EDX is an elemental chemical microanalysis technique performed in conjunction with SEM. Features or phases as small as about 1 micron can be analyzed [102].

scanning Electron Microscopy experiments were completed using the MIRA3 method, and the other tests used the Energy Dispersive X-Ray Spectroscopy (TESCAN) system. To demonstrate the evolution of microstructure and prove the purity of the resulting powders were all carried out at university of kufa.

3-3-3 Transmition Electron Microscopy (TEM):

TEM is one of the most powerful techniques to characterize materials with nanometer-scale features. Due to the small de Broglie wavelength of electrons, it is capable of imaging specimens at resolutions up to the atomic level. It has multiple imaging modes that enable examination of specimens from various aspects. Bright-field TEM, in which images are generated directly by transmitted electrons, is the most commonly employed imaging mode seen in the literature [103].To examine morphology and determine particle size of obtained powders, tests were done using (Philips CM120) apparatus at (Tehran - Islamic Republic of Iran).

3-3-4 Infrared Analysis (FTIR):

Before and after calcination, the FTIR was used to identify $MgAl_2O_4$ spinel nanoparticles. The test was done using FTIR-8300 spectrometer, which is accessible in the department of polymer laboratories of the College of Material Engineering or the University of Babylon.

3-3-5 Scanning tunneling microscopy (STM):

Scanning Tunneling Microscopy (STM) is one of the application modes for XE series SPM. STM is the ancestor of all scanning probe microscopes. It was invented in 1981 by Gerd Binnig and Heinrich Rohrer at IBM Zurich. Five years later they were awarded the Nobel prize in physics for its invention. The STM was the first instrument to generate real-space images of surface with, so-called, atomic resolution (atomic lattice resolution to be precise) [104].

The operation of STM and Conductive AFM is identical except that one uses a sharpened and conducting tip in STM instead of a conductive AFM cantilever as in Conductive AFM. A bias voltage is applied between the tip and the sample. When the tip is brought within about 10 Å of the sample, electrons from the sample begin to “tunnel” through the 10 Å gap into the tip or vice versa, depending upon the sign of the bias voltage .The resulting tunneling current varies with tip-to-sample spacing, and both the sample and the tip must be conductors or semiconductors. Thus, STM cannot image insulating materials. If the separation between the tip and the sample changes by 10% (about 1 Å), the tunneling current changes by an order of magnitude. This exponential dependence gives STMs their remarkable sensitivity. STMs can image the surface of the sample with subangstrom precision vertically, and atomic resolution laterally [105]. To examine

morphology and determine particle size of obtained powders, tests were done at (Tehran - Islamic Republic of Iran).

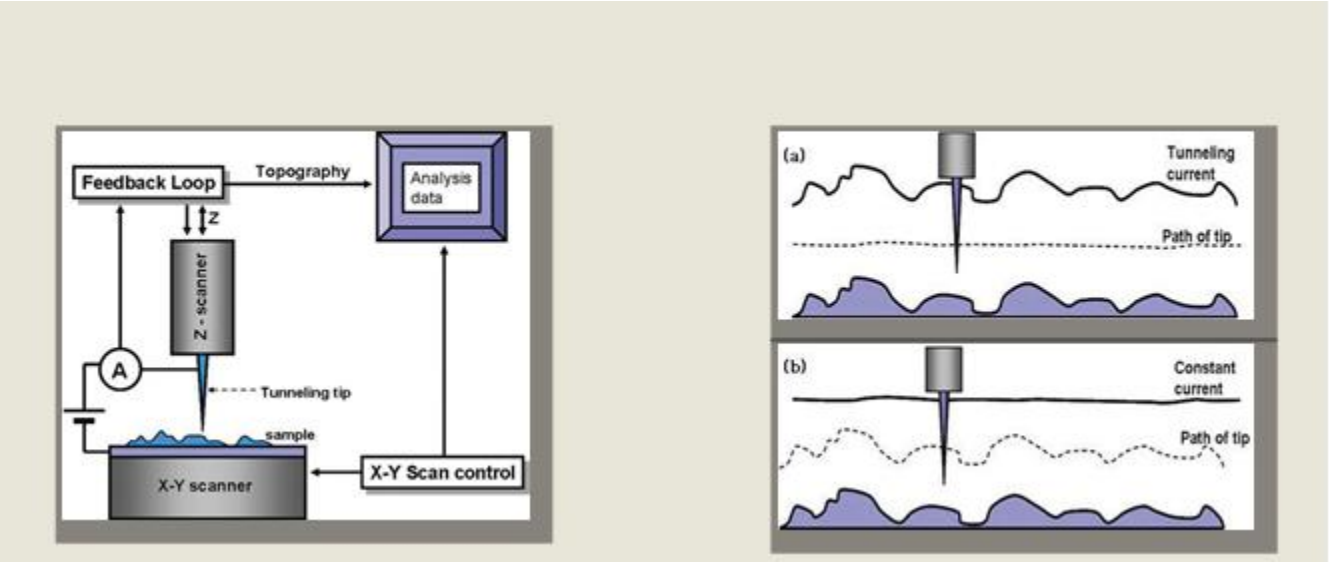

Figure (3-4).Schematic diagram of the XE-series STM system and Comparison of (a) constant-height and (b) constant-current mode for STM [106]

3-3-6 Vibrating Samples Magnometer (VSM):

Vibrating Sample Magnetometer (VSM) systems are used to measure the magnetic properties of materials as a function of magnetic field [107].

The extracted parameters from the hysteresis loop, that are most often used to characterize the magnetic properties of magnetic media, include; the saturation magnetization (Ms), the remanence (Mr), and the coercivity (Hc). The basic principle of operation for a vibrating sample magnetometer is that a changing magnetic flux will induce a voltage in a pickup coil [108]. The VSM test used to measure the magnetic properties of undoped and doped spinel nanoparticle with general formula $MgAl_2O_4$. The test was carried out at Tehran-Iran using a model (Cryogenic VSM).

Chapter 4

Results
&
Discussion

4.1 Introduction:

In This chapter includes experimental results were obtained from the measurements, and tests performed on samples prepared were carried out measurements and tests the following, where the X-ray diffraction test results show that undoped and doped $MgAl_2O_4$ nanoparticles have a single-phase at 800 °C and gave the measurements required to calculate the interplane distance, lattice constant, and crystalline size. SEM test show Surface morphology examinations, where the nanoparticles synthesized are estimated to be angular, uniform. FTIR analyze confirmed the presence of $MgAl_2O_4$ pure and doped as well as FTIR analysis shows its composition and structure. TEM can reveal even the finest details of the internal structure, in some cases as small as individual atoms and determine particles size for grain. STM gave the information about the sample's surface topography and VSM analysis indicates (Ms) value for the synthesis nanoparticles. Changes in particle size, crystallite size, the lattice parameter, and magnetic properties result from doping $MgAl_2O_4$samples with new and different ions concentrations. These changes make it possible to utilize the new doped ion in different applications.

4.2 The Properties doped and undoped $MgAl_2O_4$:

4.2.1 The Structural Properties:

4.2.1.1 X-Ray Diffraction Test:

The X-ray diffraction pattern for $MgAl_2O_4$ spinel nanoparticles spinel and doped with iron (III) ion are calcined at 800 ^{0}c for (4 h) is shown in Figure (4-1). The results of the XRD pattern indicate that $MgAl_2O_4$ spinel is pure, with a cubic and a single-phase spinel formed at a temperature of 800 °C. It can be observed that ultrafine spinel phase ($MgAl_2O_4$) in good agreement with card-No. (96-900-7136) and crystallite size of (10.81) were obtain at a temperature of 800 °C.

This mean that the clear gel transformation ultrafine powder of $MgAl_2O_4$ spinel. Crystalline intensity peaks of MA ($MgAl_2O_4$) spinel appeared at (2θ) value (18.86, 31.16,44.79, 55.46, 59.25, 65.03, 66.49). The peaks are responding to (111), (220), (311), (400), (511) and (444) diffraction plans respectively MA phase is identified as a cubic structure with space group; Fd3m and lattice size of $8.0831A^0$. The crystallite size of the formed $MgAl_2O_4$ spinel nano powders was calculated from XRD analysis using Debye-Scherer formula of the most intense peaks (311) given in Equation (3-4).

The diffraction patterns (XRD) for MA spinel doped with Fe^{+3} ion are shown in Figure (4-1a). Peaks indicate that a single-phase spinel has been obtained. Can be attributed to the doping Fe^{+3} ions with a high concentration, due to the differences in the ionic radius between Fe^{+3} (0.64 A) ions and Al^{+3} (0.54 A) ions.

The inter-planar d-spacing increases from (x = 0.0-0.05) due to increased strain in the lattice of compounds. Table 4.1 shows the the average crystallite size and values of d-spacing of undoped and doped samples.

It is also evident from Figure 4.1b that the diffraction peaks shift lightly in this position, indicating a light change in the lattice parameter. Such changing leads to a contraction or expansion in the lattice due to the introduction of a dopant with a different ionic radius in the host lattice. This suggests that the doping concentration samples successfully substituted the ions of Al^{+3} in the $MgAl_2O_4$ crystal structure with the ions of Fe^{+3}, whereas the undoped sample provided stronger purity and crystallinity phases.

Variation of the lattice constant was proportional to the difference between the ionic radius of the dopant, substituted host lattice atom and the concentration of the dopant. According to Table 4.1, the lattice parameter for undoped $MgAl_2O_4$ is equal

to (8.0831 A^0), while it is increase for doped samples. The maximum increase in lattice parameter is (8.0871A^0) at (x=0.04) for the ($MgAl_{1.96}Fe_{0.04}O_4$) sample. At x=0.05, nevertheless, the lattice parameter of the ($MgAl_{1.95}Fe_{0.05}O_4$) sample decrease.

The mean size of crystallite (D) along the planes of (311) and (400) increased for the six samples that located in the first part whereas the diffracting factor of the ions of Fe^{+3} continued to increase due to facilitating the crystalline growth and crystallization of $MgAl_2O_4$, however, it reduced for the sample of $MgAl_{1.95}Fe_{0.05}O_4$.

Table 4-1. Structural Factors of Doped and undoped ($MgAl_{2-x}Fe_xO_4$) Samples.

sample	crystallite size (nm) along (311) and (400)	space group	Lattice parameter (A^0)	d-spacinng (A^0)
$MgAl_2O_4$	10.81	#227	8.0831	2.44539
$MgAl_{1.99}Fe_{0.01}O_4$	11.68	#227	8.0836	2.44546
$MgAl_{1.98}Fe_{0.02}O_4$	10.80	#227	8.0844	2.44561
$MgAl_{1.97}Fe_{0.03}O_4$	11.36	#227	8.0866	2.44573
$MgAl_{1.96}Fe_{0.04}O_4$	12.35	#227	8.0871	2.44588
$MgAl_{1.95}Fe_{0.05}O_4$	9.14	#227	8.0858	2.44567

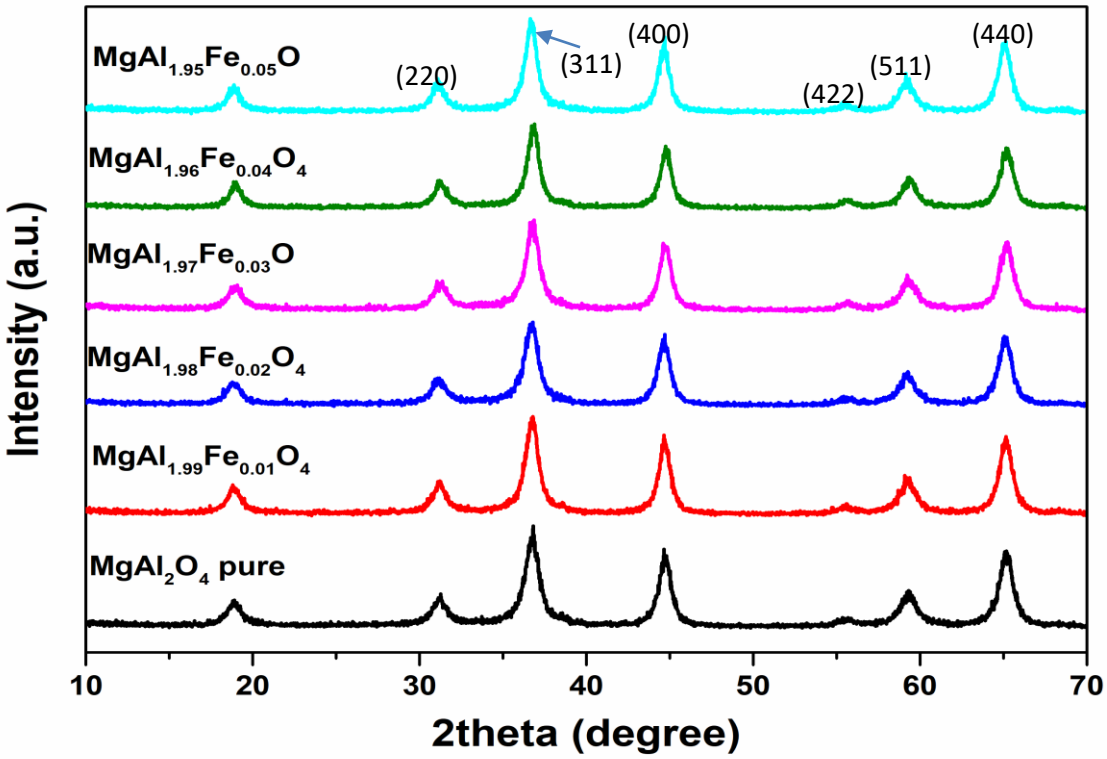

Figure (4-1a). X-ray diffraction pattern of $MgAl_2O_4$ and $MgAl_{2-x}Fe_xO_4$

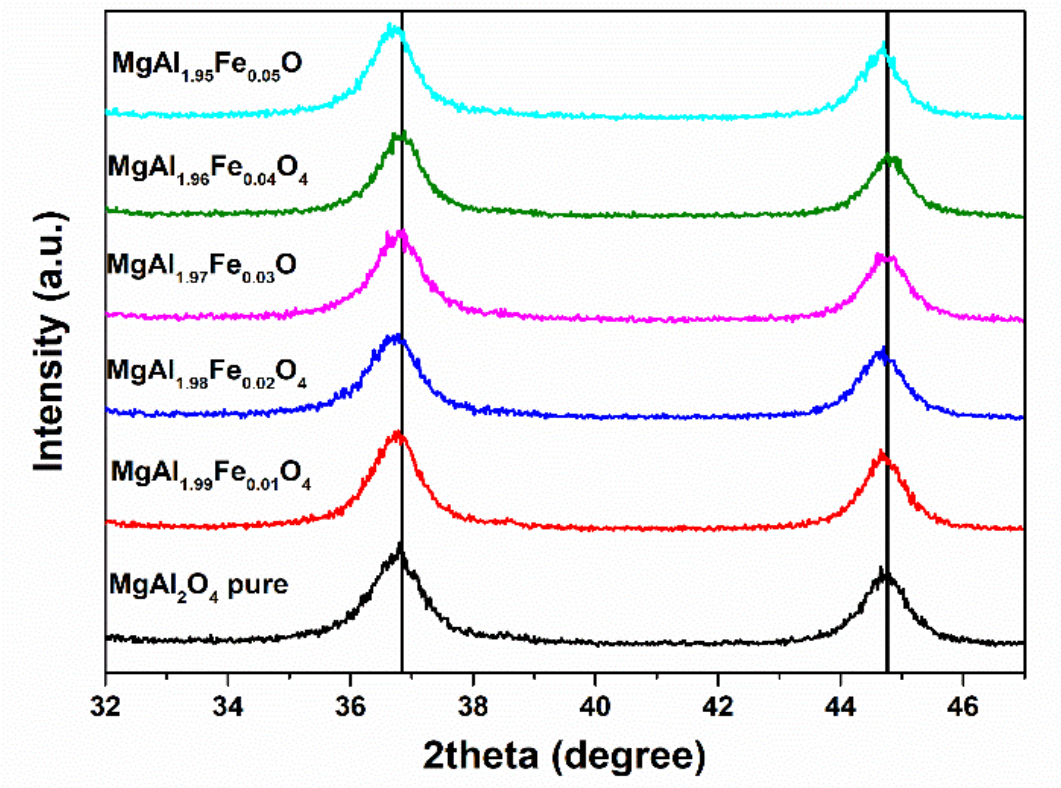

Figure (4-1b). XRD shifting of $MgAl_2O_4$ and $MgAl_{2-x}Fe_xO_4$sample for (311) and (400) plan.

In order to obtain a modification to the ($MgAl_{1.95}Fe_{0.01}Sc_{0.04}O_4$) sample as shown the in the first group.

For undoped structure of $MgAl_2O_4$, the highest intensity peak (311) is positioned at (36.7217), while the position of doped samples with different content of Fe^{+3} ions and Sc^{+3} ions were detected to be shiftied to lower value peak than positions at 2θ as shown in Figure 4.2a. This slightly shifted peak position towards less 2θ values could be recognized due to the radius of ion variance between Fe^{+3} (0.64 A^0) ions, Sc^{+3} (0.745 A^0) ions.

The Figure (4.2 b) demonstrates the shifting of the doped and undoped samples. The samples that doped with high fraction of Fe^{+3} ions are more shifted more than the samples that doped with high fraction of Sc^{+3} ions. The shifting in the diffraction peak positions establishes substitution effects and denotes a structural change due to the lattice distortion caused by the dopant ions.

The incorporation of different content of Fe^{+3} ions and Sc^{+3} ions into the crystal structure of $MgAl_2O_4$ can be causing changes in the interplaner d-spacing. This can be related to the doped samples as cleared in Table 4.2. Such dopants can be caused strain in the lattice of compounds.

The lattice parameter for undoped $MgAl_2O_4$ is (8.0831 Å), while it is larger in values for the doped samples. Such behavior could be related to the ion radius variation between the dopants and the $MgAl_2O_4$ host crystal structure. This indicating that the undoped sample have a well crystallinity and purity phase Fe^{+3} ions and Sc^{+3} ions were successfully replaced ions of Al^{+3} in the $MgAl_2O_4$ host crystal structure due to the change in the scattering centers of the the doped samples.

Crystallite size is varied according to doping different content of Fe^{+3} and Sc^{+3} ions, as shown in Table 4.2. The smallest value in the crystallite size has been recorded for the ($MgAl_{1.95}Sc_{0.05}O_4$) sample that have the maximum fraction of Sc^{+3} ions and it is free from Fe^{+3} ions. This can be related to the reduction in the grain growth afterward doping with trivalent rare-ions earth, Sc^{+3}, which can be acted as grain growth inhibitors.

Table 4-2. Structural Factors of Doped and undoped ($MgAl_{1.95}Fe_{0.05-y}Sc_yO_4$) Samples.

sample	crystallite size (nm) along (311) and (400)	space group	Lattice parameter (A^0)	d-spacinng (A^0)
$MgAl_2O_4$	10.81	#227	8.0831	2.44539
$MgAl_{1.95}Fe_{0.05-0.01}Sc_{0.01}O_4$	12.14	#227	8.0836	2.45053
$MgAl_{1.95}Fe_{0.05-0.02}Sc_{0.02}O_4$	10.62	#227	8.0844	2.45061
$MgAl_{1.95}Fe_{0.05-0.03}Sc_{0.03}O_4$	10.26	#227	8.0866	2.45078
$MgAl_{1.95}Fe_{0.05-0.04}Sc_{0.04}O_4$	9.51	#227	8.0871	2.45085
$MgAl_{1.95}Sc_{0.05}O_4$	9.02	#227	8.0858	2.45057

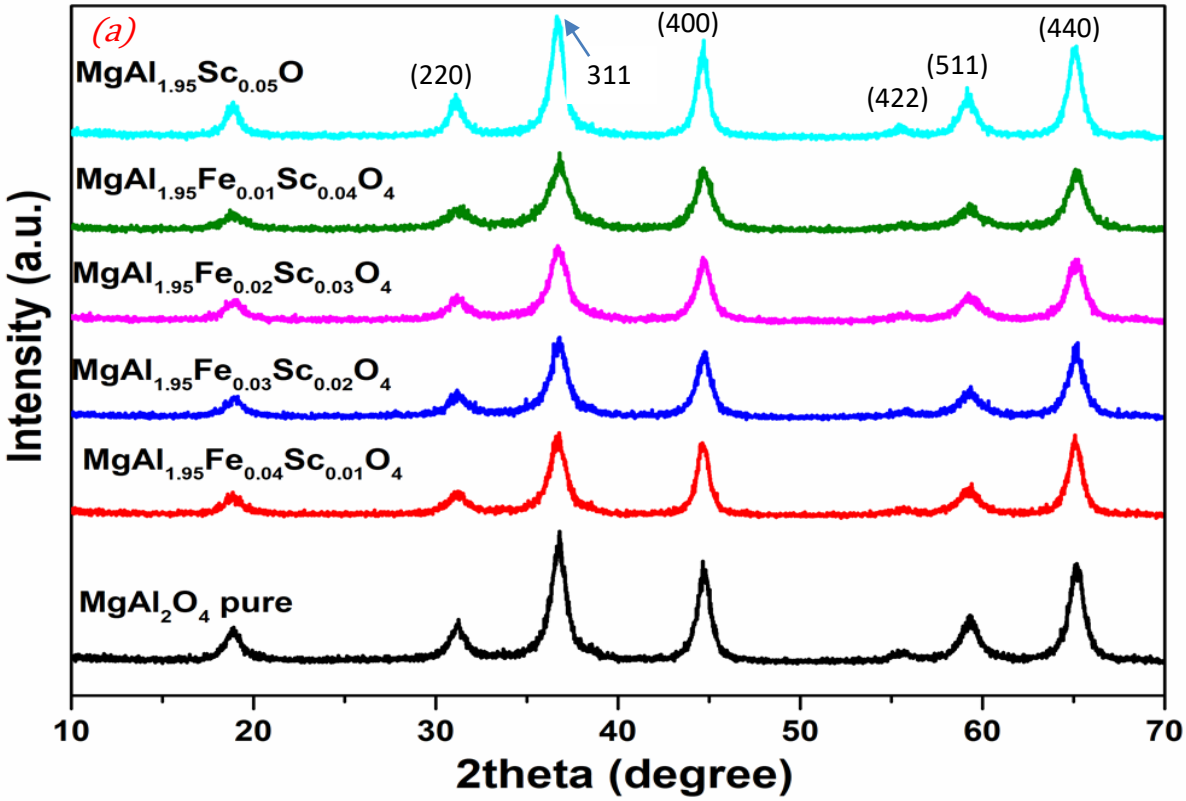

Figure (4-2 a). X-ray diffraction pattern of $MgAl_2O_4$ and $MgAl_{1.95}Fe_{0.5-y}Sc_yO_4$

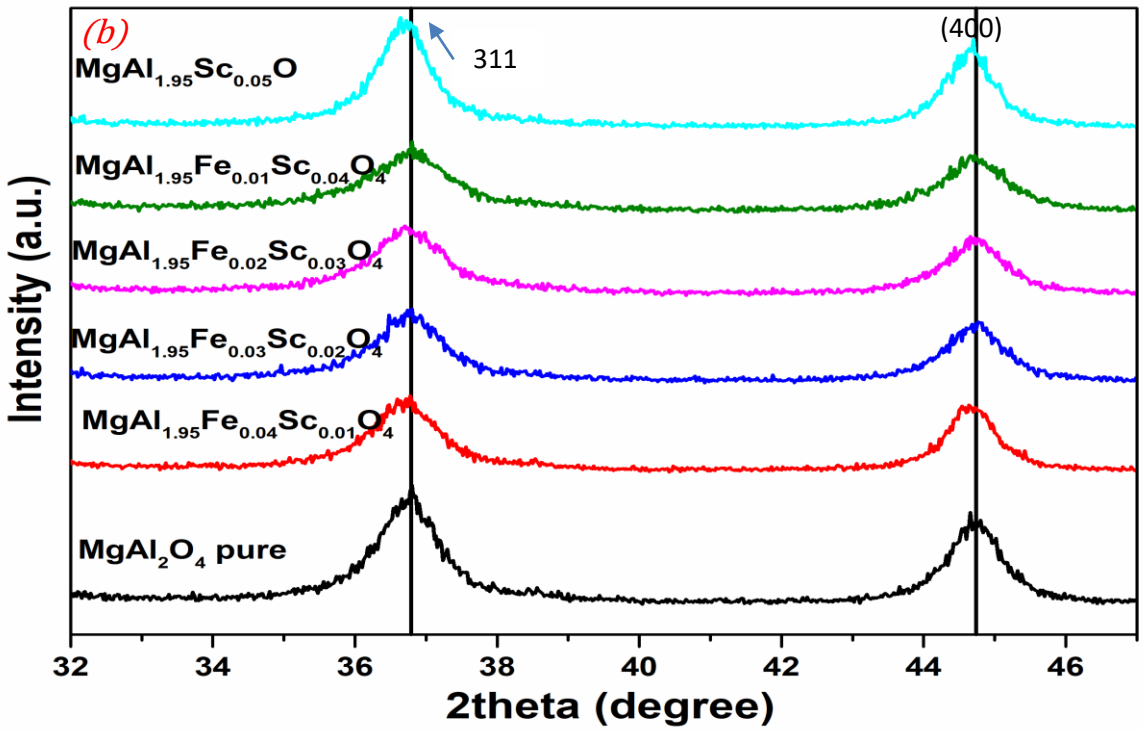

Figure (4-2 b). XRD shifting of $MgAl_2O_4$ and $MgAl_{1.95}Fe_{0.5-y}Sc_yO_4$sample for (311) and (400) plan.

4.2.1.2 FT-IR spectrum of undoped and $MgAl_2O_4$ doped:

The Figure (4-3) shows the FT-IR spectrum of $MgAl_2O_4$ nanoparticles, with curve (a) corresponding to pre-calcination and curve (b) corresponding to calcination of the precursor. It can be seen in fig. (4-3 a) before calcination, the intensity of the adsorption peaks due to the formation of organic bonds (related to citric acid and water) is very high. In fig. (4-3 b) for calcined powder at 800 ° C for (4h), the peak of organic groups was disappear in the spectrum by calcination at 800 ° C to give pure nanoparticle.

The IR spectrum (Fig. 4-3a) contained a broad band at 3448 $Cm^{-1}$and the band 2976 Cm^{-1} due to the H_2O stretching vibration, indicating the existence of water absorbed in the sample. The band centered at 2879 $Cm^{-1}$is related to the asymmetric stretching vibration of CH_2. Also, the bands at 1740 $Cm^{-1}$and 1684 Cm^{-1}represent

the stretching vibration of carboxyl group (COO^{-1}) of metal-complexed citrate ions and the stretching vibration of CAO is observed at 1189 $Cm^{-1}$and 1114 Cm^{-1}. These bands (C=O and C-O) are from the ester groups and formed as a result of esterification reactions. After calcination, these bands disappeared and indicated that the CA are removed completely and it can be said that there is almost no organic bond by calcinations at 800 °C. .

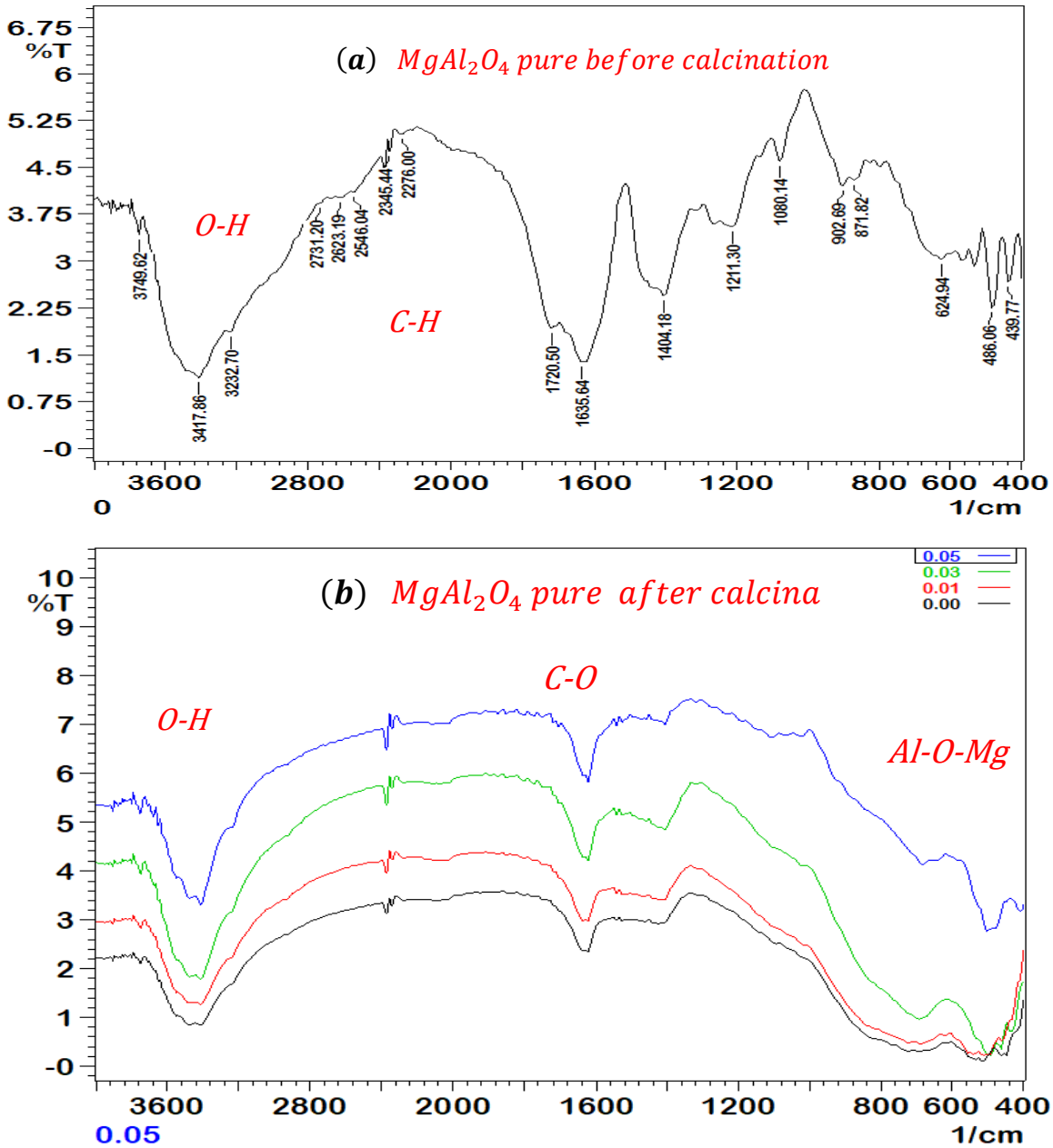

Figure (4.3) FTIR spectra of $MgAl_2O_4$ and $MgAl_{2-x}Fe_xO_4$ nanoparticles calcined at 800 °C

Two peaks presented at 529 $cm^{-1}$and 690 cm^{-1}, correspond with the vibrations of Al-O-Mg, which their peaks intensities increase with increasing the ratio Fe^{+3} ion from (0.00 to 0.05) and indicate that the crystal obtained was $MgAl_2O_4$and Fe^{+3}: $MgAl_2O_4$ spinel. This is a description nearly corresponds with [109] and with corresponds to the XRD test.The intensity of spectrum corresponding to the spinel $MgAl_2O_4$ and spinel Fe^{+3}: $MgAl_2O_4$, the O-H bonds and the peaks belong to the organic bonds are very low in intensity and the adsorption density appears to be due to an increase in inorganic bonds. The links have become stronger. This achievement confirms the results of X-ray diffraction, in the wave number between 400 to 1000 Cm^{-1}, the absorption related to Al-O-Mg bonds appears, in other words, the peak Fe^{+3} corresponds to the spinel $MgAl_2O_4$

Finally, we note after the substitution occurs between Fe^{+3} and Al^{+3}in the octahedral sites, the peak intensity of the Al^{+3} bond decreases and the peak intensity of the Fe^{+3} bond increases, which indicates the replacement of Fe^{+3} ion with Al^{+3}, (Figure 4.3b).

The same applies to the addition of the scandium ion, the peak intensity of the Al^{+3} bond stay the same in stage Fe^{+3} doping and the peak intensity of the Fe^{+3} bond decreases. This indicates that Fe^{+3} is replaced by Sc^{+3}, while the aluminum remains constant. (Figure 4-4). However, shift and variation in intensities are occurred for doped ($MgAl_{2-x}Fe_xO_4$) and ($MgAl_{1.95}Fe_{0.05-y}Sc_yO_4$) Samples, which indicates the incorporation of Fe^{+3} and Sc^{+3} ions in the $MgAl_2O_4$ lattice. This is a description nearly corresponds with [109].

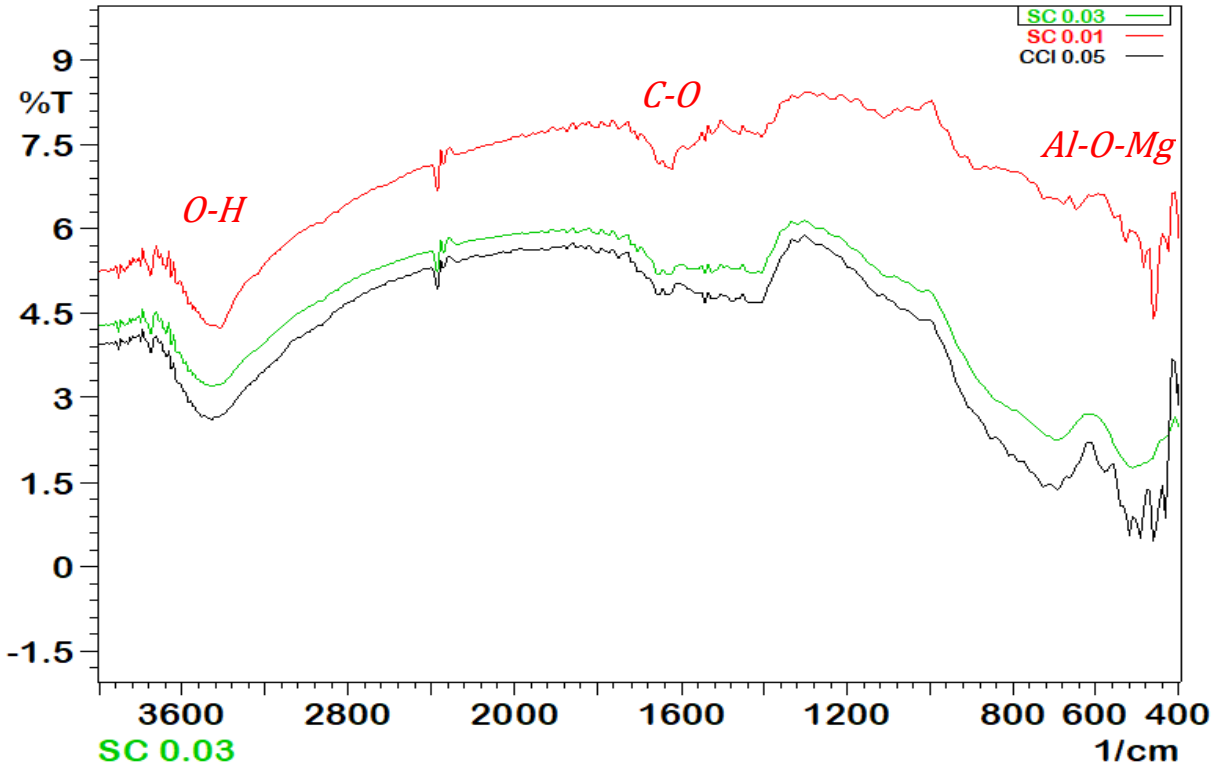

Figure (4-4) FTIR spectra of $MgAl_{1.95}Fe_{1-x}Sc_xO_4$ nanoparticles calcined at 800°C

4.2.1.3 Scanning Electron Microscope (SEM) Test and (EDX):

The surface morphology of the powders magnesium aluminate spinel was investigated by scanning electron microscopy (SEM). Fig. (4-5) is relative to the $MgAl_2O_4$ powders calcined at 800 °C; Fig. (4-7) is relative to the ratio Fe^{+3} ion (0.03) and Fig. (4-9) is relative to the ratio Fe^{+3} ion (0.05). The SEM micrographs show that the obtained $MgAl_2O_4$ powders at in all ratio are very small, uniform and suitable dimensions.Also, the shape are as angular shape and the particles size increase due to the growth of particles with increasing the ratio Fe^{+3}: $MgAl_2O_4$ from (x= 0.01 - 0.05) and the particles a little agglomerated. As can be seen clearly in fig. (4-5) the $MgAl_2O_4$ particles form completely porous and angular structures that are perfectly bonded together.

In Figure (4-7) and (4-9), Spinel is morphologically similar in both cases, and in both cases the appearance of the particles is "angular". The element analysis performed by the EDX method is shown in Figure (4-6) ,(4-8),(4-10) where the effect of the ratio iron ion on the mean diameter of particles was investigated.

At SEM micrographs, the EDX provides the type and weight percent of each element present in the selected point of sample. We can notice the differences between EDX analysis of undoped and doped $MgAl_2O_4$. which resulted in the increase in the percentage of O, Fe^{+3} ion and decrease in the percentage of Al^{+3} ion. Furthermore, EDX analysis revealed that the highest ratio of Oxygen atom was 57.52 % at the ratio iron ion (0.05) this directly suggests that the introduction of Fe^{+3} was at the expense of Al^{+3}.

The results of EDX analysis show that the amount of Mg^{+2} and Al^{+3} ions in the resulting powder compared to their load, not only do not differ much but also have a very good compatibility with each other. Table (4-3) shows the Mg^{+2} and Al^{+3} ions levels from the EDX results and Table (4-4),(4-5) shows the Mg^{+2}, Al^{+3} and Fe^{+3} levels from the EDX results.

Table (4-3) Mg^{+2} and Al^{+3} levels from the EDX analysis of $MgAl_2O_4$

Element	Series	Wt.%	At.%
Mg	K-series	16.25	13.29
Al	K-series	34.38	25.34

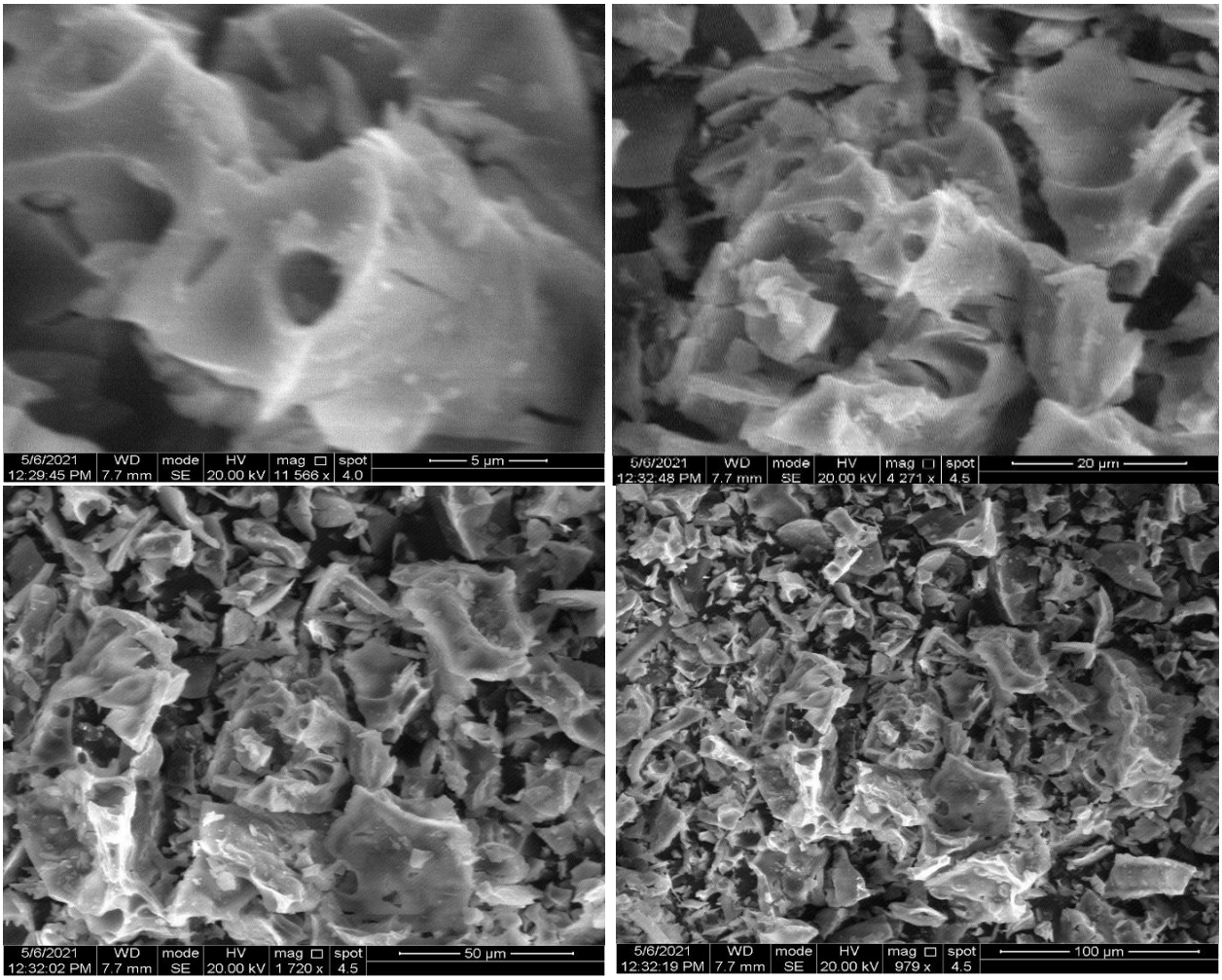

Figure 4.5 SEM image of $MgAl_2O_4$ powder calcined at 800 ^oC in four different magnifications

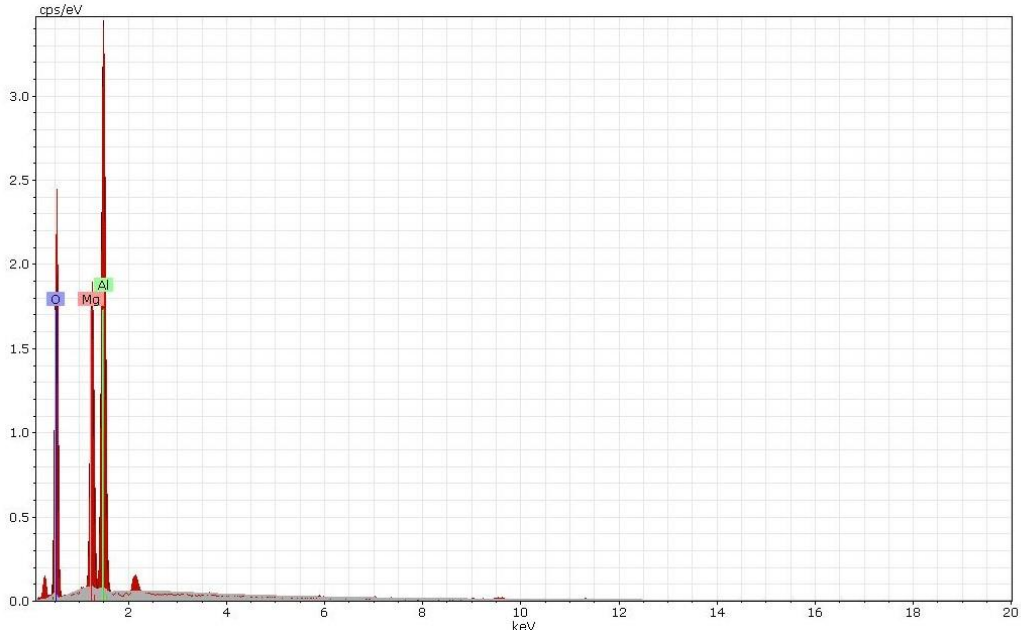

Figure 4-6. EDX analysis of spinel nanoparticles $MgAl_2O_4$ calcined at 800 °C

Table (4-4). Mg^{+2}, Al^{+3} and Fe^{+3} levels from the EDX analysis of $MgAl_{1.97}Fe_{0.03}O_4$.

Element	Series	Wt.%	At.%
Mg	K-series	16.36	13.46
Al	K-series	33.55	24.87
Fe	K-series	1.07	0.38

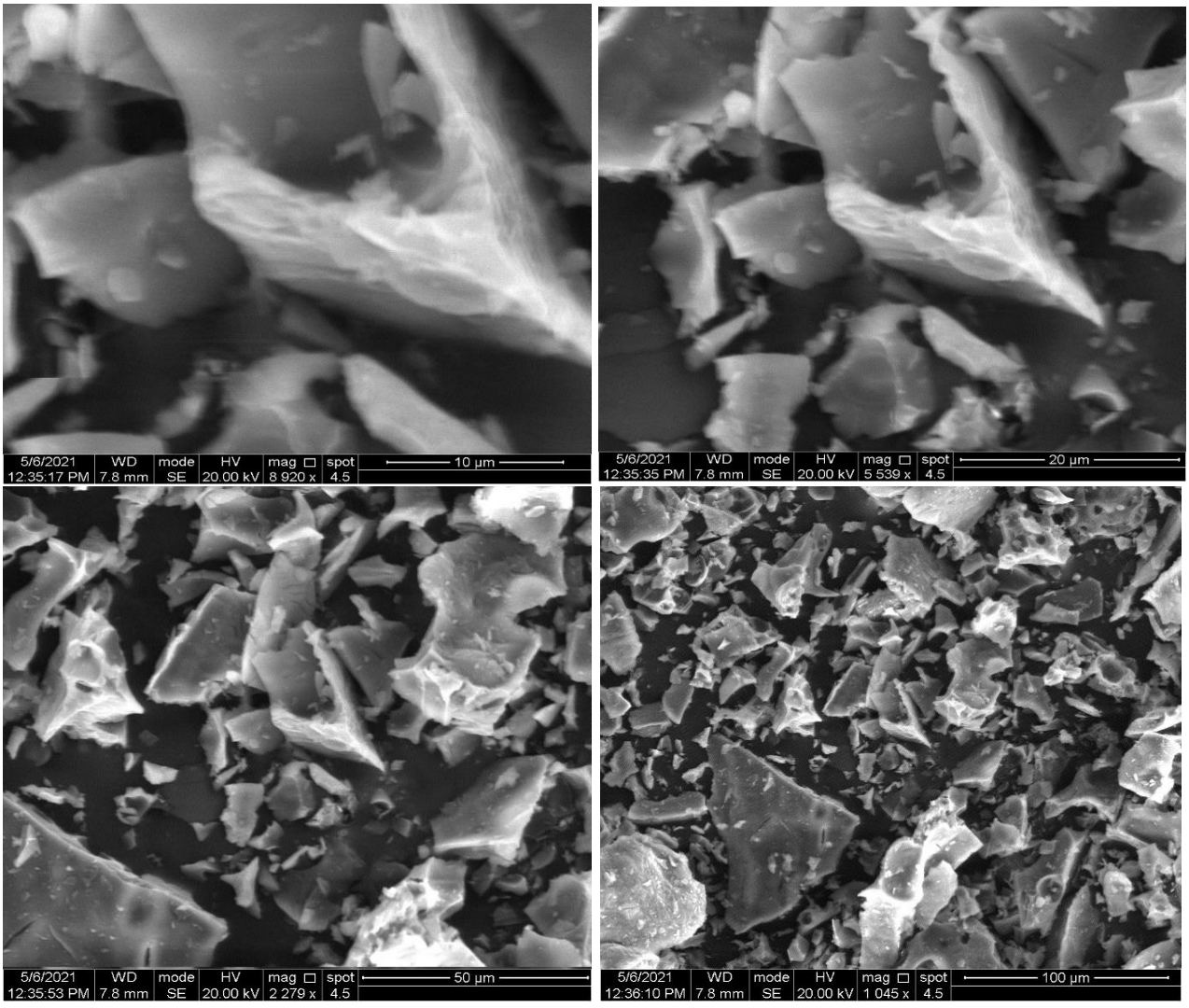

Figure 4.7 SEM image of s $MgAl_{1.97}Fe_{0.03}O_4$ powder calcined at 800 °C in four different magnifications.

Fig. (4-8) EDX analysis of spinel nanoparticles $MgAl_{1.97}Fe_{0.03}O_4$ calcined at 800°C.

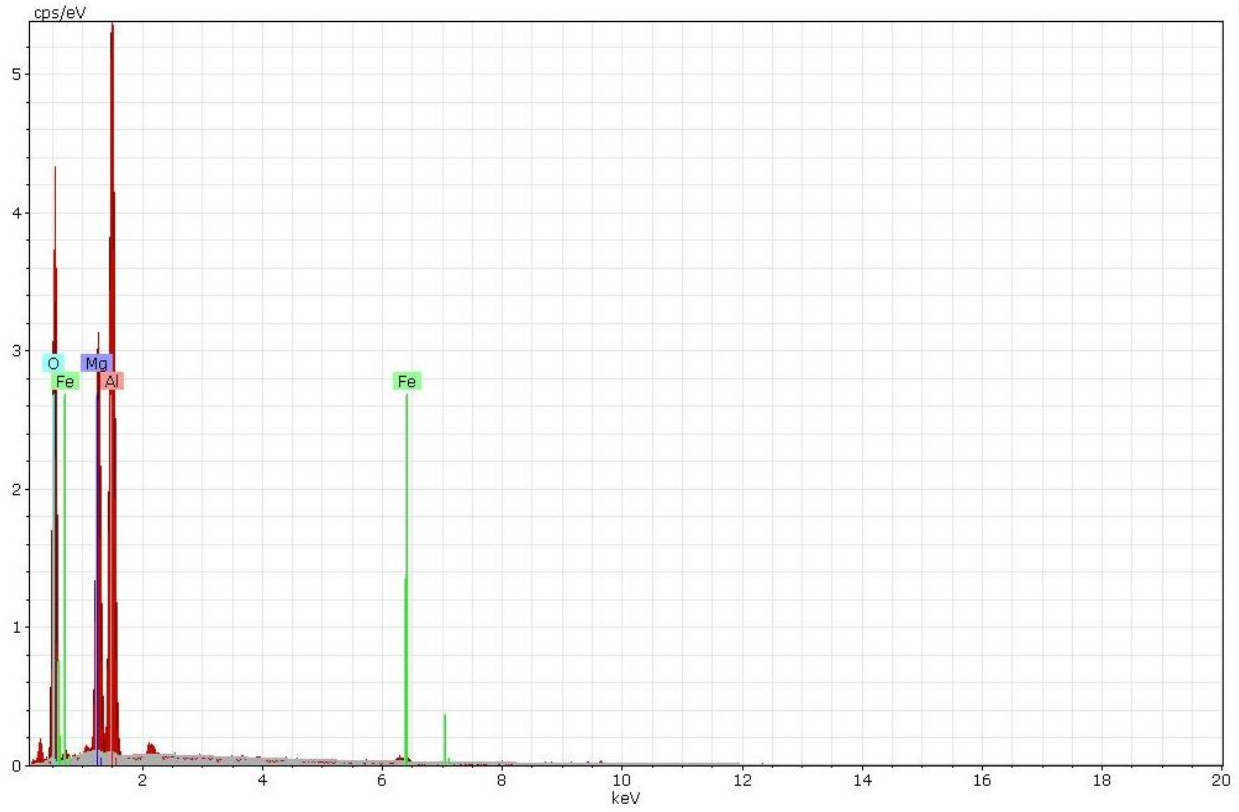

Table 4-5. Mg^{+2}, Al^{+3} and Fe^{+3} levels from the EDX analysis of $MgAl_{1.95}Fe_{0.05}O_4$.

Element	Series	Wt.%	At.%
Mg	**K-series**	**17.09**	**14.48**
Al	**K-series**	**35.29**	**26.93**
Fe	**K-series**	**2.93**	**1.08**

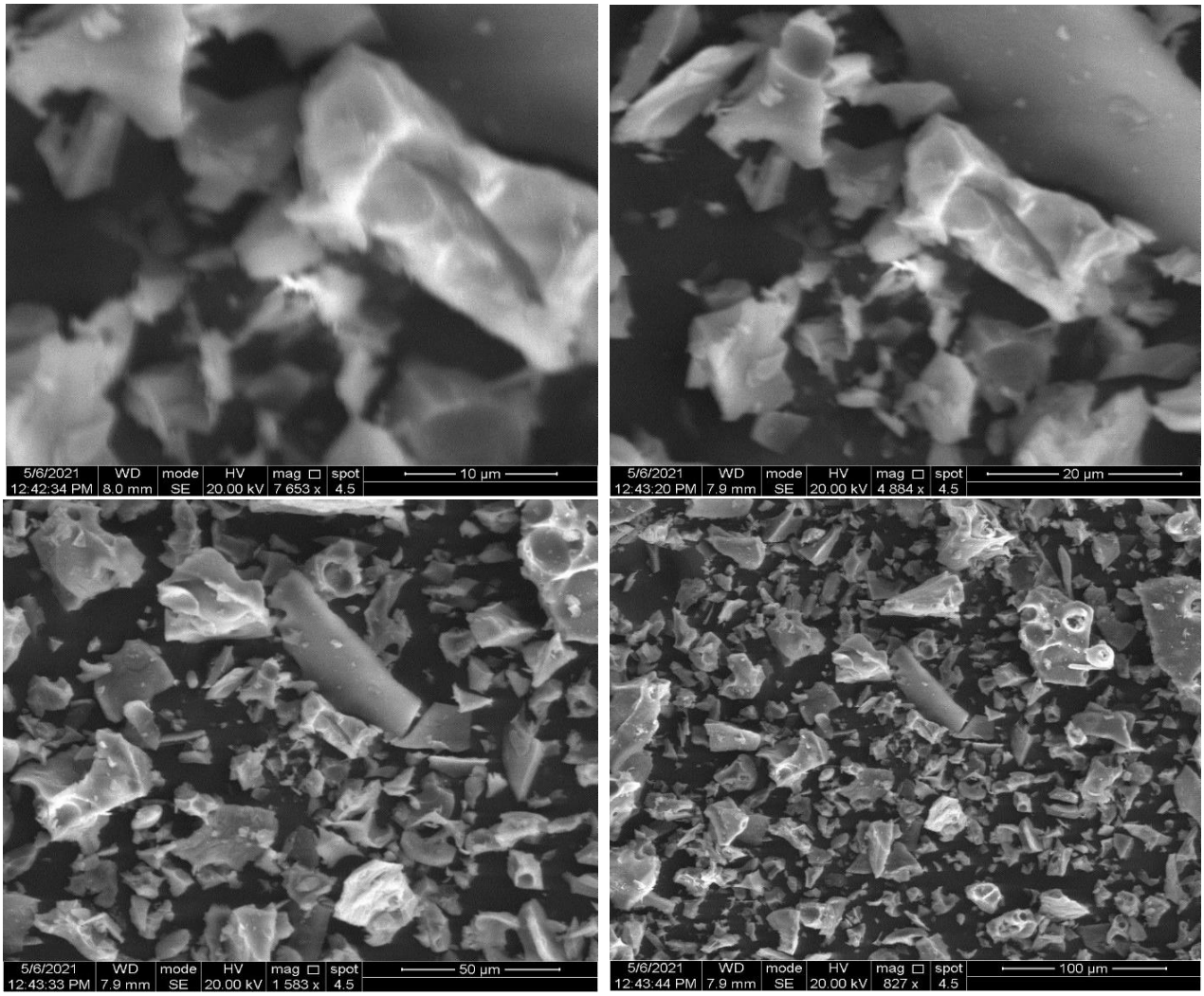

Figure 4.9 SEM image of s $MgAl_{1.95}Fe_{0.05}O_4$ powder calcined at 800 °C in four different magnifications.

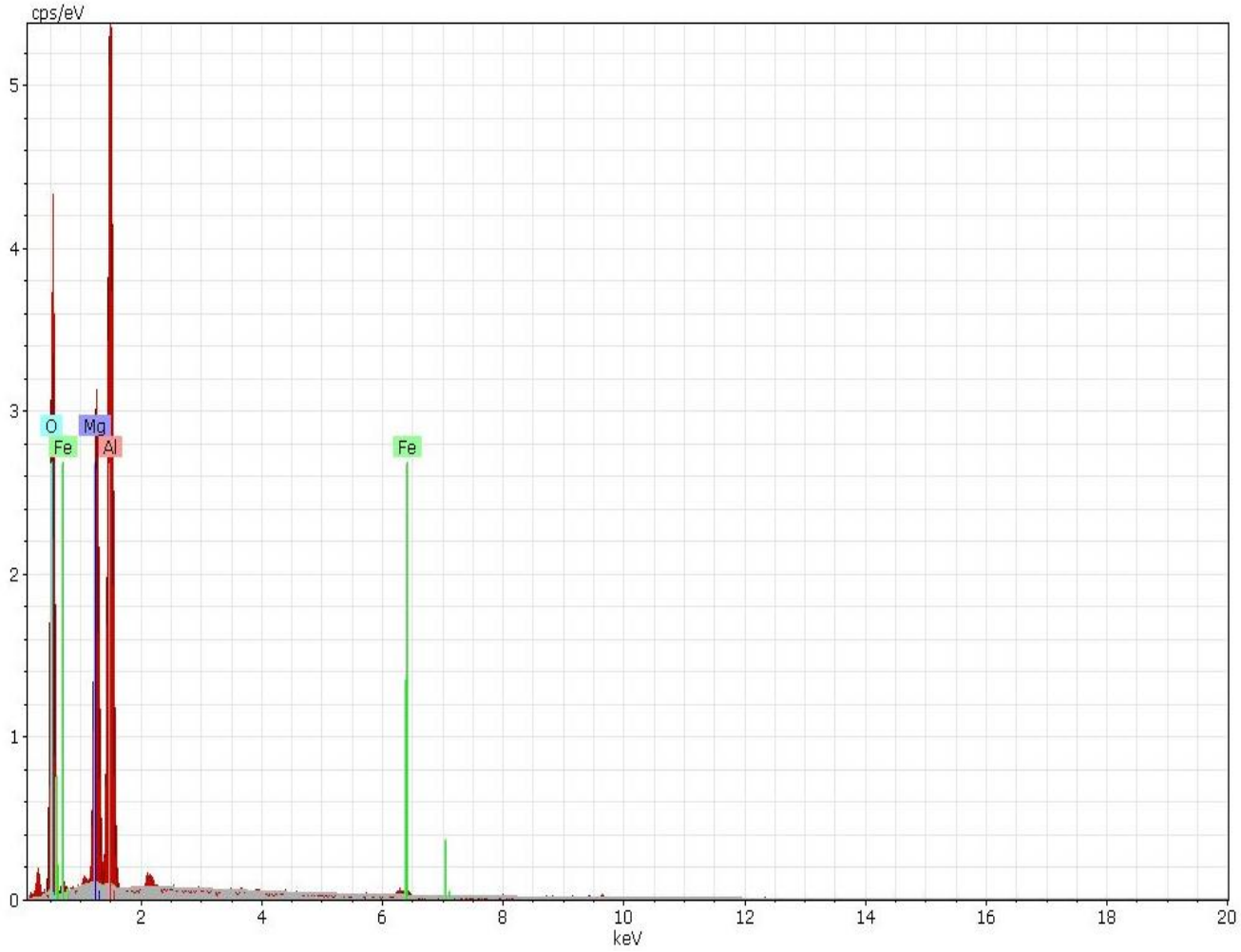

Figure 4-10. EDX analysis of spinel nanoparticles $MgAl_{1.95}Fe_{0.05}O_4$ calcined at 800 ° C

4.2.1.4 Transmission Electron Microscope (TEM) test:

TEM was used to evaluate the $MgAl_2O_4$ spinel crystallite grains microstructure as shown in Fig.(4-11). The result showed that the $MgAl_2O_4$ spinel grain size was concentrated within the range of 20-50 nm, and $MgAl_2O_4$ spinel grain morphology was near spherical. TEM micrograph seems to indicate some connected porous structure with typical domain size of the order of 14 nm, where the average particle size was is calculated by averaging from 57 particles with the ImageJ. Which is in good with XRD.

TEM was also used to characterize the morphological feature of the $MgAl_2O_4$ spinel powders after calcination at 800°C with increasing the ratio Fe^{+3} as shown in Fig. (4-12). It was also found that the $MgAl_{1.97}Fe_3O_4$ spinel powders were approximately spherical in morphology and had the average particle size of about 16.76 nm. In addition, the porous channels mostly due to the accumulation of $MgAl_2O_4$ spinel particles were also observed. Furthermore, the particle size distribution of $MgAl_{1.97}Fe_3O_4$ spinel powders calcined at 800°C includes of nonmetric particles with a narrow size distribution.

Additionally, as observed from the cross section TEM micrograph of the calcined sample in Fig. (4-13), that contains $MgAl_{1.95}Fe_{0.02}Sc_{0.03}O_4$, the particles were relatively small, uniform and plate like with have needle morphology, whose average grain size was distributed within the range of 20-30nm. Compared with the powder $MgAl_2O_4$ and $MgAl_{1.97}Fe_{0.03}O_4$, the size of the calcined particles increased and no obvious abnormal growth was observed in these grains. The grains also contacted closely to form many small and evenly distributed open pores with clear boundary among grains. It suggested that the $MgAl_2O_4$ spinel powders might be used for the preparation of porous ceramic materials.

.

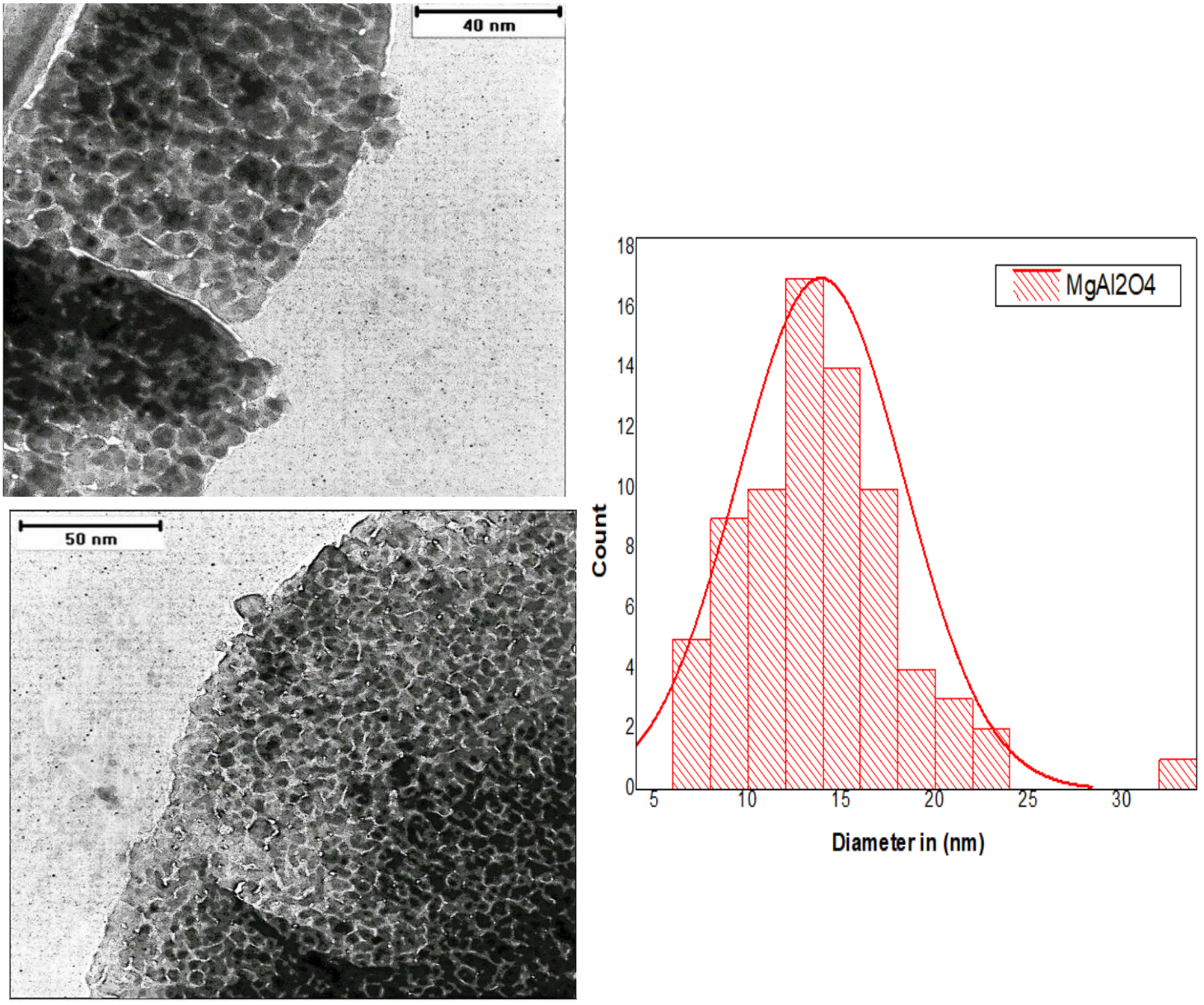

Figure 4.11 TEM image of $MgAl_2O_4$ powder in two different magnifications with analysis particle size.

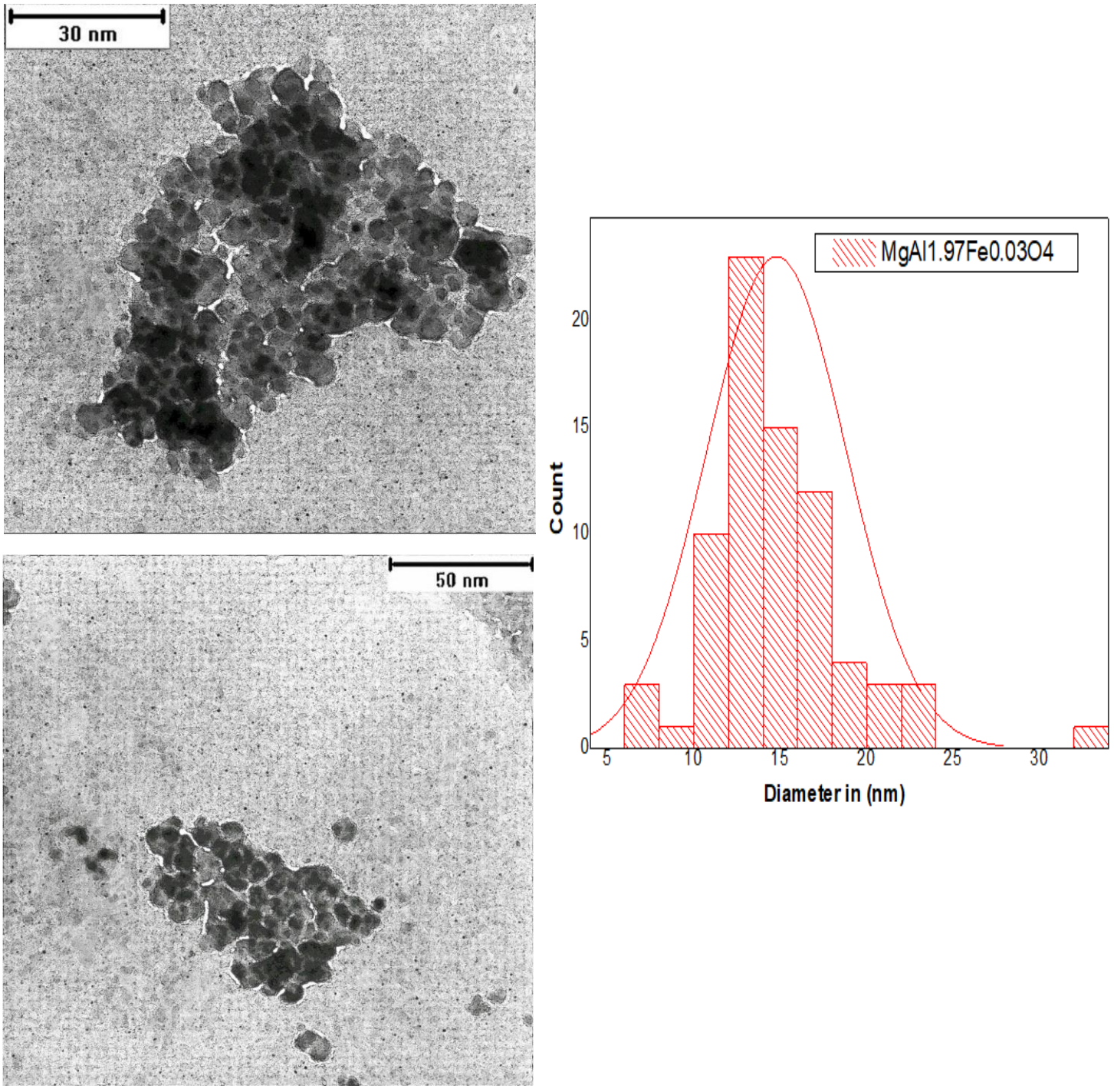

Figure 4.12 TEM image of $MgAl_{1.97}Fe_{0.03}O_4$ powder in two different magnifications with analysis particle size.

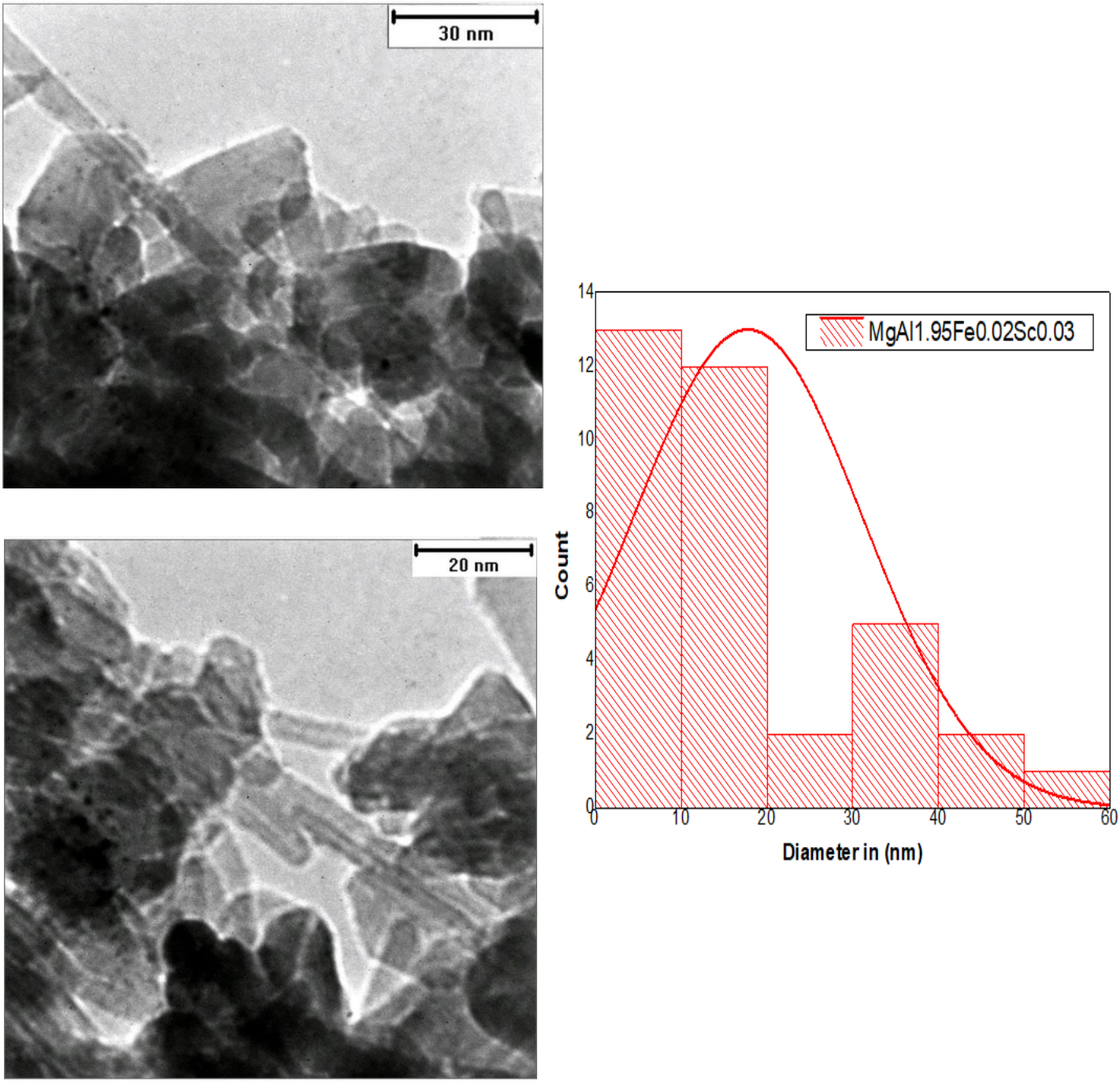

Figure 4.13 TEM image of $MgAl_{1.95}Fe_{0.02}Sc_{0.03}O_4$ powder in two different magnifications with analysis particle size.

4.2.1.5 Scanning Tunnelling Microscope (STM) test:

In figure (4.14) shows the STM image of the surface of a $MgAl_2O_4$ nanoparticles which has been calcination at 800 °C for 4 hour at a rate of 5 ° C / min . This produces a powder that is smooth (rms roughness is approximately 1.05 nm) with no cracks and that has homogenously distributed grains with point defects. To check the uniformity of the powder structure, the STM images were obtained by scanning at about 10 different regions and all showed similar morphologies.

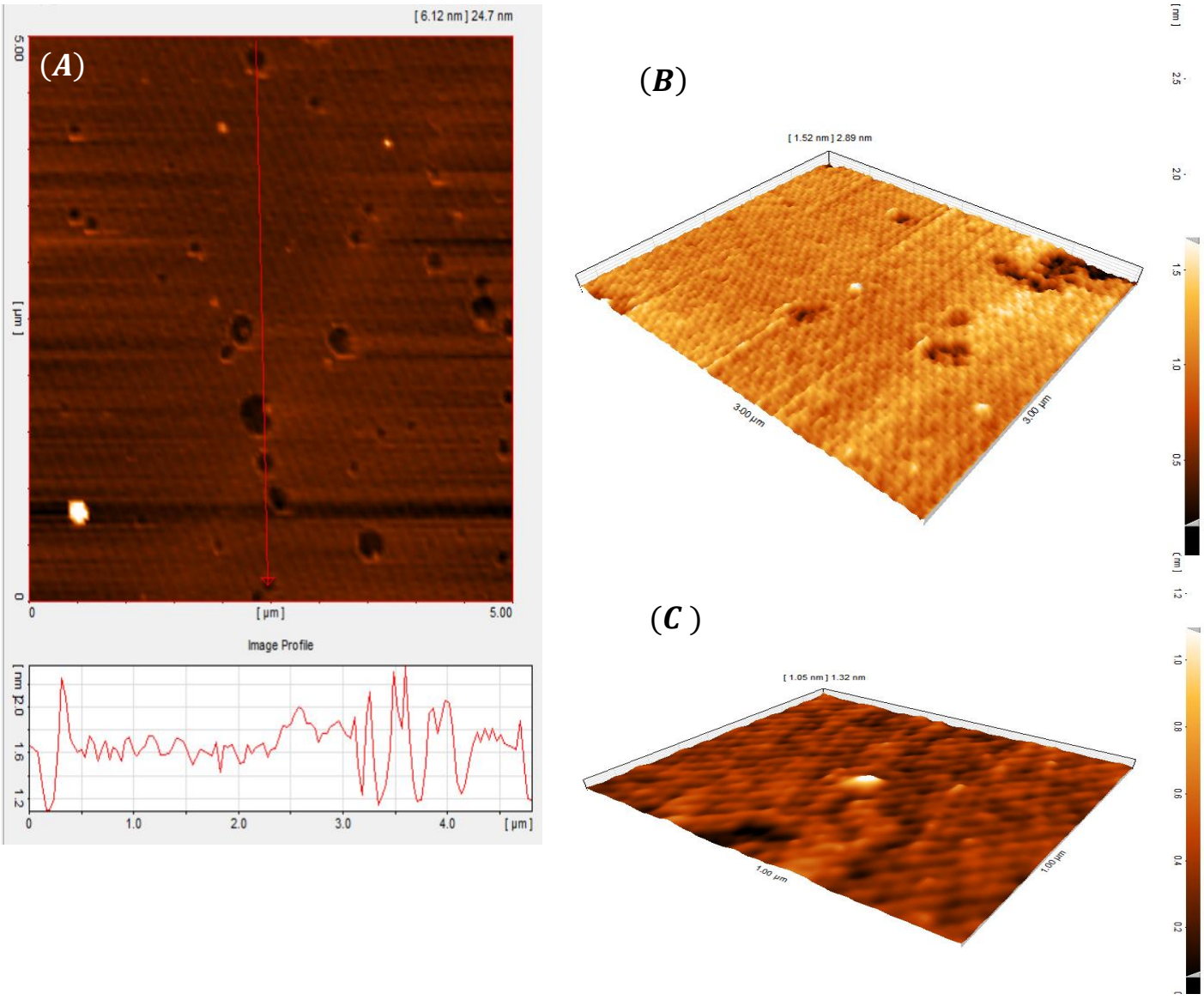

Figure 4.14 STM images of the $MgAl_2O_4$ powder in three different magnifications

When adding quantities of Fe^{+3} ion for $MgAl_2O_4$ from (0.01 to 0.05) (figure 4.15), the powder is still smooth, but the roughness increases to 1.24 nm because the particle size has increased.

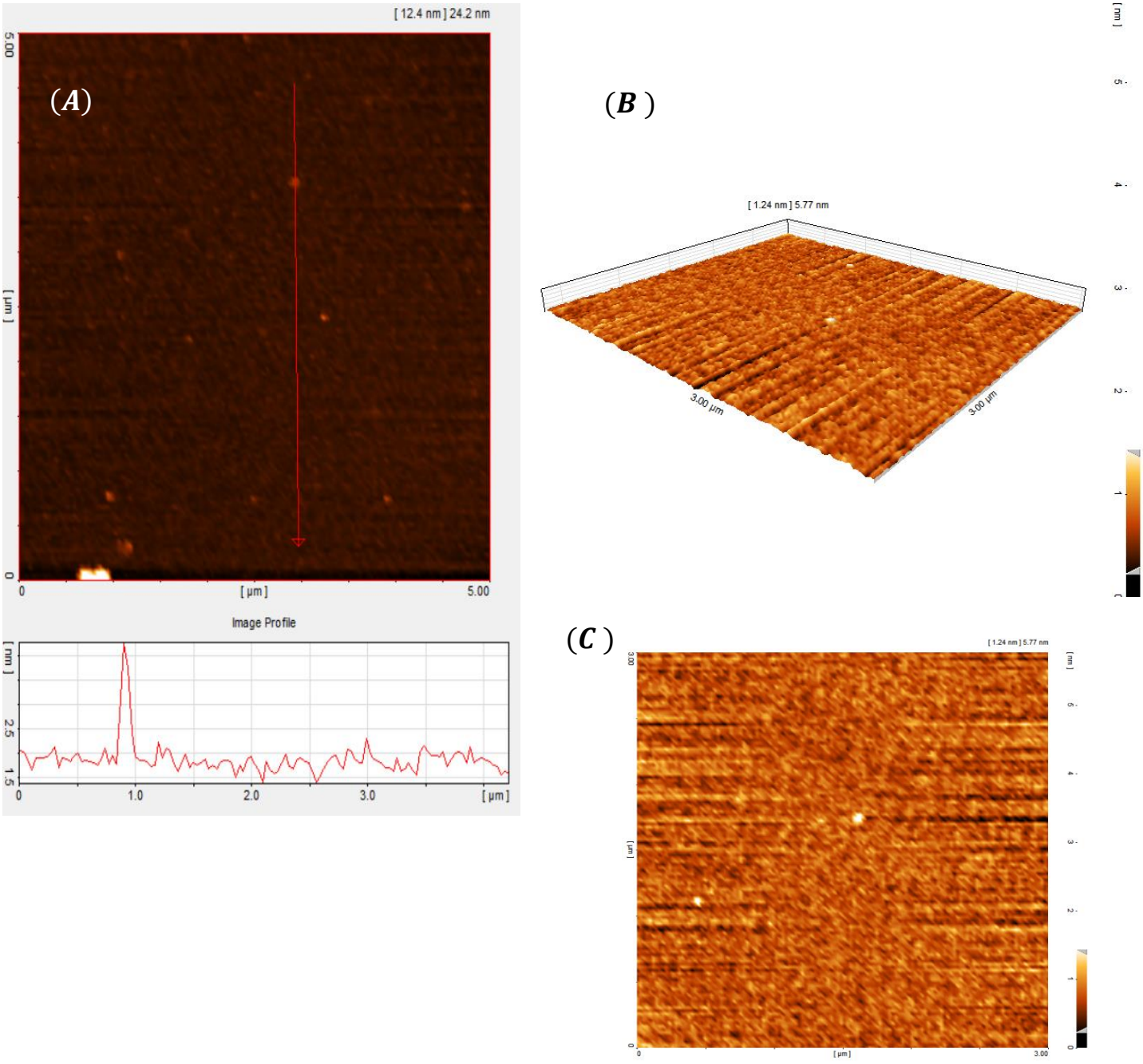

Figure 4.15 STM images of the $MgAl_{1.95}Fe_{0.05}O_4$powder in three different magnifications.

In figure 4.16 shows the STM images of the surface of $MgAl_{1.95}Sc_{0.05}O_4$ nanoparticles of different thicknesses (number of layers) which have been calcinated at 800 °C for 4 h at a rate of 5 °C / min . The morphology of these powder is significantly different from those $MgAl_2O_4$ and $MgAl_{1.95}Fe_{0.05}O_4$ (figure 4.14 and figure 4.15), where The roughness has increased to 1.32 nm for the$MgAl1.95Sc0.05O4$. After calcinatied at 800 °C the surface of the powder is smooth and the surface has regions consisting out of features of similar hills and valleys.

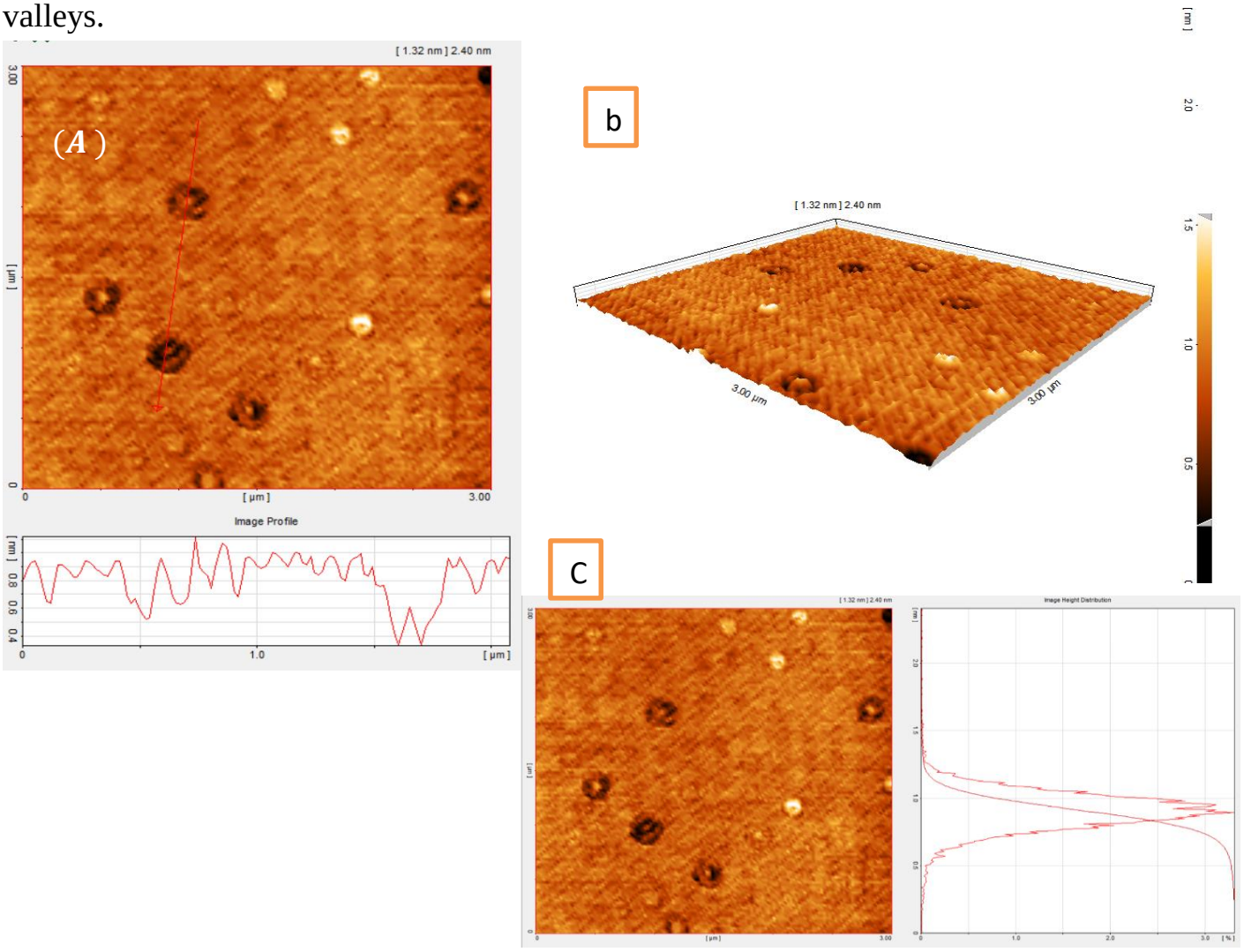

Figure 4.16 STM images of the $MgAl_{1.95}Sc_{0.05}O_4$powder in three different magnifications.

4.2.2 The Magnetic Properties:

4.2.2.1 Vibrating Sample Magnometer (VSM) measurement:

The magnetic properties of the $MgAl_2O_4$ nanoparticles were measured through vibrating sample magnetometer (VSM) at a maximum applied field of (14,000 Oe) at room temperature. Figure (4.17) shows magnetic hysteresis loops of $MgAl_2O_4$ nanoparticles prepared by sol-gel method using citric acid as a catalyst after calcination at (800 °C). were found the remanent magnetization (M_R) is 0.00119 emu/g, the coercive field (H_C) is (182 Oe) and the magnetization at saturation (M_S) is estimated to be only 0.00231 emu/g (the saturation magnetization M_S was determined from the extrapolation of curve of H/M vs H). This is a description nearly corresponds with [112].

The origin of ferromagnetism in $MgAl_2O_4$ is assumed to be resulting from the oxygen vacancies at the surface of the nanoparticles [113]. The magnetic order in the lattice of the pure and the doped $MgAl_2O_4$ samples can be achieved by providing a certain density of vacancies, which can consider the necessary condition for ferromagnetism. Such vacancies or other defects in the lattice were achieved nearly localized magnetic moments. This vacancies were usually labeled as F and V centers, which corresponding to the missing oxygen atom or Al atom respectively, in the host lattice of $MgAl_2O_4$ [114].

The reason behind the encouraging magnetic moment was spin polarization of 2p electrons of O atoms that is close to the negative charge [115]. However, The cations were enclosed by an octahedron of anions with filled valence p bands and the bonding anion p orbitals with lobes point to the cation site would be the generality energetically favoured attraction orbitals to provide the vacancies. So that the

vacancies were necessary to charge recompense by a cation vacancy at the center of such an octahedron [116].

To understand the magnetic properties of $MgAl_{2-x}Fe_xO_4$ nanoparticles where (x=0.01, 0.02, 0.03, 0.04, 0.05), it is characterized using vibrating sample magnetometer (VSM). The hysteresis loop traced at (800°C) temperature for $MgAl_{2-x}Fe_xO_4$ is shown in Fig. (4-17). The hysteresis loop explains the soft ferrimagnetic nature of the synthesized $MgAl_{2-x}Fe_xO_4$. The values of the saturation magnetization M_S, coercivity H_c and retentivity M_R are obtained. The experimental magnetic moment (mB) is determined from the saturation magnetization (M_S) data. The negligible coercivity indicated that the $MgAl_{2-x}Fe_xO_4$ nanoparticles of different particle sizes exhibited a typical superparamagnetic nature with small interactions between the particles. A small volume fraction of ferromagnetic phases was embedded in the superparamagnetic matrix. The increase of all the parameters with the nanoparticle size, such as maximum magnetization (Mmax), coercivity H_c , and remnant ratio (Mr/Mmax) indicated that inter-particle interactions increased with the increase of nanoparticle size. The values of magnetic parameters such as M_S, H_C and M_R of nanoparticles of $MgAl_{2-x}Fe_xO_4$ obtained from the VSM data are illustrated in the table (4-6).

Table (4-6). The values of magnetic parameters of $MgAl_{2-x}Fe_xO_4$ obtained from the VSM data.

Samples	Hc (Oe)	Mr (emu/g)	Ms (emu/g)
$MgAl_2O_4$	182	0.00119	0.00231
$MgAl_{1.99}Fe_{0.01}O_4$	250	0.00117	0.00268
$MgAl_{1.98}Fe_{0.02}O_4$	305	0.00131	0.00251

$MgAl_{1.97}Fe_{0.03}O_4$	251	0.00122	0.00234
$MgAl_{1.96}Fe_{0.04}O_4$	260	0.00126	0.00259
$MgAl_{1.95}Fe_{0.05}O_4$	223	0.00139	0.00282

Therefore the decrease in saturation magnetization can be attributed to the effect of Nano regime on it. In addition, can be attributed to the following: firstly, the grain size of our samples is much smaller than that of bulk materials, which induces an increase in the number of grain boundaries, the large surface and interface supplying more pinning sites for domain walls. Secondly, following the increase of the added quantities, the grain size of the powder increases and the microstructure become well crystallized. This is a description nearly corresponds with [117].

To understand the magnetic properties of $MgAl_{1.95}Fe_{0.05-y}Sc_yO_4$ nanoparticles where (y=0.0,0.01,0.02,0.03,0.04,0.05) ,it is characterized using vibrating sample magnetometer (VSM). The hysteresis loop traced at (800°C) temperature for $MgAl_{1.95}Fe_{0.05-y}Sc_yO_4$ is shown in Fig. (4-18). the values of magnetic parameters such as M_S, H_C and M_R of nanoparticles of $MgAl_{1.95}Fe_{0.05-y}Sc_yO_4$ obtained from the VSM data are illustrated in the table below (4-7).

The difference in the value of M_S can be explained in the light of cation distribution. Any change in the concentration and nature of the ions in B-site should cause resultant magnetization to be different from reported one. In the present work the proposal of cation distribution has been done to reproduce experimental values of magnetic moment and lattice constant. The increase in M_S value can be further attributed to the site occupancies of metal cations in the B-site. In nanoparticles, inter-ionic separation may face an extension due to less number of structural matters in the surrounding of each particle. Thus, the nanosize of the spinel particles and

ultimate change of the nature of ions in the respective size could have caused reduction of magnetization in $MgAl_{2-x}Fe_xO_4$ and $MgAl_{1.95}Fe_{0.05-y}Sc_yO_4$. Thus in nanoregime, the magnetization is said to be dependent on grain size and cation distribution .This is a description nearly corresponds with [118].

Table (4-7). The values of magnetic parameters of $MgAl_{1.95}Fe_{0.05-y}Sc_yO_4$ obtained from the VSM data.

Samples	Hc (Oe)	Mr (emu/g)	Ms (emu/g)
$MgAl_2O_4$	182	0.00119	0.00231
$MgAl_{1.95}Fe_{0.04}Sc_{0.01}O_4$	215	0.00133	0.00254
$MgAl_{1.95}Fe_{0.03}Sc_{0.02}O_4$	254	0.00101	0.00261
$MgAl_{1.95}Fe_{0.02}Sc_{0.03}O_4$	276	0.00106	0.00255
$MgAl_{1.95}Fe_{0.01}Sc_{0.04}O_4$	297	0.00115	0.00371
$MgAl_{1.95}Sc_{0.05}O_4$	200	0.00107	0.00299

Typical super-paramagnetic ‘S’-like shape of hysteresis loops were observed in some samples .Those ‘S’-like shape loops can be divided into two parts: curvature parts and linear parts. The linear parts are attributed to the antiferromagnetic parts of the samples, while the curvature parts may contribute to the change of the inversion parameter induced by the preparation techniques when the particle size decreases to nanoscale. This is a description nearly corresponds with [119].

It is observed from figure (4.18) that the saturation magnetization initially increase for the samples ($MgAl_{1.95}Fe_{0.04}Sc_{0.01}O_4$) with the increasing of Sc^{+3} ions and decrease of Fe^{+3} ions concentration in the $MgAl_2O_4$ host lattice as compared with the undoped $MgAl_2O_4$ sample. Due to a small separation between Fe^{+3} and Sc^{+3} ions which results increase of local magnetization with the Fe^{+3} and Sc^{+3} groups, which

are mediated by F-center exchanging coupling (FCE) interactions [120], and then start to decrease suggesting that further increase in the Sc^{+3} ions and decrease in the Fe^{+3} ions may results super-exchange interactions between Fe^{+3} and Sc^{+3} ions mediated by oxygen ions. This super-exchange interaction results the antiferromagnetic ordering, which minimize the FM ordering in the Fe^{+3} and Sc^{+3} doped $MgAl_2O_4$ host lattice.

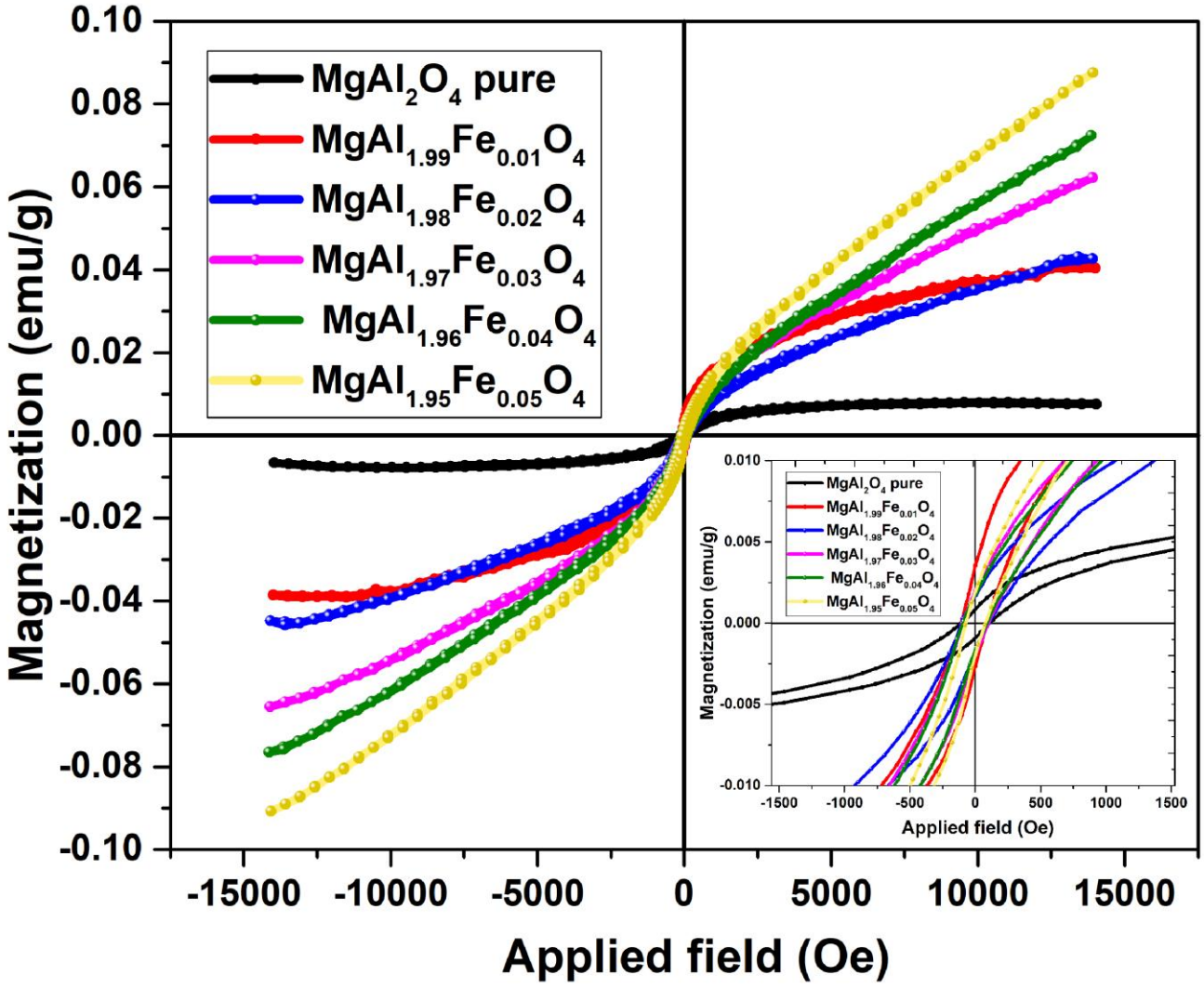

Figure 4.17 Hysteresis loops at 800 °C temperature for $MgAl_2O_4$ and $MgAl_{2-x}Fe_{1-x}O_4$ with different the added quantities.

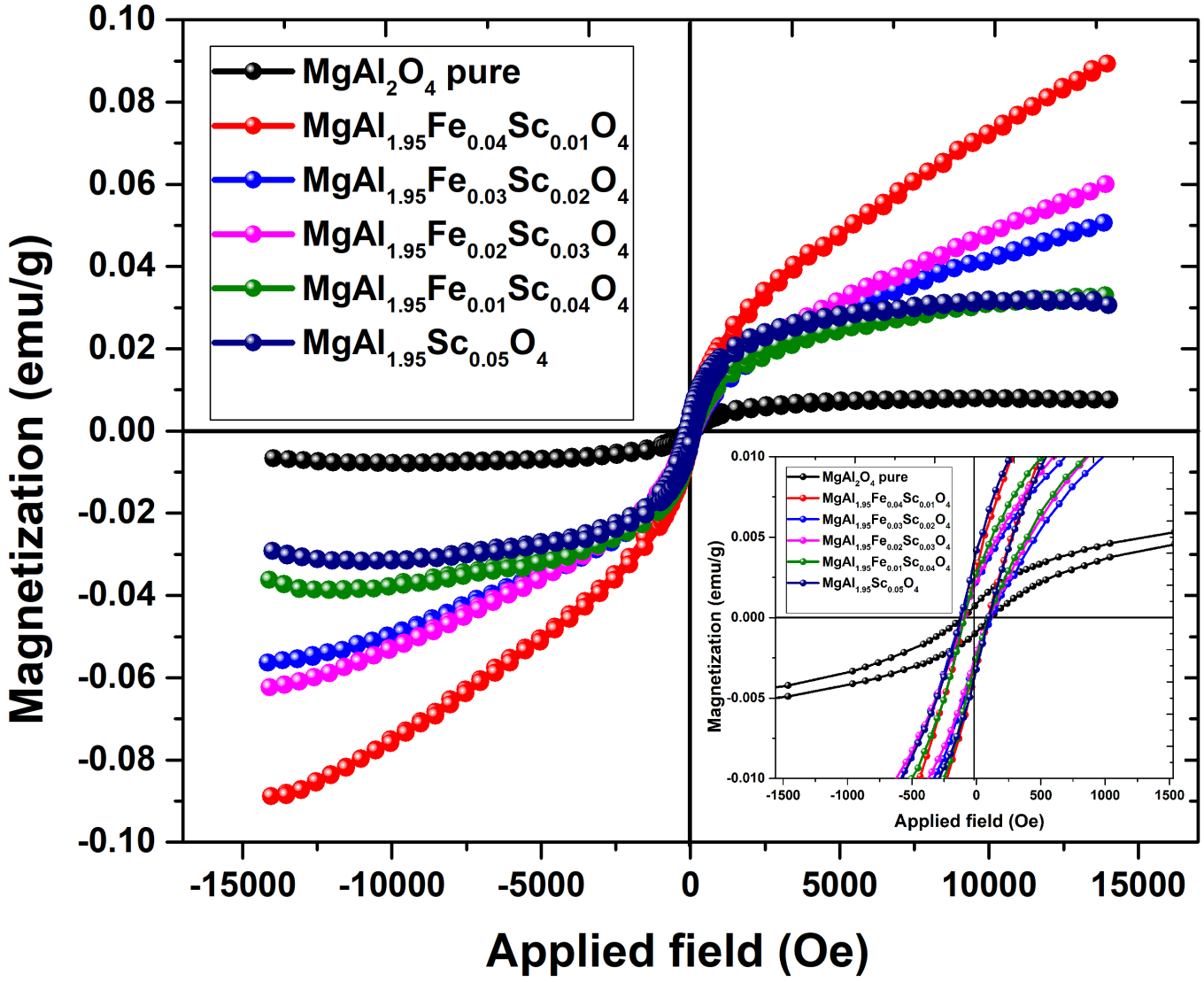

Figure 4.18 Hysteresis loops at 800 °C temperature for $MgAl_2O_4$ and $MgAl_{1.95}Fe_{0.05-x}Sc_xO_4$ with different the added quantities.

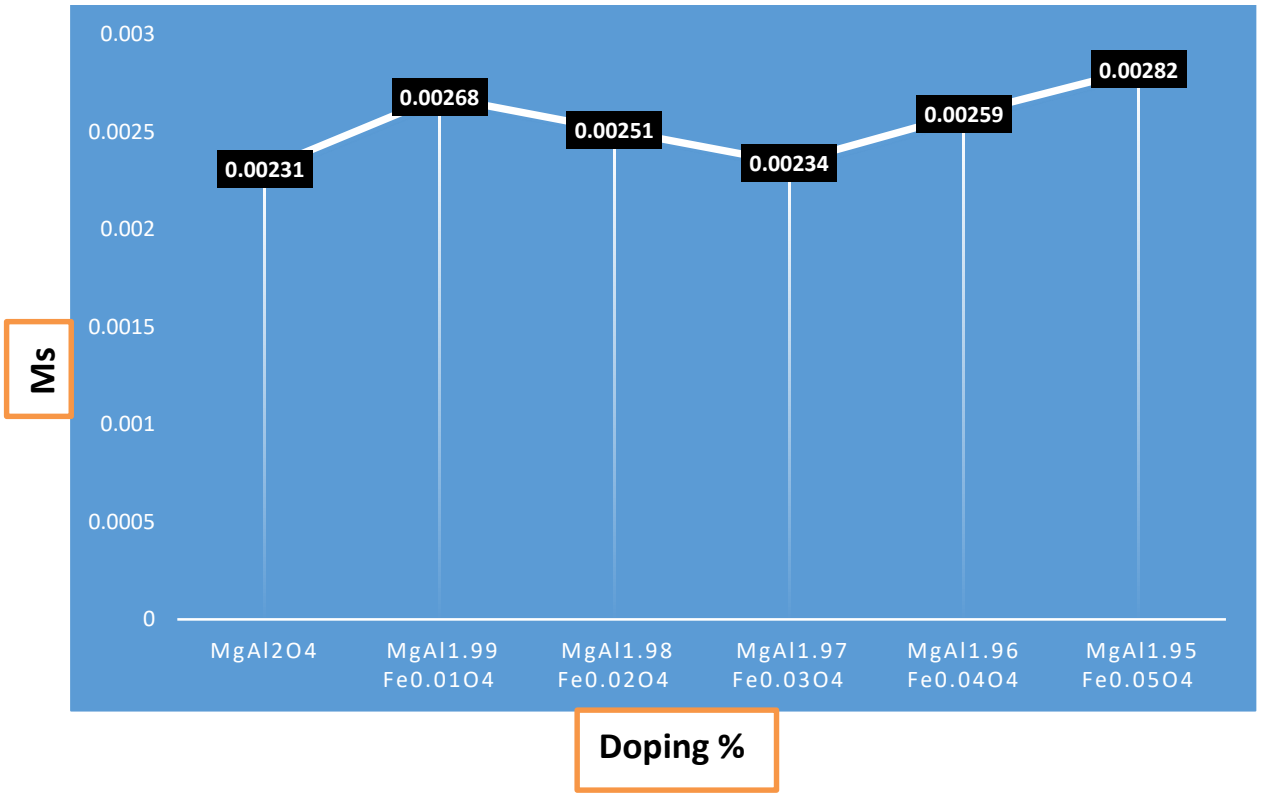

Figure (4-19) The value of Ms with different doping concentration of Fe^{+3} ions.

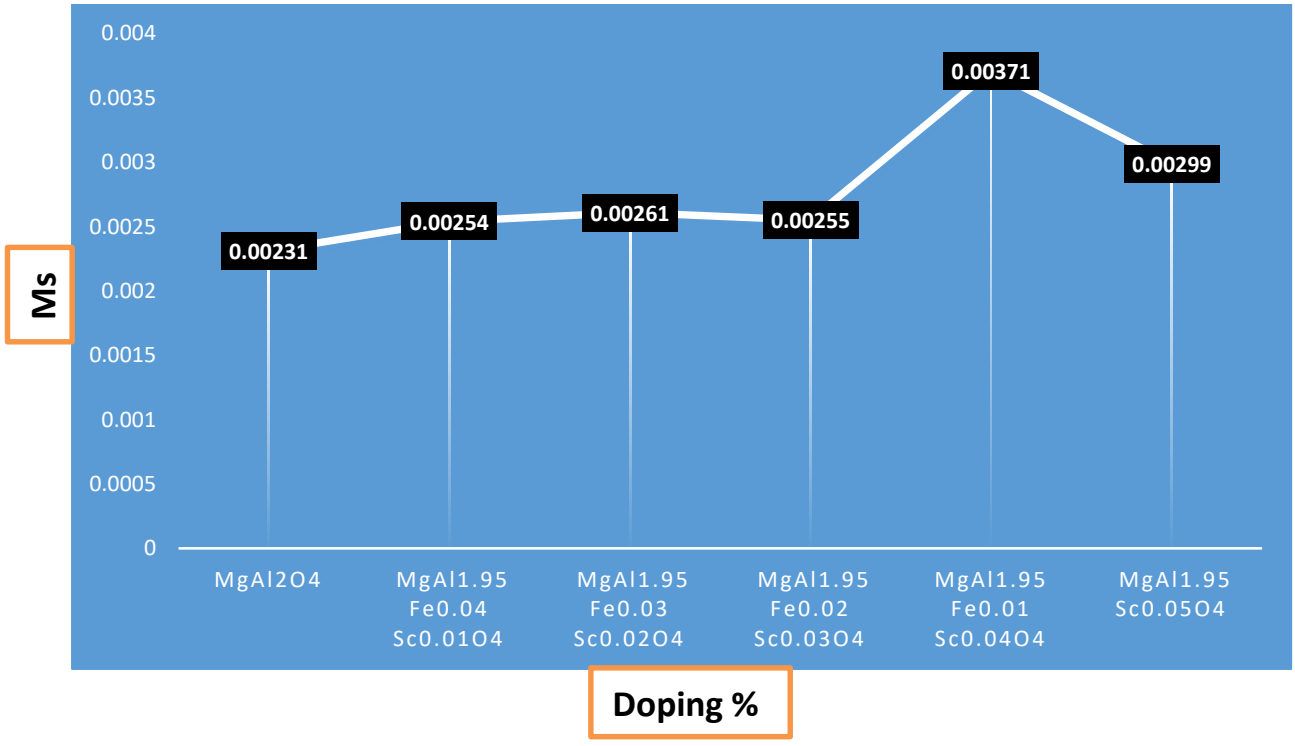

Figure (4-20) The value of Ms with different doping concentration of Sc^{+3} ions.

Chapter 5

Conclusions & Recommendations

5.1 Conclusions:

The following conclusions have been drawn in accordance with the obtained findings of the current study:

1. Undoped and doped $MgAl_2O_4$ nanopowder were successfully synthesized by modified sol–gel method. All samples have identical crystal structure. In the doped group of $MgAl_{2-x}Fe_xO_4$ and $MgAl_{1.95}Fe_{0.05-y}Sc_yO_4$ samples, the structures have little been changed due to incorporating Fe^{+3} ions an Sc^{+3} ions into the cubic lattice structure of $MgAl_2O_4$. These changes were detected as a little shift to a lower (2θ) companied with an increase in the lattice parameter. In the inter-planar d-spacing and in the crystallite size
2. Despite the large ionic radius of Fe^{+3} ions and Sc^{+3} ions compared to the $MgAl_2O_4$ host lattice structure, the sol-gel method is suitable for preparing undoped and doped samples with little changes in their structures and sufficient change in their magnetic properties according to the doped groups.
3. The peaks appearing in the range of 531-690 cm^{-1} in the FTIR spectrum obtained from the synthesized material indicate the formation of spinel. The molecular structures for the doped and undoped samples of $MgAl_{2-x}Fe_xO_4$ and $MgAl_{1.95}Fe_{0.05-y}Sc_yO_4$ samples have the same framework, but the doped samples have a variation in the broad of peaks. Furthermore, there were variation in the intensities due to incorporate of $Fe^{+3}$and Sc^{+3} ions the fingerprint area between 1000-400cm^{-1}. The lattice vibrations were also affected by the cation mass and bonding power.

4. The morphology of the undoped and doped groups have been clarified the agglomeration of the spherical or quasi-spherical nanoparticles by employing the SEM and TEM. The purity of all samples have been confirmed.
5. The topographical images obtained by STM indicate that doped and undoped $MgAl_2O_4$ powders consist of nanometer-sized individual particles and of particle clusters. However, the doped samples have a variation in the dark and bright spots at a scale that is characterized by the magnetic exchange length. The test may contribute to an improved understanding of the basic physical phenomena.
6. The hysteresis loops at temperature 800 °C have different magnetization Ms according to the doping concentration, which can be observed in $MgAl_2O_4$. The maximum M_s value in the $MgAl_{2-x}Fe_xO_4$ samples group was in ($MgAl_{1.95}Fe_{0.05}O_4$) sample, while the maximum M_s value in the $MgAl_{1.95}Fe_{0.05-y}Sc_yO_4$ samples group was in ($MgAl_{1.95}Sc_{0.05}O_4$) sample.

5.2 Recommendation:

1. Synthesis $MgAl_{2-x}Fe_xO_4$ and $MgAl_{1.95}Fe_{0.05-y}Sc_yO_4$ groups with different polybasic hydroxyl carboxylic acid and Caleinated with different temperatures and rate °C\min to investigate their effect on the structural, morphology and magnetic properties.
2. Analysis the electronic structure and electrical behavior of undoped and doped sample for $MgAl_2O_4$ by scanning tunneling spectroscopy (STS) and photoluminescence properties.
3. Study the effect of increase the concentration of Fe ions with constant and varying doping of rare earth Sc^{+3} in the $MgAl_{2-x}Fe_xO_4$ at $x > 0.05$ and investigate their effect on structure, electronic and magnetic properties.
4. Doping ($MgAl_{2-x}TM_xO_4$) group with different transition ions less and greater than an ionic radius to investigate the effect of these ions on the structure, Uv and Pl.

Reference

Reference

1. Kingery, W. D., Bowen, H. K., & Uhlmann, D. R. (1976). *Introduction to ceramics* (Vol. 17). John wiley & sons.
2. Sindel, M., Travitzky, N. A., & Claussen, N. (1990). Influence of Magnesium-Aluminum Spinel on the Directed Oxidation of Molten Aluminum Alloys. *Journal of the American Ceramic Society*, *73*(9), 2615-2618.
3. Salmones, J., Galicia, J. A., Wang, J. A., Valenzuela, M. A., & Aguilar-Rios, G. (2000). Synthesis and characterization of nanocrystallite MgAl2O4 spinels as catalysts support. *Journal of materials science letters*, 1033-1037.
4. Lavina, B., Salviulo, G., & Giusta, A. D. (2002). Cation distribution and structure modelling of spinel solid solutions. *Physics and Chemistry of Minerals*, *29*(1), 10-18.
5. Ganesh, I., Johnson, R., Rao, G. V. N., Mahajan, Y. R., Madavendra, S. S., & Reddy, B. M. (2005). Microwave-assisted combustion synthesis of nanocrystalline MgAl2O4 spinel powder. *Ceramics international*, *31*(1), 67-74.
6. Lee, M. (2007). *Ionic conductivity measurement in magnesium aluminate spinel and solid state galvanic cell with magnesium aluminate electrolyte* (Doctoral dissertation, University of Colorado at Boulder).
7. Hosseini, S. M. (2008). Structural, electronic and optical properties of spinel MgAl2O4 oxide. *Physica status solidi (b)*, *245*(12), 2800-2807.
8. Wilding, M. C. (2008). Aluminates. In *Ceramic and glass materials* (pp. 49-70). Springer, Boston, MA.

9. Ivanov, V. V., & Talanov, V. M. (2010). Principle of modular crystal structure. *Crystallography Reports*, *55*(3), 362-376.
10. Ivanov, V. V., & Talanov, V. M. (2013). A symbolic description of module packings and crystal structure codes. *Journal of Structural Chemistry*, *54*(2), 408-430.
11. Nuernberg, G. D., Foletto, E. L., Probst, L. F., Campos, C. E., Carreño, N. L., & Moreira, M. A. (2012). A novel synthetic route for magnesium aluminate (MgAl2O4) particles using metal–chitosan complexation method. *Chemical engineering journal*, *193*, 211-214.
12. Anghel, S. (2011). *Optical processes in α-ZnAl2S4 spinel-type single crystals doped by transition metals ions: ti, Co et V* (Doctoral dissertation, Université Claude Bernard-Lyon I).
13. Ahmed, M. A. A. (2017). *A review on the properties and uses of ferrite magnet* (Doctoral dissertation, Sudan University of Science and Technology).
14. Lakehal, A., Benrabah, B., Bouaza, A., Dalache, C., & Hadj, B. (2018). Tuning of the physical properties by various transition metal doping in Co3O4: TM (TM= Ni, Mn, Cu) thin films: A comparative study. *Chinese journal of physics*, *56*(5), 1845-1852.
15. Gritsyna, V., & Kazarinov, Y. (2018). Effects of transition-metal-doping on the radio-luminescence properties of magnesium aluminate spinel crystals. *Nuclear Instruments and Methods in Physics Research Section B: Beam Interactions with Materials and Atoms*, *3*, 7-12.
16. Osipov, V. V., Il'ichev, N. N., Shitov, V. A., Pashinin, P. P., Solomonov, V. I., Sidorin, A. V., ... & Gulyamova, E. S. (2019, December). Fabrication and characterization of highly transparent Fe2+: MgAl2O4 ceramics. In *XIV*

International Conference on Pulsed Lasers and Laser Applications (Vol. 11322, p. 113220M). International Society for Optics and Photonics.

17. Satalkar, M., & Kane, S. N. (2016, October). On the study of Structural properties and Cation distribution of Zn0. 75-xNixMg0. 15Cu0. 1Fe2O4 nano ferrite: Effect of Ni addition. In *Journal of Physics: Conference Series* (Vol. 755, No. 1, p. 012050). IOP Publishing.
18. Sai, R., Kulkarni, S. D., Bhat, S. S., Sundaram, N. G., Bhat, N., & Shivashankar, S. A. (2015). Controlled inversion and surface disorder in zinc ferrite nanocrystallites and their effects on magnetic properties. *RSC advances*, *5*(14), 10267-10274.
19. Sander, D., Valenzuela, S. O., Makarov, D., Marrows, C. H., Fullerton, E. E., Fischer, P., ... & Berger, A. (2017). The 2017 magnetism roadmap. *Journal of Physics D: Applied Physics*, *50*(36), 363001.
20. Tatarchuk, T., Al-Najar, B., Bououdina, M., & Ahmed, M. A. (2019). Catalytic and photocatalytic properties of oxide spinels. *Handbook of ecomaterials*, *3*, 1701-1750.
21. Talebi, R., Khademolhoseini, S., & Rahnamaeiyan, S. (2016). Preparation and characterization of the magnesium aluminate nanoparticles via a green approach and its photocatalyst application. *Journal of Materials Science: Materials in Electronics*, *27*(2), 1427-1432.
22. Nassar, M. Y., Ahmed, I. S., & Samir, I. (2014). A novel synthetic route for magnesium aluminate (MgAl2O4) nanoparticles using sol–gel auto combustion method and their photocatalytic properties. *Spectrochimica Acta Part A: Molecular and Biomolecular Spectroscopy*, *131*, 329-334.

23. Sanjabi, S., & Obeydavi, A. (2015). Synthesis and characterization of nanocrystalline MgAl2O4 spinel via modified sol–gel method. *Journal of Alloys and Compounds*, *645*, 535-540.
24. Ewais, E. M., El-Amir, A. A., Besisa, D. H., Esmat, M., & El-Anadouli, B. E. (2017). Synthesis of nanocrystalline MgO/MgAl2O4 spinel powders from industrial wastes. *Journal of Alloys and Compounds*, *691*, 822-833.
25. Akbar Hosseini, S. (2017). Investigation of the structural, photocatalytic and magnetic properties of MgAl2O4/NiTiO3 nanocomposite synthesized via sol–gel method. *Journal of Materials Science: Materials in Electronics*, *28*(14), 10765-10771.
26. Rahaman, M. N. (2017). *Ceramic processing*. CRC press.
27. Pierre, A. C. (2020). *Introduction to sol-gel processing*. Springer Nature.
28. Cao, G. (2004). *Nanostructures & nanomaterials: synthesis, properties & applications*. Imperial college press.
29. Kelsall, R., Hamley, I. W., & Geoghegan, M. (Eds.). (2005). *Nanoscale science and technology*. John Wiley & Sons.
30. Patil, K. C. (2008). *Chemistry of nanocrystalline oxide materials*: combustion synthesis, properties and applications. World Scientific.
31. Kharton, V. V. (Ed.). (2012). *Solid state electrochemistry II: electrodes, interfaces and ceramic membranes*. John Wiley & Sons.
32. Tsurkan, V., von Nidda, H. A. K., Deisenhofer, J., Lunkenheimer, P., & Loidl, A. (2021). On the complexity of spinels: Magnetic, electronic, and polar ground states. *Physics Reports*.
33. Liu, M., Jain, A., Rong, Z., Qu, X., Canepa, P., Malik, R., ... & Persson, K. A. (2016). Evaluation of sulfur spinel compounds for multivalent battery cathode applications. *Energy & Environmental Science*, *9*(10), 3201-3209.

34. Pilania, G., Kocevski, V., Valdez, J. A., Kreller, C. R., & Uberuaga, B. P. (2020). Prediction of structure and cation ordering in an ordered normal-inverse double spinel. *Communications Materials*, *1*(1), 1-11.
35. Ganesh, I. (2013). A review on magnesium aluminate (MgAl2O4) spinel: synthesis, processing and applications. *International Materials Reviews*, *58*(2), 63-112.
36. El Jabbar, Y., Lakhlifi, H., El Ouatib, R., Er-Rakho, L., Guillemet-Fritsch, S., & Durand, B. (2021). Preparation and characterisation of green nano-sized ceramic pigments with the spinel structure AB2O4 (A= Co, Ni and B= Cr, Al). *Solid State Communications*, 114394.
37. Hosseini, S. M. (2008). Structural, electronic and optical properties of spinel MgAl2O4 oxide. *physica status solidi (b)*, *245*(12), 2800-2807.
38. Zhang, W., Bock, D. C., Pelliccione, C. J., Li, Y., Wu, L., Zhu, Y., ... & Wang, F. (2016). Insights into ionic transport and structural changes in magnetite during multiple-electron transfer reactions. Advanced Energy Materials, 6(10), 1502471.
39. Naka, T., Nakane, T., Ishii, S., Nakayama, M., Ohmura, A., Ishikawa, F., ... & Uchikoshi, T. (2020). Cluster glass transition and relaxation in random spinel CoGa2O4. *arXiv preprint arXiv:2010.13291*.
40. Waychunas, G. A. (2018). Crystal chemistry of oxides and oxyhydroxides. Oxide Minerals, 11-68.
41. Iqbal, M. J., Ismail, B., Rentenberger, C., & Ipser, H. (2011). Modification of the physical properties of semiconducting MgAl2O4 by doping with a binary mixture of Co and Zn ions. *Materials Research Bulletin*, *46*(12), 2271-2277.

42. Issa, B., Obaidat, I. M., Albiss, B. A., & Haik, Y. (2013). Magnetic nanoparticles: surface effects and properties related to biomedicine applications. *International journal of molecular sciences*, *14*(11), 21266-21305.

43. Isea, R., Vegas, A., & Ramos-Gallardo, A. (1998). Distribution of the MM distances in the oxides of the group 13 elements and their spinels and delafossites. *Acta Crystallographica Section B: Structural Science*, *54*(1), 35-40.

44. Heiba, Z. K., Mohamed, M. B., Arda, L., & Dogan, N. (2015). Cation distribution correlated with magnetic properties of nanocrystalline gadolinium substituted nickel ferrite. *Journal of Magnetism and Magnetic Materials*, *391*, 195-202.

45. Sickafus, K. E., Wills, J. M., & Grimes, N. W. (1999). Structure of spinel. *Journal of the American Ceramic Society*, *82*(12), 3279-3292.

46. .Murphy, S. T., Uberuaga, B. P., Ball, J. B., Cleave, A. R., Sickafus, K. E., Smith, R., & Grimes, R. W. (2009). Cation diffusion in magnesium aluminate spinel. *Solid State Ionics*, *180*(1), 1-8.

47. Cox, P. A. (2010). *Transition metal oxides: an introduction to their electronic structure and properties* (Vol. 27). Oxford university press.

48. Gritsyna, V. T., Afanasyev-Charkin, I. V., Kazarinov, Y. G., & Sickafus, K. E. (2006). Optical properties of magnesium aluminate spinel crystals implanted with helium ions. *Vacuum*, *81*(2), 174-178.

49. Sharafat, S., Ghoniem, N. M., Cooke, P. I., Martin, R. C., Najmabadi, F., Schultz, K. R., ... & TITAN Team. (1993). Materials analysis of the TITAN-I reversed-field-pinch fusion power core. *Fusion engineering and design*, *23*(2-3), 99-113.

50. Bauerfeind, K. C., Roß, R., & Bredow, T. (2020). Theoretical Study of Polar Spinel Surfaces: Effect of Termination and Cation Inversion on Structure and Stability. *The Journal of Physical Chemistry C*, *124*(52), 28520-28530.
51. Dekkers, R., & Woensdregt, C. F. (2002). Crystal structural control on surface topology and crystal morphology of normal spinel (MgAl2O4). *Journal of crystal growth*, *236*(1-3), 441-454.
52. Lee, M. (2007). *Ionic conductivity measurement in magnesium aluminate spinel and solid state galvanic cell with magnesium aluminate electrolyte* (Doctoral dissertation, University of Colorado at Boulder).
53. Alvar, E. N., Rezaei, M., & Alvar, H. N. (2010). Synthesis of mesoporous nanocrystalline MgAl2O4 spinel via surfactant assisted precipitation route. *Powder Technology*, *198*(2), 275-278.
54. Saberi, A., Golestani-Fard, F., Willert-Porada, M., Negahdari, Z., Liebscher, C., & Gossler, B. (2009). A novel approach to synthesis of nanosize MgAl2O4 spinel powder through sol–gel citrate technique and subsequent heat treatment. *Ceramics International*, *35*(3), 933-937.
55. Ganesh, I., Reddy, G. J., Sundararajan, G., Olhero, S. M., Torres, P. M., & Ferreira, J. M. (2010). Influence of processing route on microstructure and mechanical properties of MgAl2O4 spinel. *Ceramics International*, *36*(2), 473-482.
56. Gilks, D., Nedelkoski, Z., Lari, L., Kuerbanjiang, B., Matsuzaki, K., Susaki, T., ... & Lazarov, V. K. (2016). Atomic and electronic structure of twin growth defects in magnetite. *Scientific reports*, *6*(1), 1-8.
57. Goldstein, A. (2012). Correlation between MgAl2O4-spinel structure, processing factors and functional properties of transparent parts (progress review). *Journal of the European Ceramic Society*, *32*(11), 2869-2886.

58. Irifune, T., Zou, Y., Greaux, S., Zhou, C., Whitaker, M. L., Higo, Y., & Li, B. (2012, December). Ultrasonic elastic wave velocity measurements of polycrystalline MgAl2O4 spinel at high pressure and high temperature. In *AGU Fall Meeting Abstracts* (Vol. 2012, pp. MR43C-2334).
59. Gracia, L., Beltrán, A., Andrés, J., Franco, R., & Recio, J. M. (2002). Quantum-mechanical simulation of MgAl 2 O 4 under high pressure. *Physical Review B*, *66*(22), 224114.
60. Wilding, M. C. (2008). Aluminates. In *Ceramic and glass materials* (pp. 49-70). Springer, Boston, MA.
61. Wilding, M. C. (2008). Aluminates. In *Ceramic and glass materials* (pp. 49-70). Springer, Boston, MA.

62. Ball, J. A., Pirzada, M., Grimes, R. W., Zacate, M. O., Price, D. W., & Uberuaga, B. P. (2005). Predicting lattice parameter as a function of cation disorder in MgAl2O4 spinel. *Journal of Physics: Condensed Matter*, *17*(48), 7621.
63. Ball, J. A., Pirzada, M., Grimes, R. W., Zacate, M. O., Price, D. W., & Uberuaga, B. P. (2005). Predicting lattice parameter as a function of cation disorder in MgAl2O4 spinel. *Journal of Physics: Condensed Matter*, *17*(48), 7621.
64. Wang, L., & Liang, T. (2012). Ceramics for high level radioactive waste solidification. *Journal of Advanced Ceramics*, *1*(3), 194-203.
65. Ha, S. D., & Ramanathan, S. (2011). Adaptive oxide electronics: A review. *Journal of applied physics*, *110*(7), 14.
66. Gutfleisch, O., Willard, M. A., Brück, E., Chen, C. H., Sankar, S. G., & Liu, J. P. (2011). Magnetic materials and devices for the 21st century: stronger, lighter, and more energy efficient. *Advanced materials*, *23*(7), 821-842.

67. Yu, X., Hu, Y., Zhou, L., Cao, F., Yang, Y., Liang, T., & He, J. (2011). Research progress of nanostructured materials for heterogeneous catalysis. *Current Nanoscience*, *7*(4), 576-586.
68. Doble, M., Rollins, K., & Kumar, A. (2010). *Green chemistry and engineering*. Academic Press.
69. Khomskii, D. (2014). *Transition metal compounds*. Cambridge University Press.
70. Reddy, B. M., Reddy, G. K., Khan, A., & Ganesh, I. (2007). Synthesis of monophasic Ce0.5Zr0.5O2 solid solution by microwave-induced combustion method. *Journal of materials science*, *42*(10), 3557-3563.
71. Yogapriya, M. (2012). *SOL-GEL Synthesis, Crystal Structure, Magnetic, Electronic and Optical Properties in Bi2+ xAxD4-3xO7+ δ (A= Al, Ce, Yb, Ga; D= Ni, Pd) Nanocomposite Oxides* (Doctoral dissertation).
72. Liang, S., Wang, H., Li, Y., Qin, H., Luo, Z., Huang, B., ... & Chen, L. (2020). Rare-earth based nanomaterials and their composites as electrode materials for high performance supercapacitors: a review. *Sustainable Energy & Fuels*, *4*(8), 3825-3847.
73. Furlani, E. P. (2001). *Permanent magnet and electromechanical devices: materials, analysis, and applications*. Academic press.
74. Du Merac, M. R. (2014). *The role of impurities, LIF, and processing on the sintering, microstructure, and optical properties of transparent polycrystalline magnesium aluminate (MgAl2O4) spinel*. Colorado School of Mines.
75. Krishnan, K. M. (2016). *Fundamentals and applications of magnetic materials*. Oxford University Press.

76. Dutta, D. P., & Sharma, G. (2011). Synthesis and magnetic behavior of spinel FeAl2O4 nanoparticles. *Materials Science and Engineering: B*, *176*(2), 177-180.
77. Goldman, A. (2012). *Handbook of modern ferromagnetic materials* (Vol. 505). Springer Science & Business Media.
78. Fabrykiewicz, P., Stękiel, M., Sosnowska, I., & Przeniosło, R. (2017). Deformations of the α-Fe2O3 rhombohedral lattice across the Néel temperature. *Acta Crystallographica Section B: Structural Science, Crystal Engineering and Materials*, *73*(1), 27-32.
79. Heck, C. (2013). *Magnetic materials and their applications*. Elsevier.
80. Chen, C. W. (2013). *Magnetism and metallurgy of soft magnetic materials*. Courier Corporation.
81. Cullity, B. D., & Graham, C. D. (2011). *Introduction to magnetic materials*. John Wiley & Sons.
82. Biswas, A., Bayer, I. S., Biris, A. S., Wang, T., Dervishi, E., & Faupel, F. (2012). Advances in top–down and bottom–up surface nanofabrication: Techniques, applications & future prospects. *Advances in colloid and interface science*, *170*(1-2), 2-27.
83. Rashad, M. M., Zaki, Z. I., & El-Shall, H. (2009). A novel approach for synthesis of nanocrystalline MgAl 2 O 4 powders by co-precipitation method. *Journal of Materials Science*, *44*(11), 2992-2998.
84. Xu, J., Yang, H., Fu, W., Du, K., Sui, Y., Chen, J., ... & Zou, G. (2007). Preparation and magnetic properties of magnetite nanoparticles by sol–gel method. *Journal of Magnetism and magnetic Materials*, *309*(2), 307-311.
85. Brinker, C. J., & Scherer, G. W. (2013). *Sol-gel science: the physics and chemistry of sol-gel processing*. Academic press.

86. Danks, A. E., Hall, S. R., & Schnepp, Z. J. M. H. (2016). The evolution of 'sol–gel'chemistry as a technique for materials synthesis. *Materials Horizons*, *3*(2), 91-112.
87. Carter, C. B., & Norton, M. G. (2013). Sols, gels, and organic chemistry. In *Ceramic Materials* (pp. 411-422). Springer, New York, NY.
88. Raab, C., Simkó, M., Fiedeler, U., Nentwich, M., & Gazsó, A. (2011). Production of nanoparticles and nanomaterials (NanoTrust Dossier No. 006en–February 2011).
89. Sumida, K., Liang, K., Reboul, J., Ibarra, I. A., Furukawa, S., & Falcaro, P. (2017). Sol–gel processing of metal–organic frameworks. *Chemistry of Materials*, *29*(7), 2626-2645.
90. Chandradass, J., Balasubramanian, M., Bae, D. S., Kim, J., & Kim, K. H. (2010). Effect of water to surfactant ratio (R) on the particle size of MgAl2O4 nanoparticle prepared via reverse micelle process. *Journal of alloys and compounds*, *491*(1-2), L25-L28.
91. Wiglusz, R. J., Grzyb, T., Lis, S., & Strek, W. (2010). Hydrothermal preparation and photoluminescent properties of MgAl2O4: Eu3+ spinel nanocrystals. *Journal of luminescence*, *130*(3), 434-441.
92. Torkian, L., Amini, M. M., & Bahrami, Z. (2010). Synthesis and characterization of a nanorefractory dimetaloxide spinel. *e-Journal of Surface Science and Nanotechnology*, *8*, 112-114.
93. Ianoş, R., Lazău, R., & Barvinschi, P. (2011). Synthesis of Mg1− xCoxAl2O4 blue pigments via combustion route. *Advanced Powder Technology*, *22*(3), 396-400.
94. Tong, J. F., & Chen, D. M. (2012). A novel way to synthesis magnesium aluminate spinel powders by polymer Gel reaction. In *Key Engineering Materials* (Vol. 512, pp. 600-603). Trans Tech Publications Ltd.

95. Nassar, M. Y., Ahmed, I. S., & Samir, I. (2014). A novel synthetic route for magnesium aluminate (MgAl2O4) nanoparticles using sol–gel auto combustion method and their photocatalytic properties. *Spectrochimica Acta Part A: Molecular and Biomolecular Spectroscopy*, *131*, 329-334.

96. Sanjabi, S., & Obeydavi, A. (2015). Synthesis and characterization of nanocrystalline MgAl2O4 spinel via modified sol–gel method. *Journal of Alloys and Compounds*, *645*, 535-540.

97. Al Mahmood, A., Ali, M. M., Rahman, M., Islam, M. M., & Abdul, M. (2016). Synthesis and Characterization of Sodium (Na) Doped Magnesium Aluminate (MgAl2O4) Nanoparticle by Solution Combustion Method.

98. Habibi, N., Wang, Y., Arandiyan, H., & Rezaei, M. (2017). Low-temperature synthesis of mesoporous nanocrystalline magnesium aluminate (MgAl2O4) spinel with high surface area using a novel modified sol-gel method. *Advanced Powder Technology*, *28*(4), 1249-1257.

99. Ahmad, J., Qadeer Awan, M., Yasmin, R., Sabir, M., Anwar, S., Ehsan Mazhar, M., & Hamad Bukhari, S. (2018). Infrared reflectance spectroscopy of MgAl2O4 nanoparticles substituted by K+ ions. *International Journal of Modern Physics B*, *32*(06), 1850067.

100. Motloung, S. V. (2019). Effects of In3+ doping concentration on the structural, morphological and photoluminescence properties of x% In3+: MgAl2O4 nanophosphor prepared via citrate sol-gel method. *Materials Research Express*, *6*(11), 116327.

101. Vorokh, A. S. (2018). Scherrer formula: estimation of error in determining small nanoparticle size. *Наносистемы: физика, химия, математика*, *9*(3).

102. Lee, E. Y., Kim, E. S., & Kim, K. W. (2014). Scanning electron microscopy and energy dispersive X-ray spectroscopy studies on processed

tooth graft material by vacuum-ultrasonic acceleration. *Maxillofacial Plastic and Reconstructive Surgery*, *36*(3), 103.

103. Tang, C. Y., & Yang, Z. (2017). Transmission electron microscopy (TEM). In *Membrane characterization* (pp. 145-159). Elsevier.

104. Wiesendanger, R., & Güntherodt, H. J. (Eds.). (2013). *Scanning tunneling microscopy III: theory of STM and related scanning probe methods* (Vol. 29). Springer Science & Business Media.

105. Voigtländer, B. (2015). *Scanning probe microscopy: Atomic force microscopy and scanning tunneling microscopy*. Springer.

106. Braunovic, M. (2010, October). Characterization techniques for nanostructured contact materials. In *2010 Proceedings of the 56th IEEE Holm Conference on Electrical Contacts* (pp. 1-6). IEEE.

107. Pradeep, A., Priyadharsini, P., & Chandrasekaran, G. (2008). Sol–gel route of synthesis of nanoparticles of MgFe2O4 and XRD, FTIR and VSM study. *Journal of Magnetism and Magnetic Materials*, *320*(21), 2774-2779.

108. Ghanbari, D., Sharifi, S., Naraghi, A., & Nabiyouni, G. (2016). Photo-degradation of azo-dyes by applicable magnetic zeolite Y–Silver–CoFe2O4 nanocomposites. *Journal of Materials Science: Materials in Electronics*, *27*(5), 5315-5323.

109. Li, H., Wei, H. Y., Cui, Y., Sang, R. L., Bu, J. L., Wei, Y. N., ... & Zhao, J. H. (2017). Synthesis and characterisation of MgAl2O4 spinel nanopowders via nonhydrolytic sol–gel route. *Journal of the Ceramic Society of Japan*, *125*(3), 100-104.

110. Mbela, K. (2016). *Synthesis and magnetic properties of Sn, Mn and Mg substituted Fe (x) Cr (1.8− x) O (3) nano oxides* (Doctoral dissertation).

111. Li, L., Yang, Y., Liu, Z., Jesse, S., Kalinin, S. V., & Vasudevan, R. K. (2016). Correlation between piezoresponse nonlinearity and hysteresis in

ferroelectric crystals at the nanoscale. *Applied Physics Letters*, *108*(17), 172905.

112. Talebi, R., Khademolhoseini, S., & Rahnamaeiyan, S. (2016). Preparation and characterization of the magnesium aluminate nanoparticles via a green approach and its photocatalyst application. *Journal of Materials Science: Materials in Electronics*, *27*(2), 1427-1432.

113. Sundaresan, A., Bhargavi, R., & Rangarajan, N. (2006). U. Sid desh, and CNR Rao,"Ferromagnetism as a univer sal feature of nanoparticles of the otherwise nonmag netic oxides,". *Phys. Rev. B*, *74*(16), 161304.

114. Sawai, S., & Uchino, T. (2012). Visible photoluminescence from MgAl2O4 spinel with cation disorder and oxygen vacancy. *Journal of Applied Physics*, *112*(10), 103523.

115. Beltran, J. I., Muñoz, M. C., & Hafner, J. (2008). Structural, electronic and magnetic properties of the surfaces of tetragonal and cubic HfO2. *New Journal of Physics*, *10*(6), 063031.

116. Elfimov, I. S., Yunoki, S., & Sawatzky, G. A. (2002). Possible path to a new class of ferromagnetic and half-metallic ferromagnetic materials. *Physical review letters*, *89*(21), 216403.

117. Han, M., Wang, Z., Xu, Y., Wu, R., Jiao, S., Chen, Y., & Feng, S. (2018). Physical properties of MgAl2O4, CoAl2O4, NiAl2O4, CuAl2O4, and ZnAl2O4 spinels synthesized by a solution combustion method. *Materials Chemistry and Physics*, *215*, 251-258.

118. Zaki, H. M., Al-Heniti, S. H., & Hashhash, A. (2016). Effect of Al3+ ion addition on the magnetic properties of cobalt ferrite at moderate and low temperatures. *Journal of Magnetism and Magnetic Materials*, *401*, 1027-1032.

119. Saukhimov, A. A., Hobosyan, M. A., Dannangoda, G. C., Zhumabekova, N. N., Almanov, G. A., Kumekov, S. E., & Martirosyan, K. S. (2015). Solution-combustion synthesis and magnetodielectric properties of nanostructured rare earth ferrites. *International Journal of Self-Propagating High-Temperature Synthesis*, *24*(2), 63-71.

120. Kumar, S., Kim, Y. J., Koo, B. H., & Lee, C. G. (2010). Structural and magnetic properties of Ni doped CeO2 nanoparticles. *Journal of Nanoscience and Nanotechnology*, *10*(11), 7204-7207.

Appendices

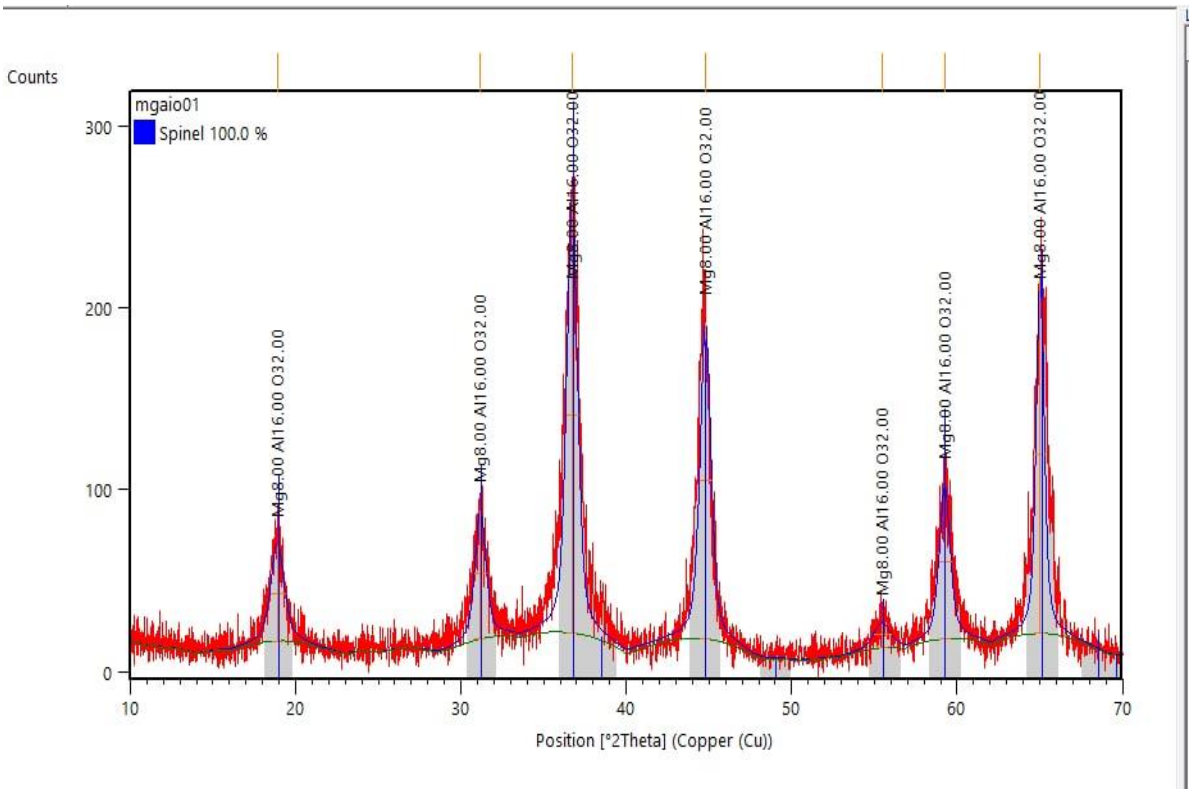

Figure1. X-ray diffraction pattern of $MgAl_2O_4$

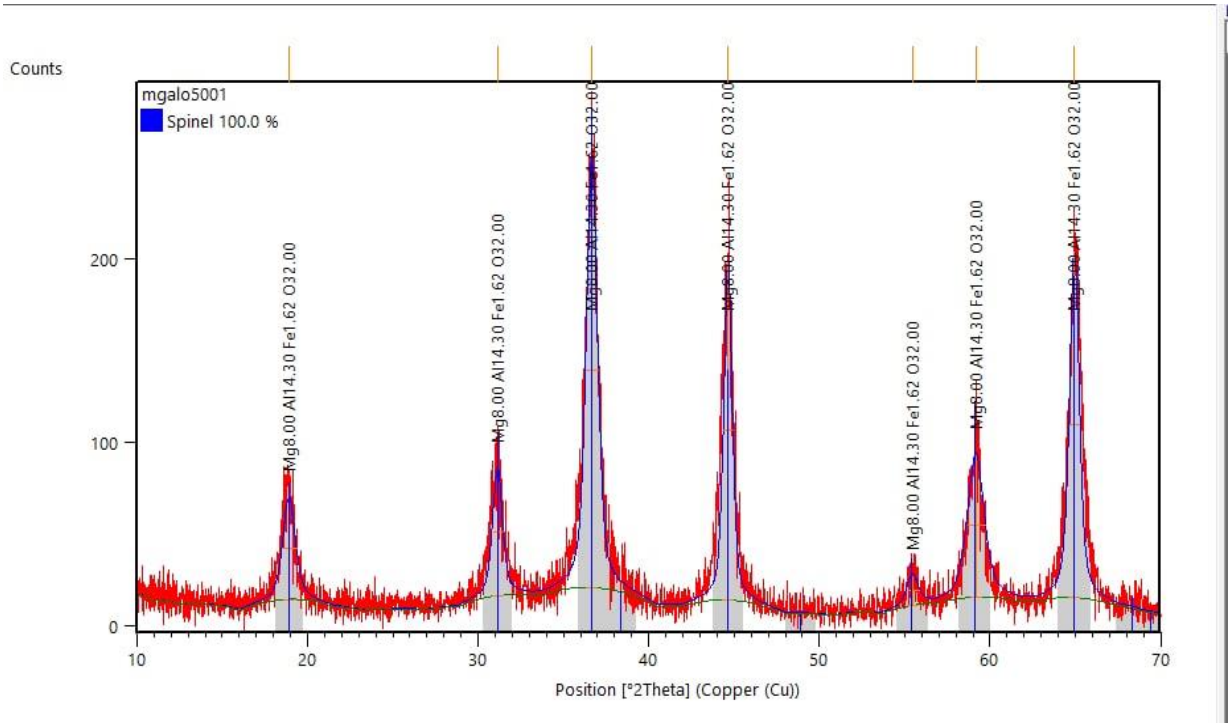

Figure2. X-ray diffraction pattern of $MgAl_{1.95}Fe_{0.05}O_4$

Anchor Scan Parameters

Dataset Name:	mgaio01
File name:	C:\Users\alnaseem\Desktop\New folder (2)\mgaio01\mgaio01.RAW
Comment:	aaaaa
Raw Data Origin:	Shimadzu-binary (.RAW)
Scan Axis:	Gonio
Start Position [°2Th.]:	10.0000
End Position [°2Th.]:	70.0000
Step Size [°2Th.]:	0.0200
Scan Step Time [s]:	0.2000
Scan Type:	Pre-set time
Offset [°2Th.]:	0.0000
Divergence Slit Type:	Fixed
Divergence Slit Size [°]:	1.0000
Specimen Length [mm]:	10.00
Receiving Slit Size [mm]:	0.3000
Measurement Temperature [°C]:	25.00
Anode Material:	Cu
K-Alpha1 [?]:	1.54060
Generator Settings:	30 mA, 40 kV
Diffractometer Number:	0
Goniometer Radius [mm]:	240.00
Dist. Focus-Diverg. Slit [mm]:	91.00
Incident Beam Monochromator:	No
Spinning:	No

Graphics

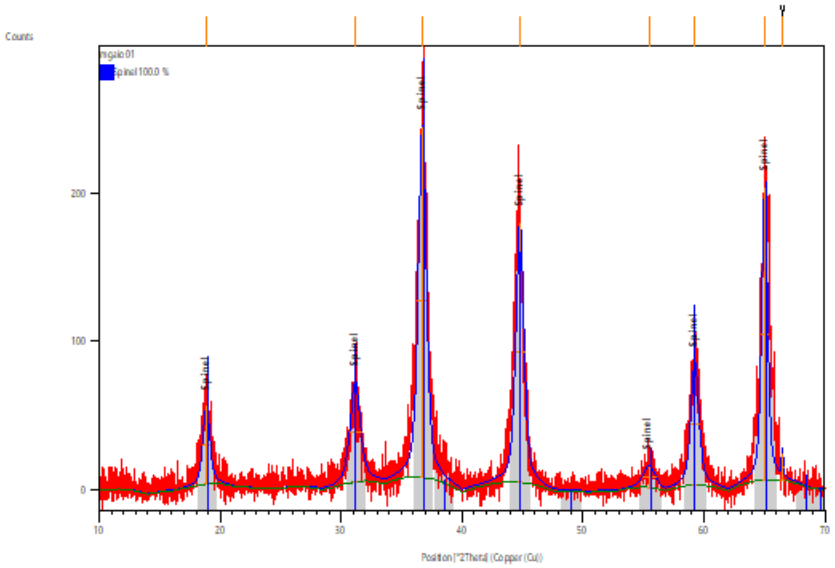

Peak List

Pos.[°2Th.]	Height [cts]	FWHMLeft[°2Th.]	d-spacing [?]	Rel. Int. [%]
18.8654	52.60	0.6720	4.70014	22.20
31.1696	67.33	0.9600	2.86715	28.42
36.7217	236.89	0.7680	2.44539	

100.00
    44.7918   174.35   0.7680   2.02176
73.60
    55.4636   14.51   1.1520   1.65537
6.13
    59.2567   82.58   0.7680   1.55814
34.86
    65.0323   196.89   0.5760   1.43301
83.12
    66.4999   18.03   0.1440   1.40490
7.61

Pattern List

Visible	Ref.Code	Score	Compound Name	Displ.[°2Th]	Scale Fac.	Chem. Formula
*	96-900-7136	92	Spinel	0.000	0.944	Al16.00 Mg8.00 O32..

Document History

Insert Measurement:
- File name = mgaio01.RAW
- Modification time = "23/04/2021 09:30:11 م"
- Modification editor = "alnaseem"

Strip K-Alpha2:
- Method = "Wide Raching"
- Intensity ratio = "0.5"
- Delta wavelength ratio = "0"
- Modification time = "23/04/2021 09:29:39 م"
- Modification editor = "alnaseem"

Subtract Background:
- Add to net scan = "Nothing"
- User defined intensity = "-5"
- Correction method = "Automatic"
- Bending factor = "2"
- Minimum significance = "0.7"
- Minimum tip width = "0"
- Maximum tip width = "1"
- Peak base width = "2"
- Use smoothed input data = "Yes"
- Granularity = "14"
- Modification time = "23/04/2021 09:30:47 م"
- Modification editor = "alnaseem"

Search Peaks:
- Minimum significance = "3"
- Minimum tip width = "0.01"
- Maximum tip width = "1"
- Peak base width = "3"
- Method = "Minimum 2nd derivative"
- Modification time = "23/04/2021 08:59:11 م"
- Modification editor = "alnaseem"

Search & Match:
- Allow pattern shift = "No"
- Auto residue = "Yes"
- Data source = "Profile and peak list"
- Demote unmatched strong = "Yes"
- Multi phase = "Yes"

- Restriction set = "Untitled"
- Restriction = "Restriction set"
- Subset name = ""
- Match intensity = "Yes"
- Two theta shift = "1"
- Identify = "Yes"
- Max. no. of accepted patterns = "5"
- Minimum score = "50"
- Min. new lines / total lines = "60"
- Search depth = "10"
- Minimum new lines = "10"
- Minimum scale factor = "0.1"
- Intensity threshold = "0"
- Use line clustering = "Yes"
- Line cluster range = "1.5"
- Search sensitivity = "1.8"
- Use adaptive smoothing = "Yes"
- Smoothing range = "1.5"
- Threshold factor = "3"
- Modification time = "23/04/2021 09:31:11 م"
- Modification editor = "alnaseem"

Determine Background:
- Add to net scan = "Nothing"
- User defined intensity = "-5"
- Correction method = "Automatic"
- Bending factor = "5"
- Minimum significance = "0.7"
- Minimum tip width = "0"
- Maximum tip width = "1"
- Peak base width = "2"
- Use smoothed input data = "Yes"
- Granularity = "20"
- Modification time = "22/02/2001 10:17:43 ص"
- Modification editor = "PANalytical"

Search Peaks:
- Minimum significance = "2"
- Minimum tip width = "0.01"
- Maximum tip width = "1"
- Peak base width = "2"
- Method = "Minimum 2nd derivative"
- Modification time = "20/02/2001 11:55:18 ص"
- Modification editor = "PANalytical"

Search & Match:
- Allow pattern shift = "No"
- Auto residue = "Yes"
- Data source = "Profile and peak list"
- Demote unmatched strong = "Yes"
- Multi phase = "Yes"
- Restriction set = ""
- Restriction = "None"
- Subset name = ""
- Match intensity = "Yes"
- Two theta shift = "0"
- Identify = "Yes"
- Max. no. of accepted patterns = "5"
- Minimum score = "27"
- Min. new lines / total lines = "40"
- Search depth = "6"
- Minimum new lines = "3"
- Minimum scale factor = "0.06"
- Intensity threshold = "0"
- Use line clustering = "Yes"
- Line cluster range = "1.5"
- Search sensitivity = "1.8"

- Use adaptive smoothing = "Yes"
- Smoothing range = "1.5"
- Threshold factor = "3"
- Modification time = "16/02/2001 11:03:07 ص"
- Modification editor = "PANalytical"

Convert Ref. Pattern to Phase:
- Modification time = "23/04/2021 09:32:50 م"
- Modification editor = "alnaseem"

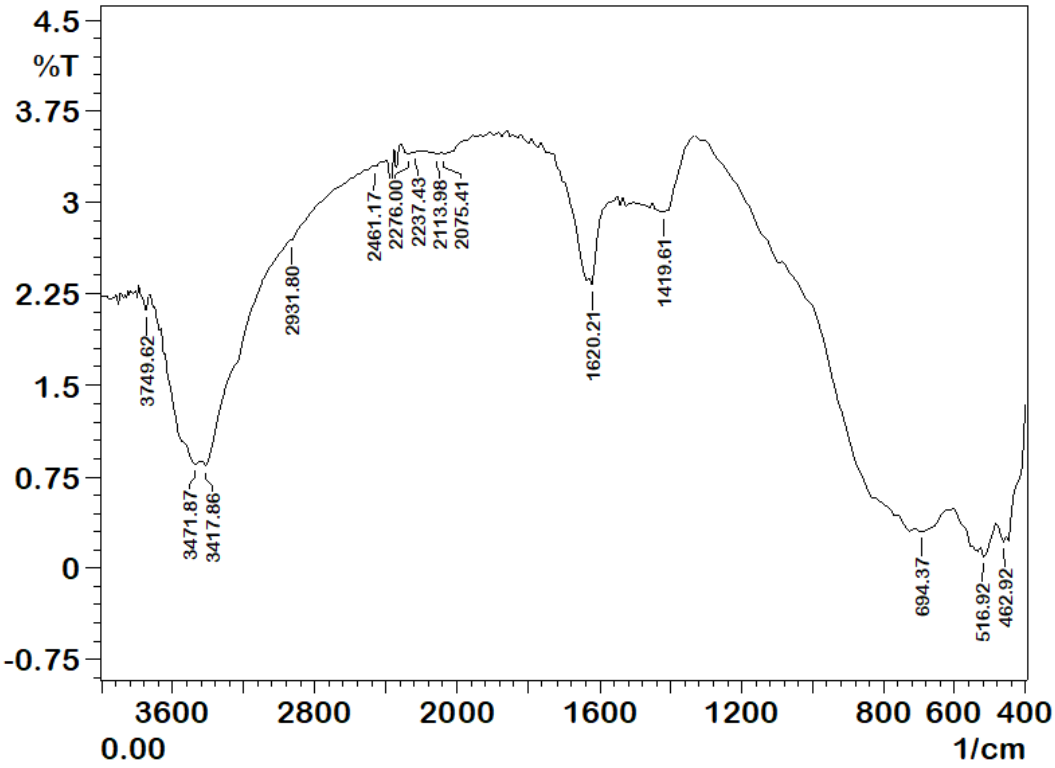

Figure(1). FTIR $MgAl_2O_4$

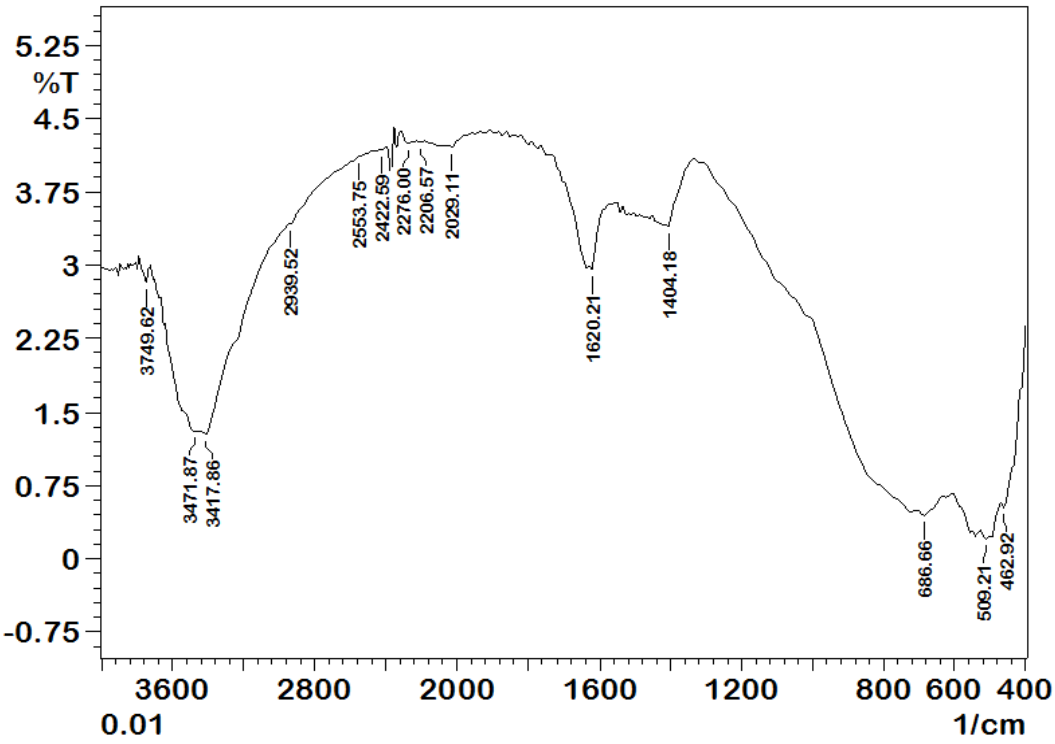

Figure(2). FTIR $MgAl_{1.99}Fe_{0.01}O_4$

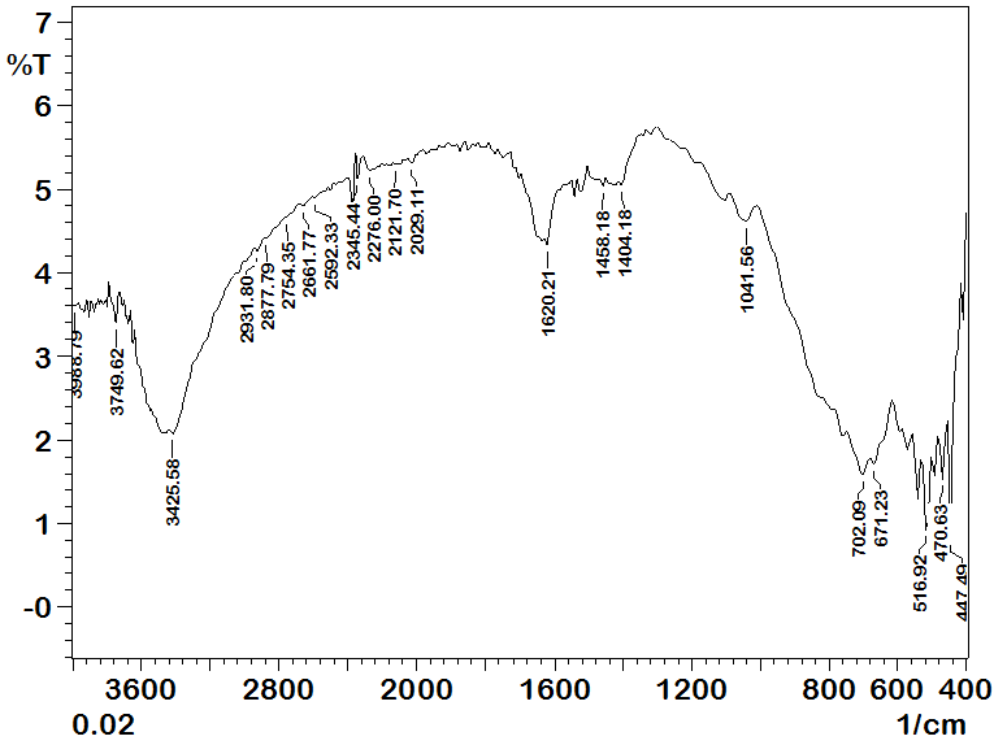

Figure(3). FTIR $MgAl_{1.98}Fe_{0.02}O_4$

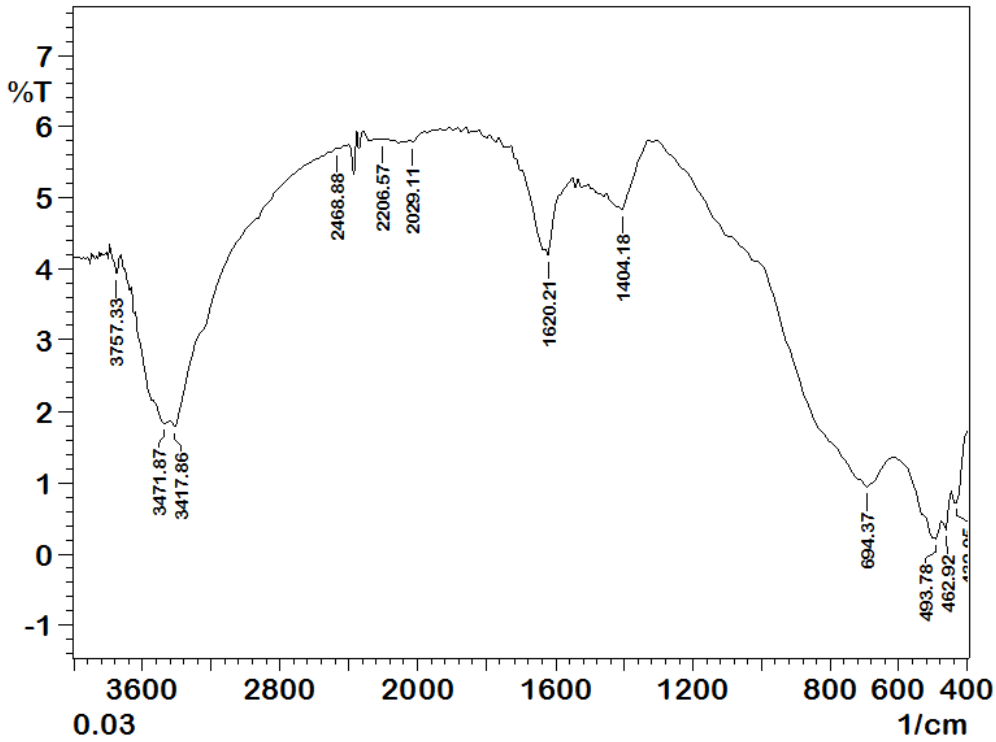

Figure(4). FTIR $MgAl_{1.97}Fe_{0.03}O_4$

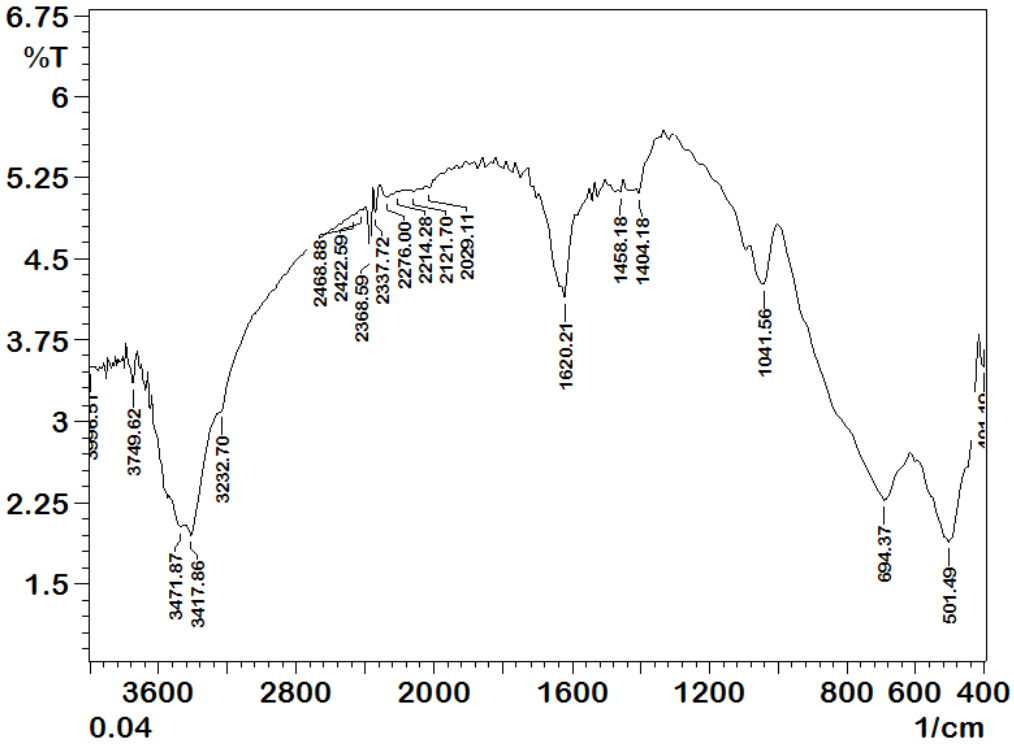

Figure(5). FTIR $MgAl_{1.96}Fe_{0.04}O_4$

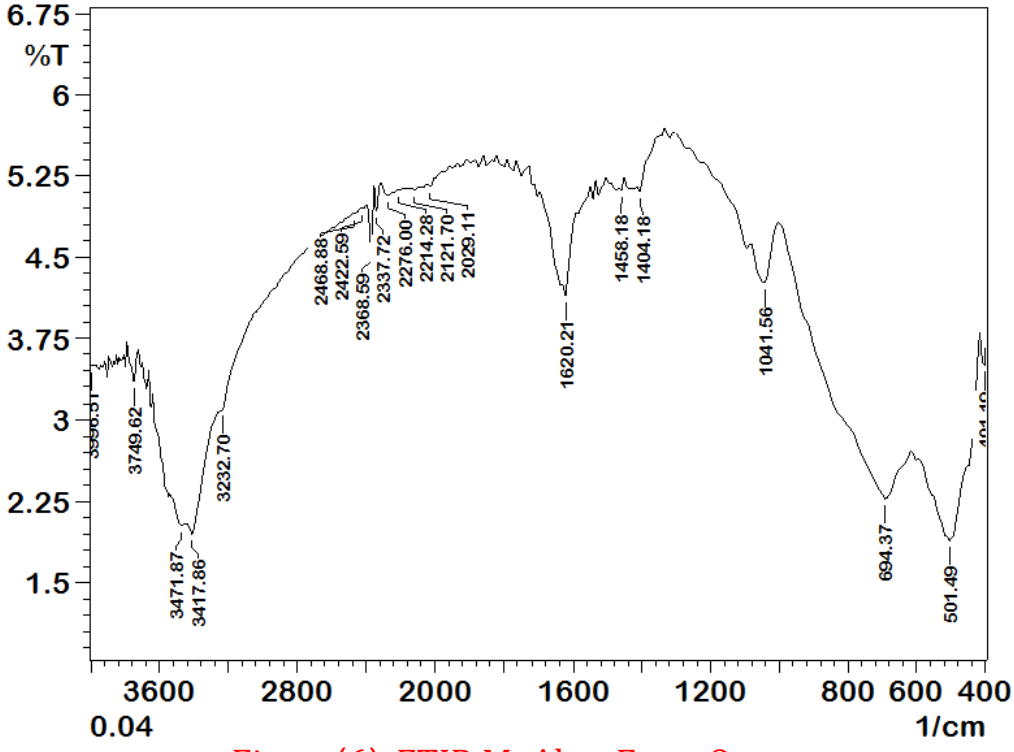

Figure(6). FTIR $MgAl_{1.95}Fe_{0.05}O_4$

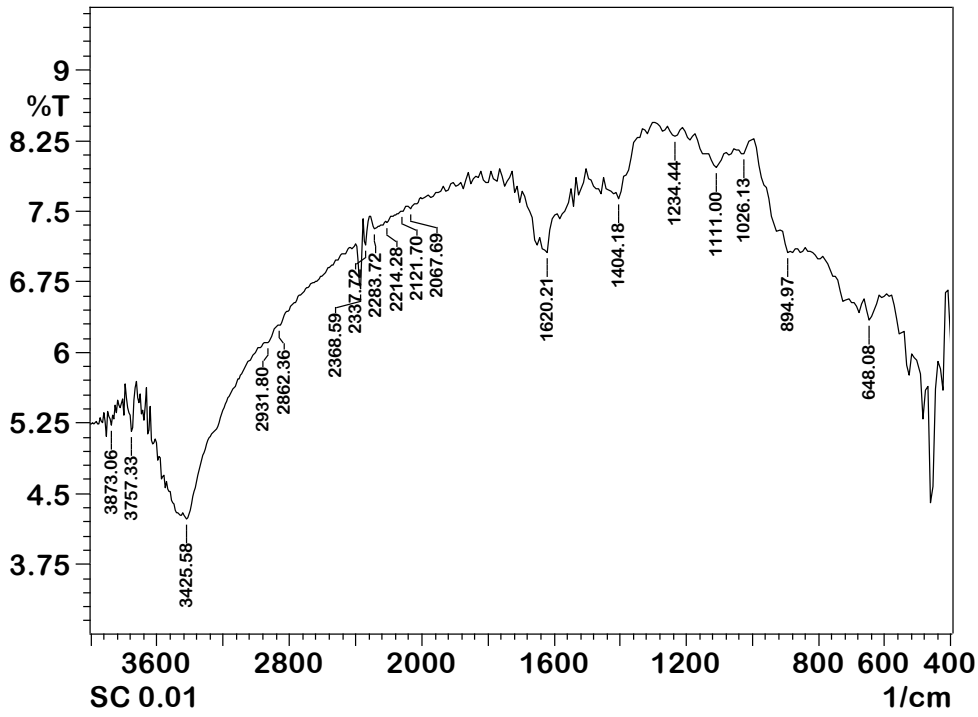

Figure(7). FTIR $MgAl_{1.95}Fe_{0.05\text{-}0.01}Sc_{0.04}O_4$

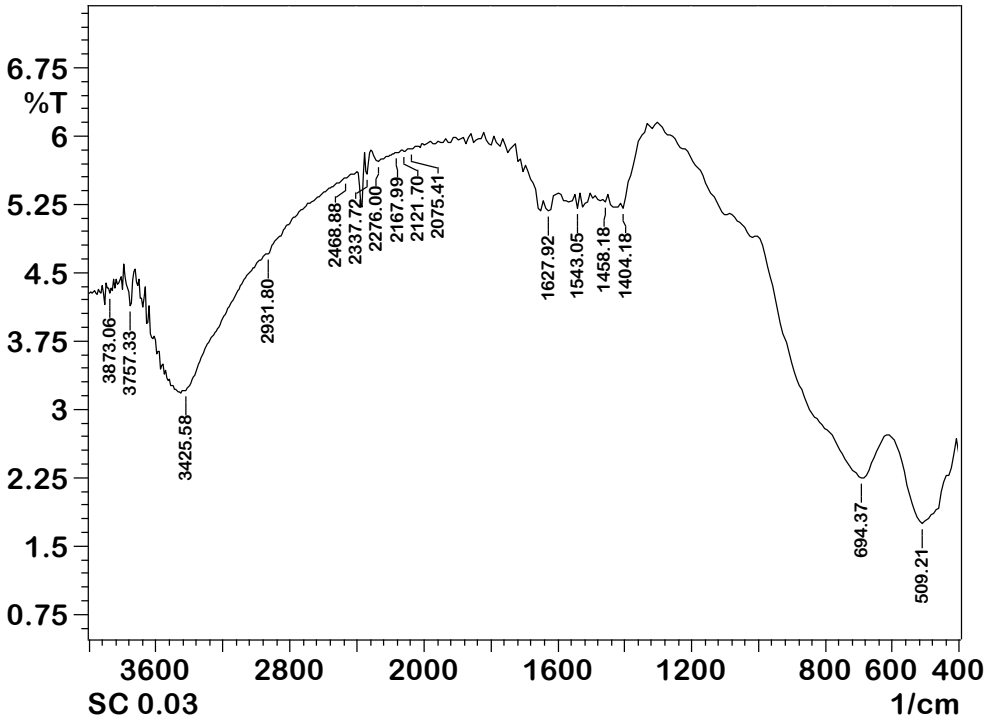

Figure(8). FTIR $MgAl_{1.95}Fe_{0.05\text{-}0.02}Sc_{0.03}O_4$

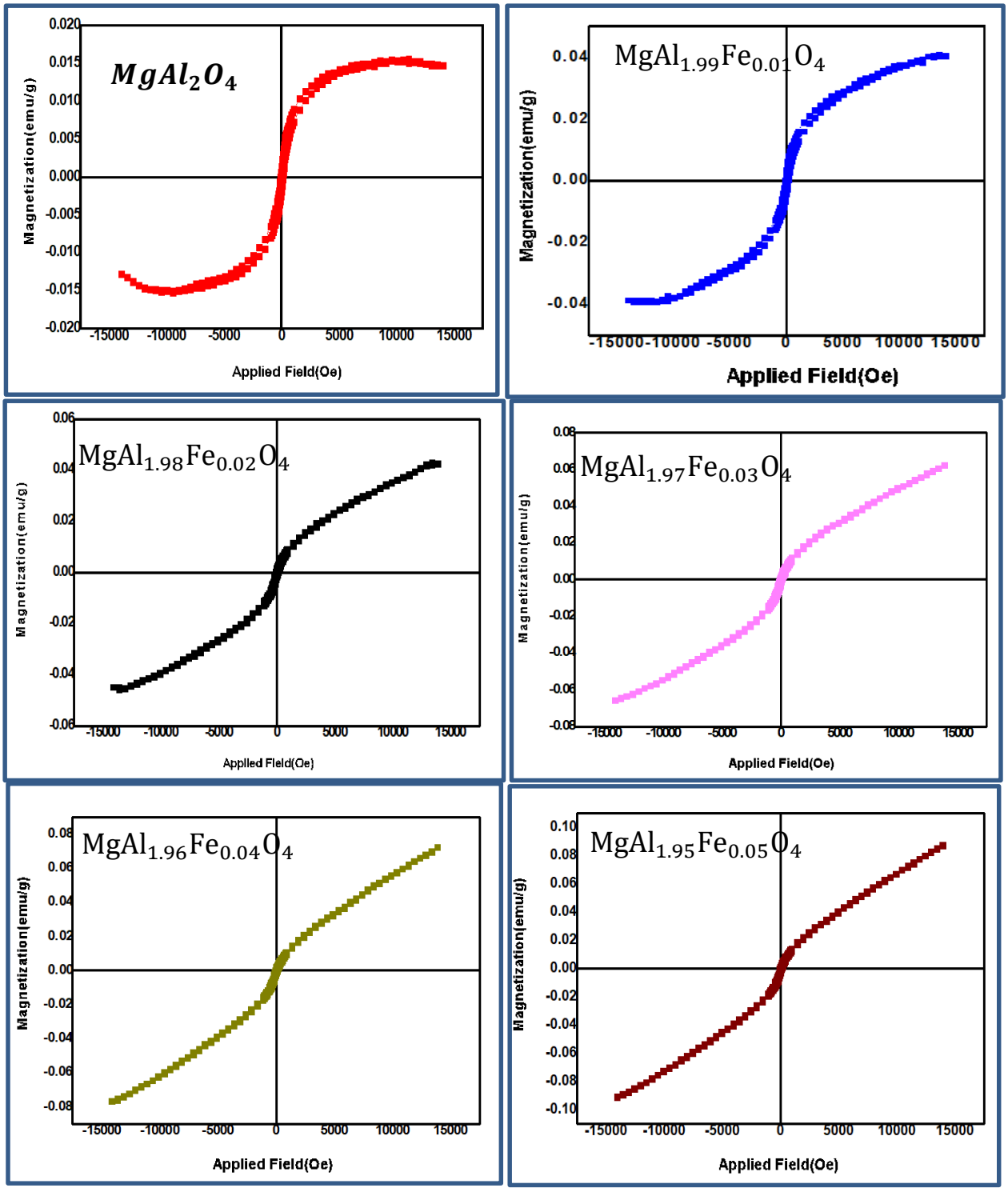

VSM for $MgAl_{2-x}Fe_{1-x}O_4$

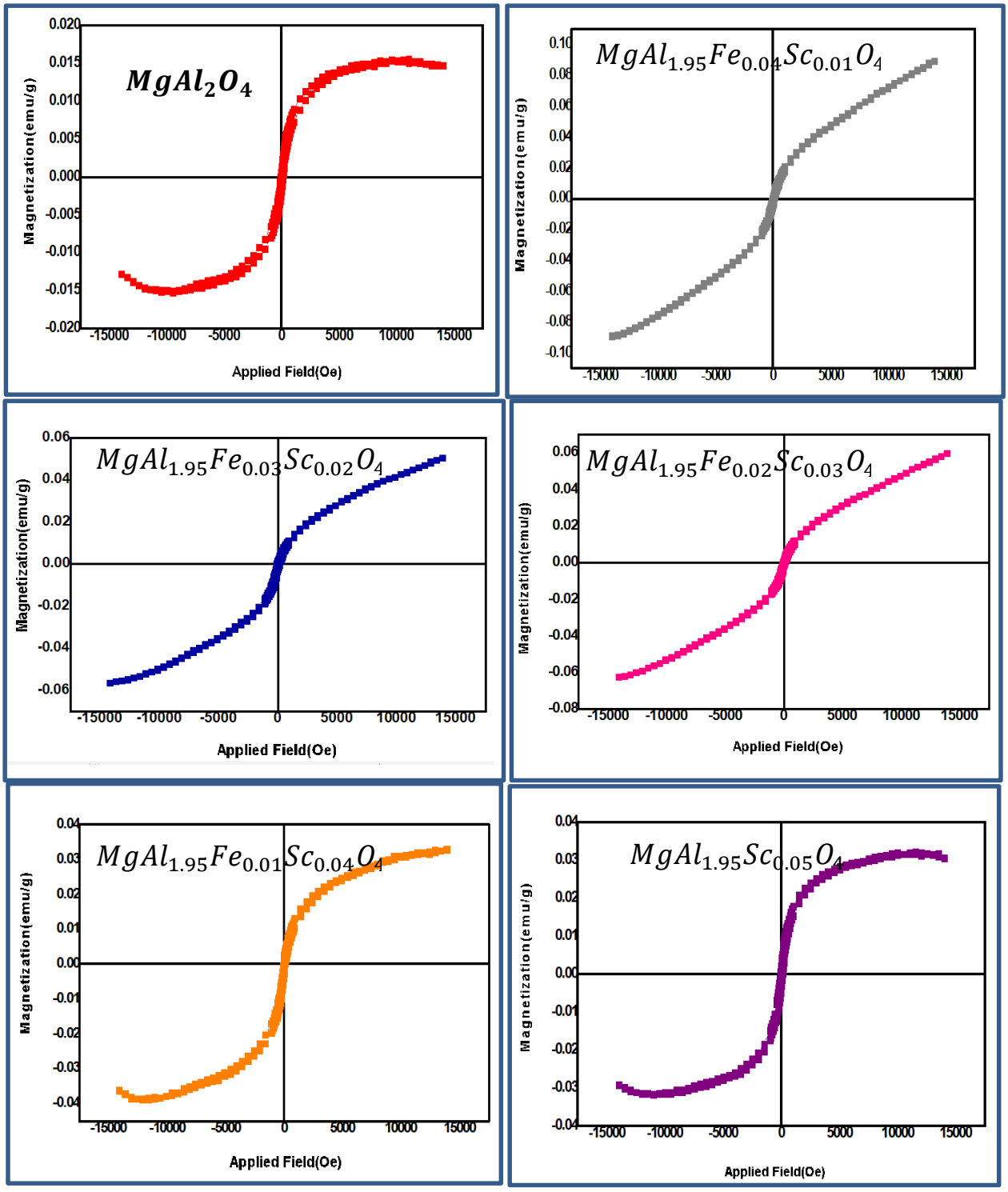

VSM for $MgAl_{1.95}Fe_{0.05-x}Sc_xO_4$

الخلاصة

الاسبنيل ألومينات المغنيسيوم ($MgAl_2O_4$) هو أحد أشهر أنواع المواد الخزفية لأكسيد المعادن بخصائص خاصة. تم تصنيع البلورات النانوية من الاسبنيل ($MgAl_2O_4$) المشوبة وغير المشوبة بطريقة sol – gel باستخدام نترات الألومنيوم، نترات المغنيسيوم، نترات الحديد، نترات سكانديوم وحمض الستريك كمواد اولية مع نسبة مولارية Al / Mg =2. بعد الحصول على مسحوق جاف، تمت معالجة السلائف بالحرارة عند درجات الحرارة المرغوبة (800 درجة مئوية) لمدة 4 ساعات بمعدل 5 درجات مئوية / دقيقة.

في البحث الحالي، تم تحضير مجموعتين رئيسيتين من الومينات المغنسيوم المشوبة والغير مشوبة. المجموعة الأولى هي ($MgAl_{2-x}Fe_xO_4$) النانوية حيث ان (x=0.0, 0.01, 0.02, 0.03, 0.04, 0.05) والمجموعة الثانية هي ($MgAl_{1.95}Fe_{0.05-y}Sc_yO_4$) النانوية حيث ان (y=0.0, 0.01, 0.02, 0.03, 0.04, 0.05).

أظهرت نتائج XRD للعينات غير المشوبة والمشوبة بان جميع العينات تتكون من تركيب بلوري موحد مع مجموعة واحدة من القمم المطابقة مع المرحلة التكعيبية لطور $MgAl_2O_4$ النانوية. بالإمكان الاستنتاج من نتائج تحليل XRD بان العينات المشوبة تعرضت للتزحيف الى مقدار اقل من زاوية 2θ في مخطط XRD مما ادى الى تغير في المسافة بين المستويات و طول وحدة الخلية البلورية و حجم الكريستالات، والتي تغيرت جميعها طبقا لنسبة الإضافة.

واظهرت نتائج التركيب الجزئي باستخدام مطياف FTIR إلى تكوين $MgAl_2O_4$ الاسبنيل حيث تظهر القمم في حدود cm^{-1} 690-531, اما بالنسبة للعينات المشوبة والغير مشوبة ل ($MgAl_{2-x}Fe_xO_4$) النانوية و($MgAl_{1.95}Fe_{0.05-y}Sc_yO_4$) النانوية بانها جميعها تمتلك نفس الهيكل التركيبي . وان العينات المشوبة حصل فيها تغيير في عرض القمم والشدة نتيجة لزيادة الاستبدال بأيونات Fe^{+3} وSc^{+3} في منطقة البصمة والتي تتراوح بين cm^{-1} 1000-400.

ومن صور اختبار SEM بينت شكل الدقائق النانوية بانها اشكال غير منتظمة بشكل كاف، تكون بشكل زاوي او تشبه الصفائح او شبة كروية وتحتوي على قنوات مسامية بسب تراكم الجزيئات. وان نقاوة جميع العينات تم تأكيدها بواسطة فحص EDX. كما لوحظ من صور اختيار TEM بينت شكل الدقائق النانوية بانها اشكال كروية او شبة كروية مع تداخلات اشكال ابرية ناتجة من نسب إضافات ايون Sc^{+3} وأظهرت النتيجة أن حجم الحبيبات لكل من العينات المشوبة والغير مشوبة كان مركزًا في نطاق 20-50 نانومتر.

تم استخدام STM لدراسة أبعاد جسيمات ألومينات المغنيسيوم المكلسة وغير المشبعة لفهم أفضل للظواهر الفيزيائية الأساسية حيث $MgAl_{2-x}Fe_xO_4$ كانت هناك جسيمات أكبر ومجموعات من الجسيمات يرجع متوسط أحجام العالية للجسيمات إلى Fe^{+3} أيون، مما يؤدي إلى تكثيف نمو الجسيمات الفردية. المساحة السطحية المحددة للمساحيق المحترقة يمكننا أن نرى أن لها طابع مسامي بسبب التكليس، حيث أظهرت انخفاضًا واضحًا في مساحات السطح لأن الجسيمات الأولية ذات الحجم الميكرومتر الفرعي قد تكتلت إلى جزيئات ثانوية أكبر. وعينات $MgAl_{1.95}Fe_{0.05-y}Sc_yO_4$النانوية لها نفس الإطار، لكن العينات المشوبة ب Fe^{+3} و Sc^{+3} لها تباين في البقع الداكنة والمشرقة في مقياس يتميز بأبعاد النانومتر.

ان نتائج المغناطسية تم قياسها بواسطة فحصVSM. حيث أظهرت النتائج ان قيم التشبع المغناطيسي Ms تعتمد على نسب التشويب. وان اقصى قيمة مغناطسييه لمجموعة $MgAl_{2-x}Fe_xO_4$ النانوية هي عند x=0.05 لعينة $MgAl_{1.95}Fe_{0.05}O_4$ بينما سجلت اقصى قيمة مغناطسية لمجموعة $MgAl_{1.95}Fe_{0.05-y}Sc_yO_4$ النانوية عندما y=0.04 لعينة $MgAl_{1.95}Fe_{0.01}Sc_{0.04}O_4$. ان نتائج المغناطسية افترضت ان كلا الايونين التشويب Fe^{+3} وSc^{+3} وبنسب مختلفة وفجوات الاوكسجين تؤدي دور مهما وإضافة الى ذلك ظهور ثلاث أنواع من حلقات الهستيريا.

جمهورية العراق
وزارة التعليم العالي والبحث العلمي
جامعة بابل
كلية هندسة المواد
قسم هندسة السيراميك ومواد البناء

تأثير التشويب بأيونات Fe^{+3} وSc^{+3} على خصائص $MgAl_2O_4$

رسالة

مقدمة إلى قسم هندسة السيراميك ومواد البناء في كلية هندسة المواد/جامعة بابل

كجزء من متطلبات نيل درجة الماجستيرفي هندسة المواد/ سيراميك

اعدت من قبل:

الخضر محمد فاضل علوان

بكالوريوس هندسة السيراميك ومواد البناء 2018

إشراف:

الأستاذ الدكتور
شاكر جاهل ادريس

الأستاذ المساعد الدكتور
شيماء جابر كريم

2021-2022 م